



Université catholique de Louvain

Ecole Polytechnique de Louvain

(Faculté des Sciences Appliquées)

LABORATOIRE DE TÉLÉCOMMUNICATIONS

ET

TÉLÉDÉTECTION

B - 1348 Louvain-la-Neuve

Belgique

Cyclic Prefixed Block Transmission for Wireless Communications: Performance Analysis and Optimization

Bertrand Devillers

Thesis presented for the Ph.D. degree
in Applied Sciences

Ph.D. committee:

Luc VANDENDORPE (UCL) - Supervisor

Ana GARCÍA ARMADA (Universidad Carlos III de Madrid)

Miguel Ángel LAGUNAS HERNÁNDEZ (Universitat Politècnica de Catalunya)

Jérôme LOUVEAUX (UCL)

Marc MOENECLAËY (Universiteit Gent)

Jean-Pierre RASKIN (UCL) - Chairman

March 2009

Remerciements

Une thèse de doctorat... certainement un aboutissement personnel, mais aussi une multitude de personnes qui y contribuent, parfois même sans s'en rendre compte!

Tout d'abord, je tiens à remercier mon promoteur, Luc Vandendorpe, pour son enthousiasme envers mon sujet de thèse, pour sa rigueur mathématique contagieuse, pour ses conseils précieux, pour la relation de confiance mutuelle, et pour son sens de l'humour. Merci aussi aux membres de mon jury, pour leurs commentaires constructifs: Ana García Armada, Miguel Ángel Lagunas Hernández, Jérôme Louveaux, Marc Moeneclaey, et Jean-Pierre Raskin.

Ma reconnaissance va également au Fonds National de la Recherche Scientifique pour avoir soutenu financièrement ce travail, tout en m'accordant une grande liberté.

Evidemment, ces années de thèse auraient été bien tristes sans les compagnons de travail. Un grand coup de chapeau à mes différents collègues de bureau qui ont réussi à me supporter: Thierry & Antoine (mes premiers mentors), Harold & Xa (bien plus que des 1/2 Dieu), Jon & Raf (que de fous rires!), Rosa, Mohieddine. Je tiens aussi à remercier de tout coeur tous les compagnons de pause de midi de ces dernières années: Xa W, Cédric, Valéry, André, David, Annabelle, Lyazid, Marilena, Onur, Mika, Ulas, Latif, Maxime, Seb, Joaquin, Quique (Federer fan), David (Barça fan), ... De manière générale, merci à tous les membres TELE, et en particulier à l'équipe DIGICOM. Finalement, gracias aux membres de l'uc3m pour leur accueil: Eloy, Felipe, Javi, Lorena, MLuz, Oscar, Rocio, Rosa, Ruben.

Puisque cette fin de thèse coïncide avec mon départ vers d'autres horizons, je me permets de remercier ici toutes les personnes qui me sont chères. Principalement, je voudrais exprimer mon énorme admiration pour ma Maman et mon Papa. Merci à eux pour les nombreux sacrifices qu'ils ont faits pour moi, et pour tout ce qu'ils m'ont donné et me donnent. Merci aussi à mes frères et soeurs pour l'exemple qu'ils m'ont toujours donné: Pierre & Anne, Benoît & Christelle, et Marie-France & Olivier. Que tous leurs merveilleux petits bouts ne grandissent pas trop vite!

Plus personnellement encore, j'aimerais remercier mes amis. Que la distance ne soit qu'une barrière ridicule face à notre amitié!

- Les tennismen et autres Pointures: Λ Prez, Λ Coach, Λ Latin lover, Fab, Hugs, Julien, Marcelo, Oli, Perny, Pov, Xa Bach, Xa Dauf, Dav, ...
- Les membres de la confrérie P&A: Baud, Ben, David, Nico d'or, Q, Régis.
- Les ex-colocs: Maya, Frans, Ben, Nico, Caro.
- Les amis du bout du monde: Thomas, TJ, Eirik, AJ, thanks guys!

A mi Gretiña! Ya sabes que te mereces que te escriba dos paginas enteras para darte las gracias por todo lo que me das a diario. Lo nuestro empezó justo cuando empezó este doctorado. Últimamente, tu mayor deseo ha sido que se acabara este doctorado de una vez! Mi deseo es que lo nuestro no se acabe nunca! Tu deseo acabó cumpliendose. Espero que el mío también se cumpla...

Abstract

Digital wireless communications have considerably changed not only the way people communicate, but also the way research is conducted in the field of telecommunications. In fact, the nature of the wireless medium has created a number of new challenging and fascinating research topics. In particular, a prerequisite for achieving higher and higher transmission rates in wireless systems is to develop strategies for efficiently dealing with the frequency selectivity of the wireless channel. A good candidate is the so-called cyclic prefixed block transmission, and in particular its two most popular variants which are the cyclic prefixed single-carrier (CPSC) and orthogonal frequency division multiplexing (OFDM) modulations. In this context, this thesis aims at analyzing and optimizing the use of cyclic prefixed block transmission for wireless communications.

Firstly, this thesis contributes to the current state-of-the-art on the performance comparison between CPSC and OFDM, focusing on the derivation of analytical results when possible. If the channel state information is not available at the transmitter side, CPSC with minimum mean square error linear receiver is shown to achieve the best trade-off between performance and complexity, as it exploits the multipath diversity under some realistic hypotheses.

Secondly, this thesis aims at using a system-based or cross-layer criterion, called goodput, for allocating resource in a coded OFDM system. Interestingly, the well-known waterfilling solution, when adequately parametrized, is proved to be near-optimal from a goodput point of view.

Finally, this thesis discusses the possibility of improving the performance of a CPSC system by exploiting the cyclic prefix for equalization purposes.

Contents

Abstract	v
Table of contents	vi
Notations and Acronyms	xi
1 Introduction	1
2 Cyclic Prefixed Block Transmission: from MC to SC	9
2.1 Introduction	9
2.2 Digital wireless transmission: the signal model	11
2.2.1 The wireless channel	11
2.2.2 A discrete-time signal model	13
2.3 Cyclic prefixed block transmission	15
2.4 From multi-carrier to single-carrier	19
2.4.1 Orthogonal frequency division multiplexing	22
2.4.2 Cyclic prefixed single-carrier	25
2.5 Multi-antenna dimension	31
2.5.1 MIMO OFDM	33
2.5.2 MIMO DFE-CPSC	38
2.6 Conclusions	38
Appendix 2.A Derivation of the MMSE DFE for CPSC	40
3 BER and Diversity	43
3.1 Introduction	43
3.2 Instantaneous bit error rate	45
3.2.1 OFDM	45

3.2.2	ZF-CPSC	46
3.2.3	MMSE-CPSC	47
3.2.4	DFE-CPSC	47
3.2.5	Instantaneous BER comparison	48
3.3	Average BER and diversity	52
3.3.1	OFDM	53
3.3.2	ML-CPSC	54
3.3.3	ZF-CPSC	58
3.3.4	MMSE-CPSC	60
3.4	Conclusions	64
	Appendix 3.A Detailed calculations	66
3.A.1	Derivation of (3.34)	66
3.A.2	Derivation of (3.46)	67
3.A.3	Derivation of (3.60)	67
	Appendix 3.B Derivation of the pdf of $x = K \min_k (h_k)$	68
	Appendix 3.C The harmonic mean - an every day life example	69
4	Achievable Bit Rate	71
4.1	Introduction	71
4.2	Mathematical preliminaries	72
4.2.1	Majorization theory	72
4.2.2	Relation between the Cholesky and eigenvalue decompositions	74
4.3	Bit rate formulation	80
4.4	Bit rate comparison	81
4.4.1	SISO	81
4.4.2	MIMO	84
4.5	Conclusions	86
	Appendix 4.A An alternative proof for Proposition 4.9	88
	Appendix 4.B About the principal submatrices of a matrix of the type $\mathbf{L}\mathbf{L}^H$	89
5	The Goodput Criterion: a Practical Trade-Off	93
5.1	Introduction	93
5.2	System model: OFDM with error-correction and retransmission mechanism	96

5.3	The waterfilling solution	100
5.4	Problem formulation	102
5.5	Discrete problem	104
5.5.1	Power allocation strategy for a given bit allocation	104
5.5.2	Bit allocation strategy	109
5.6	Relaxed problem with EBPA	110
5.7	Comparison with the waterfilling solution	113
5.8	Simulation results	115
5.9	Goodput comparison between OFDM and CPSC	119
5.10	Conclusions	121
	Appendix 5.A More on the waterfilling solution	123
6	Exploiting CP For Performance Improvement in CPSC Systems	127
6.1	Introduction	127
6.2	Proposed CPSC scheme	128
6.2.1	Conventional receiver	130
6.2.2	Proposed receiver	130
6.2.3	Power loading	135
6.3	Performance evaluation	135
6.3.1	Bit error rate	136
6.3.2	Goodput	138
6.4	Conclusions	140
7	Conclusions	143
	List of Publications	149
	Bibliography	151

Notations and Acronyms

Mathematical notations

j	imaginary unit: $j = \sqrt{-1}$
x	a scalar
x^*	the complex conjugate of x
$\text{Re}(x)$	the real part of x
$\text{Im}(x)$	the imaginary part of x
$ x $	the absolute value or norm of x
\mathbf{x}	a column vector
x_m	the $(m + 1)$ th entry of vector \mathbf{x} : $\mathbf{x} = [x_0, x_1, \dots, x_{K-1}]^T$
$x_{[i]}$	the components of \mathbf{x} in decreasing order: $x_{[0]} \geq x_{[1]} \geq \dots \geq x_{[K-1]}$
$x_{(i)}$	the components of \mathbf{x} in increasing order: $x_{(0)} \leq x_{(1)} \leq \dots \leq x_{(K-1)}$
\mathbf{x}^T	the transpose of vector \mathbf{x}
\mathbf{x}^H	the conjugate transpose of vector \mathbf{x}
$\ \mathbf{x}\ ^2$	the squared Frobenius norm of \mathbf{x} : $\ \mathbf{x}\ ^2 = \mathbf{x}^H \mathbf{x}$
\mathbf{X}	a matrix
$[\mathbf{X}]_{m,n}$	the $(m + 1)$ -th row and $(n + 1)$ -th column entry of matrix \mathbf{X}
\mathbf{X}^T	the transpose of matrix \mathbf{X}
\mathbf{X}^H	the conjugate transpose of matrix \mathbf{X}
\mathbf{X}^{-1}	the inverse of matrix \mathbf{X}
$\text{diag}(\mathbf{x})$	diagonal matrix whose entries are the elements of vector \mathbf{x}
$\text{trace}(\mathbf{X})$	the trace of matrix \mathbf{X}
$\det(\mathbf{X})$	the determinant of matrix \mathbf{X}
\mathbf{I}_N	the $N \times N$ identity matrix
$\mathbf{1}$	the all-ones column vector

\triangleq	is defined as
\cong	is approximately equal to
$E[x]$	the expected value (or mathematical expectation) of x
$[x]^+$	the positive part of x , i.e. $[x]^+ \triangleq \max(0, x)$
\check{d}	the detected value (or decision) of symbol d
\hat{d}	the estimated value of symbol d (i.e. before decision making)
$Q(\cdot)$	the Gaussian Q-function: $Q(\alpha) = \frac{1}{\sqrt{2\pi}} \int_{\alpha}^{\infty} e^{-u^2/2} du$
$H(\mathbf{x})$	the harmonic mean of the entries of vector \mathbf{x}
$ \mathcal{S} $	the cardinality of set \mathcal{S}

Acronyms

ACK	ACKnowledgment
ARQ	Automatic Repeat Request
AWGN	Additive White Gaussian Noise
BBBA	Branch-and-Bound Bit Allocation
BER	Bit Error Rate
BPSK	Binary Phase Shift Keying
cdf	cumulative distribution function
CFO	Carrier Frequency Offset
CIR	Channel Impulse Response
CP	Cyclic Prefix
CPSC	Cyclic Prefixed Single Carrier
CSI	Channel State Information
CSIT	Channel State Information at the Transmitter side
DFE	Decision Feedback Equalization
DMMT	Discrete Matrix Multitone
DMT	Discrete Multi-Tone
EBPA	Equal BER Power Allocation
ESBA	Exhaustive Search Bit Allocation
FER	Frame Error Rate
FFT	Fast Fourier Transform
FSR	Frame Success Rate
GABA	Greedy Algorithm Bit Allocation

GBN	Go-Back-N
GP	Goodput
IFFT	Inverse Fast Fourier Transform
i.i.d.	independent and identically distributed
ISI	Intersymbol Interference
MC	Multi-Carrier
MIMO	Multiple Input Multiple Output
ML	Maximum Likelihood
MMSE	Minimum Mean Square Error
MRC	Maximum Ratio Combining
MSE	Mean Square Error
NAK	Negative AcKnowledgegment
OFDM	Orthogonal Frequency Division Multiplexing
OFDMA	Orthogonal Frequency Division Multiple Access
OPA	Optimal Power Allocation
PAPR	Peak to Average Power Ratio
PEP	Pairwise Error Probability
pdf	probability density function
PSK	Phase Shift Keying
QAM	Quadrature Amplitude Modulation
QPSK	Quadrature Phase Shift Keying
RRBA	Round Relaxed Bit Allocation
SAW	Stop-And-Wait
SC	Single Carrier
SISO	Single Input Single Output
SINR	Signal to Interference plus Noise Ratio
SNR	Signal-to-Noise Ratio
SR	Selective-Repeat
SVD	Singular Value Decomposition
ZF	Zero Forcing

Introduction

1

As daily users of communication devices, we have all witnessed the continuous evolution of this technology in the last decade. This evolution as a whole is to be jointly credited to major advances in various fields of electrical engineering, one of these fields being that of telecommunications and digital wireless communications in particular. In fact, let us take the example of today's mobile phones: they provide more and more services, like mobile TV or Internet. For such applications, one of the bottlenecks of the overall system can be the rate at which the (digital) information is transmitted through the wireless medium. This constitutes the context of this thesis: the achievement of higher and higher transmission rates in digital wireless systems.

Achieving reliable and high data rate communications over wireless links remains a challenging problem, that continues to receive a lot of attention from many research groups throughout the world. In fact, the inherent nature of the wireless medium has created a number of new challenging research topics:

- **Wireless propagation: the multipath fading channel.**

The transmitted signal potentially interacts with any element of the wireless environment. Because of reflections by objects in the propagation medium, the received signal is the sum of multiple delayed and attenuated versions of the transmitted signal. Moreover, since this interaction is highly dependent on the environment configuration (e.g. position of the transmitter, reflecting objects, and receiver), the instantaneous channel can vary drastically from one configuration to

another, and consequently from one instant to another in a mobile environment. In other words, the wireless channel is referred to as multipath fading channel. At first, the multipath fading channel was seen as an imperfection which had to be compensated. However, attitudes have changed slightly as people realized that reliable communication can be achieved if the intrinsic nature of the wireless channel is exploited. In fact, since multiple replicas of the transmitted signal reach the receiver, the communication can be potentially reliable if at least one of these replicas has sufficient strength. In short, the multipath fading channel inherently provides a source of diversity, referred to as multipath diversity.

■ **Wireless medium: a ubiquitous resource.**

The wireless and wireline communications inherently differ by the accessibility of the propagation medium. The wireless medium is a resource which is accessible simultaneously from anywhere and, consequently, has to be shared by a potentially large number of transmissions. As irrelevant as it might sound, this statement lies at the basis of many research topics within wireless communications. Without being exhaustive, let us mention two of these topics: the multi-user and multi-antenna dimensions. First, the sharing of the medium by multiple users gives rise to signal interference which has to be controlled. The optimization of the multi-user environment gave birth to new challenges for multiple-access techniques, adaptive resource allocation among users, users scheduling, etc. Second, the ubiquitous nature of the wireless medium can be exploited within one single transmission by transmitting and/or receiving the signal simultaneously on multiple antennas. This multi-antenna dimension turns out to improve considerably the performance, and has received a lot of attention in the last decade. Moreover and from a more general point of view, the above-mentioned time-variability of the wireless channel has to be taken into account in all analyses, which makes all wireless research topics even richer and more challenging.

In this dissertation, the focus is mainly set on the exploitation of the first above-mentioned characteristic of the wireless medium, which is the multi-

path fading channel. For the study of digital wireless communication, the multipath fading channel translates into a discrete-time impulse response model. In particular, if the delay spread (i.e. the delay between the shortest and longest paths) of the channel is large when compared with the symbol period, the discrete-time impulse response is made up of several taps, and the channel is said to be frequency selective. In the other way around, the channel is said to be flat. In today's communication systems, the decreasing duration of symbols for higher rates results in an increasing frequency selectivity. As a consequence, in this thesis, the focus will be set on frequency selective channels.

A key issue in digital wireless communication has been to find strategies for how to deal with frequency selective channels, that is how to mitigate the intersymbol interference inherent to such channels. One well-known approach is the multi-carrier (MC) modulation, whose first efficient implementations were proposed more than 40 years ago in [1, 2]. As its name indicates, the MC modulation consists of splitting the transmission of a high rate message over various separate carrier frequencies. Each of these carriers is then operating at a lower signal rate, such that the corresponding subchannels can appear to be flat and can be equalized easily. Since then, the popularity of the MC modulation has grown significantly thanks to its implementation with fast Fourier transform (FFT) [3–5]. Nowadays, the MC modulation is widely used [6, 7] and is known as discrete multitone (DMT) and orthogonal frequency division multiplexing (OFDM) in the wireline and wireless communities respectively. The basic idea relies on the organizing of the transmission in blocks of symbols and on the addition of a cyclic prefix (CP) (as first introduced in [4]) to each transmitted block. The role of the CP is twofold: first it acts as a guard period between blocks, and second it converts the linear convolution with the channel impulse response into a cyclic one. Thanks to that, the equalization can be linearly implemented in the frequency domain, with low complexity: it only requires one inverse FFT (IFFT) operation at the transmitter side, and one FFT at the receiver side followed by symbol-by-symbol scalar multiplications. In addition to its ability to deal with frequency selective channels with low complexity, the OFDM modulation has become popular also thanks to its efficient applicability to a multi-user environment: in fact, each user can be assigned a subset of subcarriers without interfering with the

other users [8]. This is known as orthogonal frequency division multiple access (OFDMA).

More recently, it has been pointed out in [9, 10] that by keeping the cyclic extension of each block and by moving the IFFT operation of the OFDM modulation from the transmitter to the receiver side, we end up with a so-called cyclic prefixed single-carrier (CPSC) system. The CPSC system also benefits from a low complexity equalization of the multipath channel in the frequency domain. The complexity is actually mostly moved to the receiver side. On top of that, CPSC transmission has received much attention because, unlike the OFDM modulation, it does not suffer from the peak to average power ratio (PAPR) problem. This is precisely due to the absence of the IFFT operation at the transmitter side. These considerations make CPSC a good alternative candidate for the uplink [11]. Another issue which has received some attention when comparing OFDM and CPSC is their respective sensitivity to non-idealities [12]. In particular, the OFDM modulation is known to be very sensitive to carrier frequency offset (CFO), which causes intercarrier interference even for flat fading channels [13]. Despite some statements to the contrary, it is unfortunately not clear that CPSC is more robust to CFO: it also suffers from intersymbol interference if the channel is frequency selective (even though it does not when the channel is flat). Generally speaking, even if it is tractable to bring in the contribution of the non-idealities into the signal models [14], it is much more difficult to analytically derive the effects of these non-idealities on the actual performance of the systems [15]. Finally, for completeness, let us mention the following recent works on the applicability of CPSC to multi-antenna systems [16–18] and to multi-user environments [19, 20].

Both OFDM and CPSC are thus variants of the same technique called cyclic prefixed block transmission. This thesis aims at analyzing and optimizing the use of cyclic prefixed block transmission for wireless communications.

Outline

The dissertation is divided in 5 chapters. Hereunder is an overview of each of them.

Chapter 2. This chapter aims at introducing the different concepts that will be used throughout the thesis, together with the mathematics related to them. The wireless channel model is defined, as well as the corresponding discrete-time signal model for digital wireless communication. The notion of cyclic prefixed block transmission is introduced, and is then particularized successively into OFDM and CPSC. Different receiving strategies are considered, including optimal/suboptimal linear/nonlinear receivers. The multi-antenna dimension is also discussed both for OFDM and CPSC.

Chapter 3. This chapter tackles a first natural question, that is, how do OFDM and CPSC compete in terms of bit error rate (BER). This comparison has to be considered first for a given channel realization, which has been discussed in part in [21, 22]. A second step consists of integrating the fading of the channel in the comparison and leads to diversity issues. In particular, this chapter analyzes to which extent the multipath diversity is extracted by a CPSC transmission. The state-of-the-art is currently pessimistic on that issue, and has to be moderated: if it is true that the asymptotical, i.e. at infinite signal to noise ratio (SNR), diversity order achieved by CPSC is equal to one, we prove that the block size has an influence on the performance at moderate SNR. In particular, for reasonably large values of the block size, we show that the multipath diversity can be extracted by CPSC for the range of BER values typically used in practice. The influence of suboptimal linear receivers on the diversity extraction is also investigated. Note that, in this chapter, the channel is assumed to be perfectly known at the receiver side, but unknown at the transmitter side.

Publication related to Chapter 3: [23]

Chapter 4. This chapter discusses the dual comparison of that of Chapter 3. The channel is assumed to be also known at the transmitter side. This knowledge is used for adaptively allocating the bits to the different symbols of a block. This chapter is then dedicated to analytically comparing OFDM and CPSC in terms of achievable bit rate for a given target BER. The results of this chapter extend the work in [24], where the achievable bit rates of OFDM and CPSC were compared for the single input single output (SISO) case and for the high SNR regime. Our contribution is twofold: it extends the comparison to any SNR value, and to the multiple input multiple output (MIMO) case.

Note that the mathematical derivations of this chapter will make use of the majorization theory. The basics of this theory are recalled in the first part of the chapter.

Publication related to Chapter 4: [25]

Chapter 5. This chapter addresses the problem of adaptively allocating both the bits and the power among the OFDM subcarriers. The originality of this work lies in the optimization criterion used: the objective is to maximize the number of information bits delivered without error to the user by unit of time, or goodput. This criterion has been chosen in order to reach a trade-off between the bit rate and BER criteria, which is what a user is specifically looking for in some applications. Moreover, this system-based criterion allows taking into account the error-correction and retransmission mechanisms. In other words, the goodput criterion is cross-layer oriented. In this chapter, a frame-oriented transmission with convolutional coding, hard Viterbi decoding, and automatic repeat request (ARQ) retransmission protocol is considered. First, a mathematical expression for the goodput of the system is presented. Then, using that expression, different bit and power allocation strategies are derived and compared. Interestingly, these strategies can be analytically connected to a more conventional strategy (the so-called waterfilling solution) which is based on an information theoretical criterion [26]. We prove that the waterfilling solution can be goodput near-optimal if it is parametrized adequately and according to the convolutional code used, the frame length, the type of ARQ protocol used, the available transmit power, and the subcarriers gains. Finally, OFDM and CPSC are compared in the light of this new criterion.

Publications related to Chapter 5: [27–29]

Chapter 6. This chapter reconsiders the conventional CPSC scheme and proposes a modification to it. Conventionally, and in all previous chapters of this thesis, the cyclic prefix (CP) is discarded at the receiver side: while it is sometimes used for channel estimation or synchronization, the part of the received signal corresponding to the CP is conventionally not used for equalization purposes. The objective of this chapter is to propose a new CPSC receiver exploiting the whole received signal (including the CP) for data detection. With an extra FFT size and reasonable additional complexity, the pro-

posed architecture is shown to outperform the conventional CPSC receiver, both in terms of BER and goodput.

Publication related to Chapter 6: [30]

Cyclic Prefixed Block Transmission: from Multi-Carrier to Single-Carrier

2

This chapter aims at introducing the material that will be used in this thesis.

2.1 Introduction

As emphasized in the introduction chapter, the main particularity of wireless communications lies in the inherent nature of the wireless channel. The transmitted signal potentially interacts with any element constituting the wireless environment. For instance, because of reflections by objects in the propagation medium, the received signal is the sum of multiple delayed and attenuated versions of the transmitted signal. Moreover, since this interaction is highly dependent on the environment configuration (e.g. position of the transmitter, reflecting objects, and receiver), the instantaneous channel (i.e. the impulse response connecting the transmitted and received signals) can vary drastically from one configuration to another, and consequently from one instant to another in a mobile environment. In the jargon, the wireless channel is referred to as multipath fading channel. In the context of digital wireless communication, the multipath fading channel translates into a discrete-time impulse response. In particular, if the delay spread of the channel (i.e. the delay between the shortest and longest paths) is large when compared with the

symbol period, the discrete-time impulse response is made up of several taps, and the channel is said to be frequency selective. In today's communication systems, the decreasing duration of symbols for higher rates results in an increasing frequency selectivity. For this reason, in this dissertation, the focus is exclusively set on frequency selective channels.

An important issue in digital wireless communication is the equalization of the frequency selective channels. That is, the intersymbol interference (ISI) inherent to such channels has to be mitigated in order to allow reliable communication. One efficient approach is the cyclic prefixed block transmission. The basic idea relies on the organizing of the transmission in blocks of symbols and on the addition of a cyclic prefix (CP) to each transmitted block [4]. The role of the CP is twofold. First, it acts as a guard period between blocks, and avoids interblock interference. Second, it converts the linear convolution with the channel impulse response into a cyclic one. Consequently, thanks to the CP insertion, each block can be equalized independently. Furthermore, this equalization can be linearly implemented with low complexity in the frequency domain, thanks to (inverse) fast Fourier transforms ((I)FFT) operations. Depending on the linear operation implemented at the transmitted side, the cyclic prefixed block transmission particularizes into two well-known transmission techniques:

- If an IFFT operation is carried out at the transmitter side, we get a multi-carrier (MC) modulation [6], known as discrete multitone (DMT) and orthogonal frequency division multiplexing (OFDM) in the wireline and wireless communities respectively. The OFDM modulation deals with frequency selective channels with low complexity: it only requires one inverse FFT (IFFT) operation at the transmitter side, and one FFT at the receiver side followed by symbol-by-symbol scalar multiplications.
- If the IFFT operation is removed from the transmitter side, we end up with a so-called cyclic prefixed single-carrier (CPSC) system [9]. The CPSC system also benefits from a low complexity equalization of the frequency selective channel in the frequency domain. The complexity is actually mostly moved to the receiver side. On top of that, the CPSC transmission has received much attention because, unlike the OFDM

modulation, it does not suffer from the peak to average power ratio (PAPR) problem. This is precisely due to the absence of the IFFT operation at the transmitter side. These considerations make CPSC a good alternative candidate for the uplink [11].

The goal of this chapter is to introduce the mathematics behind all these concepts. The remainder of this chapter is organized as follows. Section 2.2 describes the wireless channel model, and derives the corresponding discrete-time signal model for digital wireless communication. The notion of cyclic prefixed block transmission is introduced in Section 2.3. The associated signal model is also derived. In Section 2.4, it is shown how this signal model takes the shape of either an OFDM or CPSC system depending on the linear operation implemented at the transmitter side. Different receivers (linear or not) are considered for both OFDM and CPSC systems. Finally a multi-antenna dimension is considered for both OFDM and CPSC: its mathematical description is given in Section 2.5.

2.2 Digital wireless transmission: the discrete-time signal model

This section is dedicated to deriving the discrete-time signal model for digital wireless communication, which will be used throughout this thesis. With this objective in mind, the wireless channel is first described and modeled.

2.2.1 The wireless channel

The fundamental characteristic of the wireless channel is the so-called multipath propagation illustrated in Fig. 2.1: due to reflections by objects in the propagation medium, the received signal is a superposition of multiple copies of the transmitted signal, each with different amplitude, phase and delay. The replicas from the different paths can interfere in a constructive or destructive manner, causing variations in the channel strength, or fading. At first sight, the wireless medium might thus not seem very appropriate for communication, when compared to the wireline channel for instance. However, we will

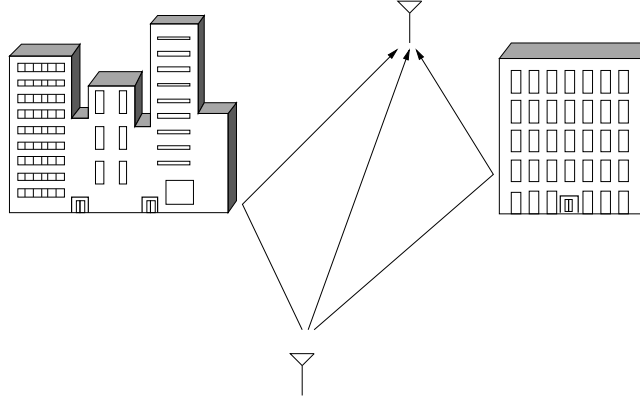


Figure 2.1 Multipath propagation.

see throughout this thesis that the multipath fading channel can actually be exploited, and that reliable communication can be achieved.

The multipath fading channel can be characterized by the following channel impulse response [31]

$$c(t) = \sum_{i=0}^{M-1} a_i \delta(t - \tau_i) \quad (2.1)$$

where M denotes the number of multipath components, and a_i and τ_i are the amplitude and the delay of the i th path, respectively. Obviously, these quantities are related to physical characteristics of the propagation environment (spatial configuration,...), but this is beyond the scope of this thesis. The interested reader can refer to [31,32] for a more detailed description. An important parameter of the multipath wireless channel is the delay spread T_d defined as the difference in arrival time between the longest and shortest path

$$T_d \triangleq \tau_{M-1} - \tau_0. \quad (2.2)$$

Since the baseband equivalent representation of the signals will be used in all mathematical developments of this thesis, we are more interested in the baseband equivalent representation of the channel impulse response (2.1), which is given by

$$c^b(t) = \sum_{i=0}^{M-1} a_i^b \delta(t - \tau_i) \quad (2.3)$$

where $a_i^b = a_i e^{-j2\pi f_c \tau_i}$, with f_c the carrier frequency. Please note that, even though it is not made explicit in (2.1) and (2.3) for simplicity, both a_i and τ_i (and therefore a_i^b) are time-varying quantities.

2.2.2 A discrete-time signal model

Assume that the baseband transmitted signal has the following conventional form

$$x(t) = \sum_n s_n u(t - nT_s) \quad (2.4)$$

where s_n are the input complex symbols, T_s is the symbol period, and $u(t)$ is the pulse shaping filter. Given the baseband channel impulse response (2.3), the baseband received signal is given by

$$\begin{aligned} r(t) &= \int_{-\infty}^{\infty} c^b(\tau) x(t - \tau) d\tau + w(t) \\ &= \sum_n s_n \int_{-\infty}^{\infty} c^b(\tau) u(t - \tau - nT_s) d\tau + w(t) \\ &= \sum_n s_n \sum_{i=0}^{M-1} a_i^b u(t - \tau_i - nT_s) + w(t) \end{aligned} \quad (2.5)$$

where $w(t)$ is the additive white Gaussian noise (AWGN). At the receiver side, the first operation is the matched pulse shaping filter

$$\begin{aligned} y(t) &= \int_{-\infty}^{\infty} u(-\tau') r(t - \tau') d\tau' \\ &= \sum_n s_n \sum_{i=0}^{M-1} a_i^b \int_{-\infty}^{\infty} u(t - \tau' - \tau_i - nT_s) u(-\tau') d\tau' \\ &\quad + \int_{-\infty}^{\infty} u(-\tau') w(t - \tau') d\tau' \end{aligned} \quad (2.6)$$

followed by sampling at rate $1/T_s$

$$\begin{aligned} y_m &= y(t = mT_s) \\ &= \sum_n s_n \sum_{i=0}^{M-1} a_i^b \int_{-\infty}^{\infty} u(mT_s - \tau' - \tau_i - nT_s) u(-\tau') d\tau' \\ &\quad + \int_{-\infty}^{\infty} u(-\tau') w(mT_s - \tau') d\tau' \end{aligned} \quad (2.7)$$

$$= \sum_l s_{m-l} \sum_{i=0}^{M-1} a_i^b p(lT_s - \tau_i) + n_m \quad (2.8)$$

where $l = m - n$, and where we defined

$$n_m \triangleq \int_{-\infty}^{\infty} u(-\tau') w(mT_s - \tau') d\tau' \quad (2.9)$$

$$p(t) \triangleq \int_{-\infty}^{\infty} u(t - \tau) u(-\tau) d\tau. \quad (2.10)$$

Note that $p(t)$ is the convolution of the pulse shaping and matched filters. Finally, by defining

$$g_l \triangleq \sum_{i=0}^{M-1} a_i^b p(lT_s - \tau_i), \quad (2.11)$$

the signal model (2.8) becomes

$$y_m = \sum_l g_l s_{m-l} + n_m. \quad (2.12)$$

In the following, g_l will be referred to as the l th (complex) tap of the channel impulse response¹. Looking at the expression (2.11), we see that, strictly speaking, each tap g_l contains the contribution of all M paths. However, $p(t)$ is typically a raised-cosine response, and is rapidly decaying with t . As a consequence, only the paths whose delays τ_i are close to lT_s will contribute significantly to the value g_l of the l th tap. The finite number M of paths will then translate into a finite number of taps denoted by L , and (2.12) finally becomes

$$y_m = \sum_{l=0}^{L-1} g_l s_{m-l} + n_m \quad (2.13)$$

where the causality constraint was also introduced such that $l \geq 0$. The number of taps L is closely related to how the values of the delay spread T_d and symbol period T_s compare to each other:

- If T_d is much smaller than T_s , then a single tap is sufficient to represent the discrete channel. The channel is said to be flat, and $L = 1$.
- If T_d is larger than T_s , then multiple taps are needed to represent the discrete channel. The channel is referred to as frequency selective, and $L > 1$. This situation is the most common one, and will be the one considered in this thesis. In fact, today's wireless communication systems

¹Strictly speaking, the g_l are the taps of the channel impulse response of the equivalent discrete model, and are related to the "true" impulse response by (2.11). However, for conciseness, we will abusively refer to g_l as taps of the channel impulse response.

are expected to achieve higher and higher rates, which implies small values of T_s .

Since the amplitudes and phases of the different paths are time-varying quantities, the channel taps g_l are also time-varying and will be modeled as random variables. In particular, we assume that a large number of paths with statistically independent amplitudes and phases contribute to a single tap, such that each tap g_l can be modeled as a circularly symmetric complex zero-mean Gaussian random variable. Additionally, it will be assumed that the random variables g_l and $g_{l'}$ ($l \neq l'$) are independent. This assumption is justified by the fact that two distinct taps are influenced by paths with difference range of delays, as commented above. Moreover, since paths with longer delays are expected to have lower amplitudes in average, the power (i.e. variance) of a given tap g_l should decrease as l increases. However, for simplicity, we will assume in this thesis that each tap g_l has variance equal to $1/L$. Note that this normalization is such that the channel impulse response has unit average power, independently of the value of L . Looking at the squared norm of a given tap, we end up with a random variable $x = |g_l|^2$ which has a chi-square distribution. Its probability density function (pdf) is given by

$$T_x(x) = L e^{-Lx}. \quad (2.14)$$

Finally, the noise samples n_m in (2.13) are also assumed to be i.i.d. circularly symmetric complex Gaussian random variables with zero mean and variance denoted by σ_n^2 .

The discrete signal model (2.13) will be used extensively throughout this thesis. This is the reason why we thought that it might be useful to dedicate a section reminding how to get to this model, and what are the assumptions related to it.

2.3 Cyclic prefixed block transmission

When the channel is frequency selective ($L > 1$), the signal model (2.13) inherently suffers from intersymbol interference (ISI): the delayed versions of the previous symbols s_k ($k < m$) interfere with the current symbol s_m . Some

equalization technique is thus needed in order to detect the transmitted symbols from the received signal (2.13). Maximum likelihood (ML) detection can be applied using the Viterbi Algorithm if the number of taps is relatively small (otherwise the algorithm's complexity rapidly grows). An alternative with lower complexity is the use of linear signal processing to suppress the ISI from the other symbols, and detect the current symbol.

A well-known approach for dealing with frequency selective channels with lower complexity is the organizing of the transmission in blocks of symbols. This method will be the one considered in this thesis. At the transmitter side, a guard interval is inserted between each pair of consecutive blocks. If the guard interval is greater or equal to the channel impulse response's maximum delay (equal to $L - 1$ symbol periods), there is no interblock interference, and the successive blocks can be detected independently, which is convenient. The introduction of a guard interval clearly implies a bandwidth efficiency loss, which is the price to pay. However, this loss can be small if the block size is much greater than the channel impulse response's maximum delay. Different alternatives have been proposed for the guard interval structure:

- Zero-padding (ZP) - the guard interval is the all-zero sequence.
- Unique Word (UW) - the guard interval is a known sequence.
- Cyclic Prefix (CP) - the guard interval is a copy of the last symbols of the subsequent block.

In this thesis, the focus will be set on the use of the CP as guard interval. The reader interested in ZP and UW can refer to [33–35] and [36–38], respectively.

Let us consider the situation depicted in Fig. 2.2 where the focus is set on the transmission of one symbol block (say symbol block i). The block size is denoted by K , such that the symbol block can be written as a $K \times 1$ vector

$$\mathbf{s} = [s_0, s_1, \dots, s_{K-1}]^T. \quad (2.15)$$

As previously said, the CP consists of prefixing a copy of at least the last $L - 1$ symbols of the block. In the following, Let us suppose a CP of length precisely equal to $L - 1$ (i.e. we assume a CP of minimal length, since the longer the CP the higher the bandwidth efficiency loss will be). The transmitted signal

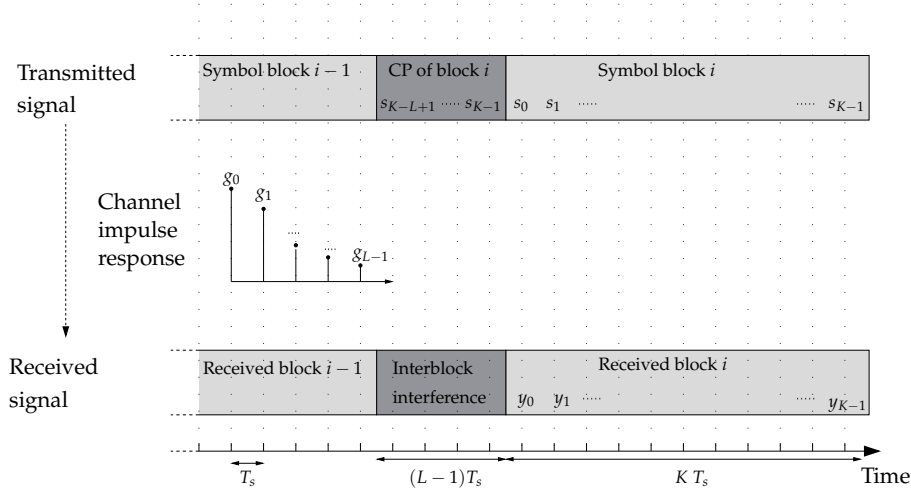


Figure 2.2 The cyclic prefix as guard interval.

(CP + symbol block) is thus represented as a $(K + L - 1) \times 1$ vector

$$\tilde{\mathbf{s}} = [s_{K-L+1}, \dots, s_{K-1}, s_0, s_1, \dots, s_{K-1}]^T. \quad (2.16)$$

Let us examine the received signal during the $K + L - 1$ symbol periods associated with the transmission of $\tilde{\mathbf{s}}$: as shown in Fig. 2.2, the first $L - 1$ samples suffer from interference from the previous block of symbol (block $i - 1$). These first $L - 1$ samples are thus ignored², and the following K samples are considered and denoted by

$$\mathbf{y} = [y_0, y_1, \dots, y_{K-1}]^T. \quad (2.17)$$

If the channel remains constant over the considered $K + L - 1$ symbol periods, the signal model (2.13) then directly translates into the following matricial relation

$$\mathbf{y} = \mathbf{G}_T \tilde{\mathbf{s}} + \mathbf{n} \quad (2.18)$$

²This operation will be referred to as the discarding of the CP at the receiver side.

where \mathbf{G}_T is a $K \times (K + L - 1)$ Toeplitz matrix

$$\mathbf{G}_T = \begin{pmatrix} g_{L-1} & g_{L-2} & \cdots & g_0 & 0 & 0 & \cdots & 0 \\ 0 & g_{L-1} & \cdots & g_1 & g_0 & 0 & \cdots & 0 \\ \vdots & & & & & & & \vdots \\ 0 & & \cdots & & 0 & g_{L-1} & \cdots & g_0 \end{pmatrix} \quad (2.19)$$

and $\mathbf{n} = [n_0, n_1, \dots, n_{K-1}]^T$ is the $K \times 1$ AWGN vector. The matrix \mathbf{G}_T is nothing more than a matricial way to express the linear convolution with the discrete channel impulse response

$$\mathbf{g} = [g_0, g_1, \dots, g_{L-1}]^T. \quad (2.20)$$

More precisely, the rows of \mathbf{G}_T are delayed and time-reversed versions of \mathbf{g} . Taking into account the structure of $\tilde{\mathbf{s}}$ in (2.16) (i.e. the fact that the first $L - 1$ elements are equal to the last $L - 1$ ones), the last equation can be rewritten in terms of \mathbf{s}

$$\mathbf{y} = \mathbf{G}_c \mathbf{s} + \mathbf{n} \quad (2.21)$$

where \mathbf{G}_c is a $K \times K$ circulant matrix whose first column is given by the channel impulse response \mathbf{g} appended by $K - L$ zeros

$$\mathbf{G}_c = \begin{pmatrix} g_0 & 0 & \cdots & 0 & 0 & g_{L-1} & \cdots & g_1 \\ g_1 & g_0 & 0 & \cdots & 0 & 0 & \ddots & \vdots \\ \vdots & g_1 & g_0 & 0 & 0 & \ddots & 0 & g_{L-1} \\ g_{L-1} & \vdots & g_1 & \ddots & 0 & \ddots & 0 & 0 \\ 0 & g_{L-1} & \vdots & \ddots & g_0 & \ddots & \ddots & 0 \\ \vdots & 0 & g_{L-1} & \ddots & g_1 & g_0 & 0 & 0 \\ \vdots & \vdots & 0 & \ddots & \vdots & \ddots & \ddots & 0 \\ 0 & 0 & \cdots & 0 & g_{L-1} & \cdots & g_1 & g_0 \end{pmatrix}. \quad (2.22)$$

In other words, the CP converts the linear convolution into a cyclic one. And the reason for choosing the particular structure of the CP as guard interval is that we end up with a circulant matrix in the signal model (2.21), and that

circulant matrices have convenient properties. Let us introduce the K -point fast Fourier transform (FFT) of the channel impulse response

$$\boldsymbol{\omega} = [\omega_0, \omega_1, \dots, \omega_{K-1}]^T \quad (2.23)$$

$$\omega_k = \sum_{l=0}^{L-1} g_l e^{-j2\pi \frac{kl}{K}}. \quad (2.24)$$

It is well-known that a circulant matrix can be decomposed as [39]

$$\mathbf{G}_c = \mathbf{W}^H \boldsymbol{\Omega} \mathbf{W} \quad (2.25)$$

where $\boldsymbol{\Omega}$ is a diagonal matrix with the frequency channel response $\boldsymbol{\omega}$ on its diagonal

$$\boldsymbol{\Omega} = \text{diag}(\boldsymbol{\omega}), \quad (2.26)$$

and \mathbf{W} (resp. \mathbf{W}^H) is the $K \times K$ FFT (resp. IFFT) unitary matrix, defined by

$$[\mathbf{W}]_{k,k'} = \frac{1}{\sqrt{K}} e^{-j2\pi \frac{kk'}{K}}. \quad (2.27)$$

In other words, the channel matrix \mathbf{G}_c in the signal model (2.21) has always the same eigenvectors, independently of the realization of \mathbf{g} . This is precisely the convenient property we were referring to.

The cyclic prefixed block transmission is summarized in the block diagram in part (a) of Fig. 2.3. It basically consists of adding a CP at the transmitter side, and discarding it at the receiver side. The resulting signal model (2.21) will be used extensively in this thesis. Together with (2.25), it results in the equivalent scheme in part (b) of Fig. 2.3. Remember that this model assumes that the channel remains constant over the duration of a block, and that the CP is greater or equal to the channel impulse response's maximum delay. It is also worth noting a first trade-off in the choice of the block size K : it simultaneously has to be sufficiently large to reduce the efficiency loss induced by the CP, and sufficiently small for the channel to remain constant over its duration.

2.4 From multi-carrier to single-carrier

Based on the material presented in the previous sections of this chapter, let us go one step further and consider the block diagram depicted in Fig. 2.4.

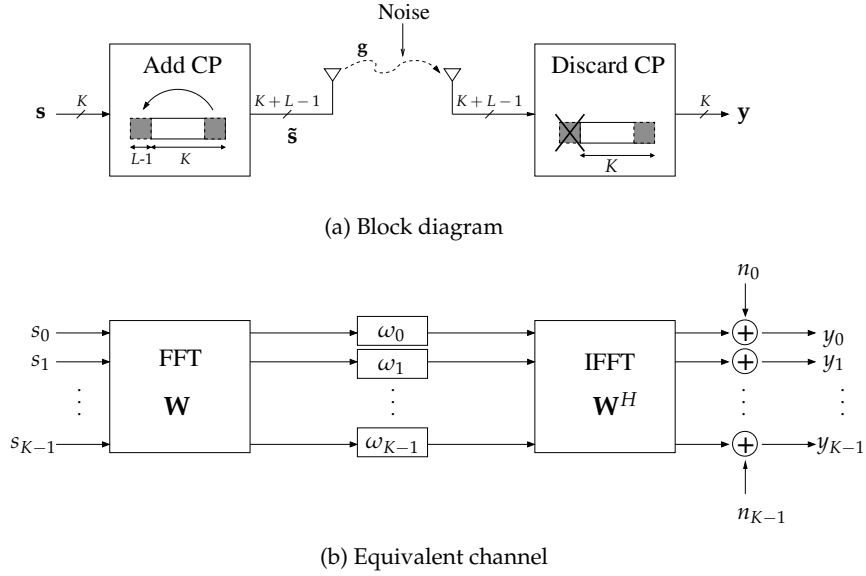


Figure 2.3 Cyclic prefixed block transmission.

This scheme assumes that the vector \mathbf{s} is a linearly precoded version of the $K \times 1$ data symbol vector \mathbf{d}

$$\mathbf{s} = \mathbf{P} \mathbf{d} \quad (2.28)$$

$$\mathbf{d} = [d_0, d_1, \dots, d_{K-1}]^T. \quad (2.29)$$

Throughout this thesis, the data symbols d_k will always be taken from a constellation (BPSK, QPSK, 16-QAM, or 64-QAM) that has unit energy, that is $E[d_k d_k^*] = 1$. The matrix \mathbf{P} is the precoding matrix, which should not alter the total transmit power, i.e. $\text{trace}(\mathbf{P}^H \mathbf{P}) = K$. The detection operation was also included in Fig. 2.4. By detection, we mean the operation which generates the detected data vector $\hat{\mathbf{d}}$ from the received vector \mathbf{y} . This operation may be partly/totally made of linear processing, or not.

In the following, we will see that special choices of the precoding matrix \mathbf{P} lead to multi-carrier or single-carrier systems.

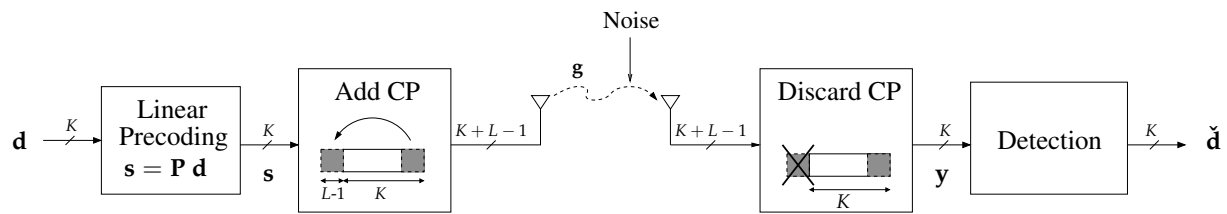


Figure 2.4 Linearly precoded cyclic prefixed block transmission: block diagram.

2.4.1 Orthogonal frequency division multiplexing

In section 2.3, we stressed that the good thing about adding a CP is that we end up with a channel matrix \mathbf{G}_c whose eigenvectors are the columns of the FFT matrix, independently of the channel realization. From that, it is natural to consider the case where the precoding matrix is equal to the conjugate transpose of the matrix of right-eigenvectors of \mathbf{G}_c in (2.25), i.e.

$$\mathbf{P} = \mathbf{W}^H \quad (2.30)$$

$$\mathbf{s} = \mathbf{W}^H \mathbf{d}. \quad (2.31)$$

In other words, an IFFT is taken on the data symbols \mathbf{d} before transmitting them. In this particular case, the received signal (2.21) becomes

$$\mathbf{y} = \mathbf{G}_c \mathbf{s} + \mathbf{n} \quad (2.32)$$

$$= \mathbf{W}^H \mathbf{\Omega} \mathbf{W} \mathbf{W}^H \mathbf{d} + \mathbf{n} \quad (2.33)$$

$$= \mathbf{W}^H \mathbf{\Omega} \mathbf{d} + \mathbf{n} \quad (2.34)$$

where (2.25), (2.31), and the unitary property of the FFT matrix have been used. Let us look right away at the ML detection of the data symbol vector \mathbf{d} using the received signal (2.34)

$$\check{\mathbf{d}}_{\text{ML}} = \underset{\mathbf{d}}{\operatorname{argmin}} \|\mathbf{y} - \mathbf{W}^H \mathbf{\Omega} \mathbf{d}\|^2 \quad (2.35)$$

$$= \underset{\mathbf{d}}{\operatorname{argmin}} (\mathbf{\Omega}^{-1} \mathbf{W} \mathbf{y} - \mathbf{d})^H \mathbf{\Omega}^H \mathbf{\Omega} (\mathbf{\Omega}^{-1} \mathbf{W} \mathbf{y} - \mathbf{d}). \quad (2.36)$$

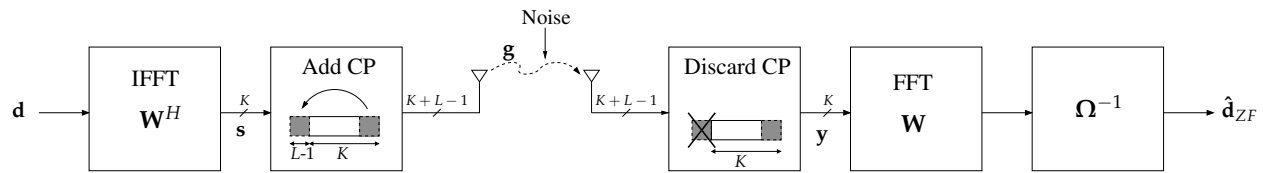
Since the matrix $\mathbf{\Omega}^H \mathbf{\Omega}$ is diagonal with positive entries on its diagonal, the equation (2.36) suggests that the ML detection is strictly equivalent to taking symbol-by-symbol decisions on the linear zero-forcing (ZF) estimate

$$\hat{\mathbf{d}}_{\text{ZF}} = \mathbf{\Omega}^{-1} \mathbf{W} \mathbf{y}. \quad (2.37)$$

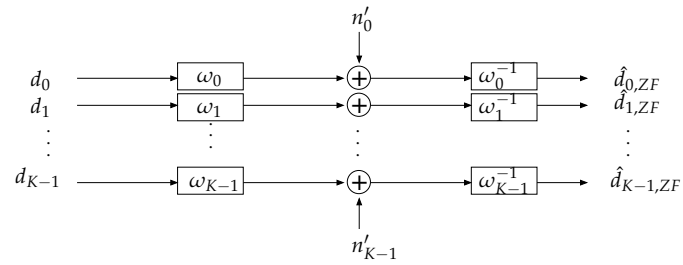
In that sense, the ZF linear receiver is optimal for the particular scenario considered in this subsection. Let us thus consider the linear ZF receiver which, from (2.37), is nothing more than taking an FFT on the received signal followed by K scalar multiplications (since $\mathbf{\Omega}^{-1}$ is a diagonal matrix), as depicted in part (a) of Fig. 2.5. Inserting (2.34) into (2.37), we get

$$\hat{\mathbf{d}}_{\text{ZF}} = \mathbf{d} + \mathbf{\Omega}^{-1} \mathbf{W} \mathbf{n} \quad (2.38)$$

$$= \mathbf{d} + \mathbf{\Omega}^{-1} \mathbf{n}' \quad (2.39)$$



(a) Block diagram



(b) Equivalent scheme

Figure 2.5 OFDM system.

where $\mathbf{n}' \triangleq \mathbf{W} \mathbf{n}$ is the equivalent noise which has the same statistical properties as \mathbf{n} . On the basis of (2.39), the equivalent scheme drawn in part (b) of Fig. 2.5 can be established. We see that the transmission scheme considered in this subsection actually consists of multiplexing the K data symbols on K independent fading AWGN channels. The K fading gains are given by the K elements of the frequency channel response ω (2.23)-(2.24). This scheme is known as orthogonal frequency division multiplexing (OFDM): it divides the spectrum into narrowband orthogonal subcarriers, each symbol being transmitted on a single subcarrier. The OFDM modulation is thus basically a multi-carrier (MC) modulation, and has become very popular thanks to its low complexity [6]. In fact, as shown in part (a) of Fig. 2.5, it only requires one IFFT operation at the transmitter side, and one FFT at the receiver side followed by K symbol-by-symbol scalar multiplications. Remember that (I)FFT operations can be implemented with low complexity, especially if the block length K is chosen to be a power of two.

Thanks to its capability to deal with frequency selective channels with low complexity, it is not surprising to find the OFDM modulation in most standards for wireless communications [40, 41]. Further analysis of the performance of the OFDM modulation will be presented in the next chapters of this thesis. However, we can already formulate two drawbacks of this technique:

1. Let us concentrate for a minute on the variability in the power of a transmitted sample s_k . In particular, let us look at the following ratio

$$\text{PAPR} = \frac{\max(|s_k|^2)}{\mathbb{E}[|s_k|^2]} \quad (2.40)$$

which is referred as the peak to average power ratio (PAPR). The PAPR is comparing the maximum value that the power of a s_k can take, with its mean value. Using (2.31), we rewrite $s_k = \frac{1}{\sqrt{K}} \sum_{i=0}^{K-1} d_i e^{j2\pi \frac{k}{K} i}$. On the one hand, it is obvious that the magnitude of a s_k is maximum if all d_i align in phase after rotation. For instance, this happens for s_0 if $d_0 = \dots = d_{K-1} = d$. In such case, $|s_0|^2 = K|d|^2$. With the hypothesis of constellations with unit energy, we can assume³ that $\max(|d|^2) \cong 1$,

³For constellations with unit energy, the maximum squared norm of a point of the constellation is greater or equal to one, $\max(|d|^2) \geq 1$. To be more specific, it is equal to one for BPSK and QPSK constellations, and equal to 1.34 and 1.53 for 16-QAM and 64-QAM constellations, respectively.

such that

$$\max(|s_k|^2) \cong K. \quad (2.41)$$

On the other hand, the denominator in (2.40) is calculated as

$$E[|s_k|^2] = E \left[\frac{1}{\sqrt{K}} \sum_{i=0}^{K-1} d_i e^{j2\pi \frac{k i}{K}} \frac{1}{\sqrt{K}} \sum_{i'=0}^{K-1} d_{i'}^* e^{-j2\pi \frac{k i'}{K}} \right] \quad (2.42)$$

$$= \frac{1}{K} \sum_{i=0}^{K-1} \sum_{i'=0}^{K-1} E[d_i d_{i'}^*] e^{j2\pi \frac{k(i-i')}{K}} \quad (2.43)$$

$$= 1 \quad (2.44)$$

such that the PAPR for an OFDM system is approximately equal to the block size

$$\text{PAPR}^{\text{OFDM}} \cong K. \quad (2.45)$$

This is a rather bad news since a high PAPR means a potential performance loss: in fact, a significant distortion can affect the OFDM signal whose power fluctuations may fall into the nonlinear characteristic of the power amplifiers typically used in radio transmitters. This imperfection is often referred to as the OFDM's PAPR problem. Note the additional trade-off (besides the one mentioned at the end of Section 2.3) in the choice of the block size K : increasing K reduces the efficiency loss due to the CP, but also increases the PAPR. Note also that different techniques have been proposed to solve the OFDM's PAPR problem [42–48], but this particular topic is beyond the scope of this thesis.

2. Looking at the estimate (2.39), we see that if the channel is in deep fade on one subcarrier, the symbol transmitted on that subcarrier will be affected by a noise with potentially infinite variance. For reliable transmission, some preprocessing should thus be added to the pure OFDM system of Fig. 2.5. The channel coding stage (error correction code + interleaver) can do the job, at least partially. Another solution is the addition of extra linear precoding so that each symbol is spread over all subcarriers. This last possibility leads to the next subsection.

2.4.2 Cyclic prefixed single-carrier

Let us consider the possibility of introducing an additional precoding stage to the OFDM system right before the IFFT operation in part (a) of Fig. 2.5.

Based on the suggestion just made when mentioning the second drawback of OFDM, this precoding stage can be designed such that each symbol is spread over all K subcarriers or frequencies. Such precoder can be implemented by an FFT operation, for instance. In this case, this FFT operation actually cancels out with the IFFT operation in part (a) of Fig. 2.5, leading to a matrix \mathbf{P} in Fig 2.4 equal to the $K \times K$ identity matrix \mathbf{I}_K

$$\mathbf{P} = \mathbf{I}_K \quad (2.46)$$

such that

$$\mathbf{s} = \mathbf{d}. \quad (2.47)$$

In other words, the data symbols are sent unaltered in a single-carrier fashion. The difference with respect to classical single-carrier systems is the addition of the CP to each block. Consequently, this transmission scheme is known as cyclic prefixed single-carrier (CPSC).

Since the data symbols are transmitted unaltered (2.47), the PAPR as defined in (2.40) is just the one associated with the constellation used and is approximately equal to one⁴

$$\text{PAPR}^{\text{CPSC}} \cong 1, \quad (2.48)$$

and

$$\text{PAPR}^{\text{CPSC}} = \frac{\text{PAPR}^{\text{OFDM}}}{K}. \quad (2.49)$$

That is, CPSC is solving the OFDM's PAPR problem. This is one of the reasons why CPSC was introduced in the literature [9,11] and has gained in popularity for practical implementations [49].

Using (2.25) and (2.47), the received signal (2.21) becomes

$$\mathbf{y} = \mathbf{G}_c \mathbf{d} + \mathbf{n} \quad (2.50)$$

$$= \mathbf{W}^H \mathbf{\Omega} \mathbf{W} \mathbf{d} + \mathbf{n}. \quad (2.51)$$

Unlike for OFDM, the type of receiver used will have an influence on the performance of a CPSC system. In the following subsections, let us describe four possible receivers for detecting \mathbf{d} from \mathbf{y} in (2.51).

⁴More precisely, the PAPR is equal to one for BPSK and QPSK transmission. For 16-QAM and 64-QAM, however, the PAPR is equal to 1.34 and 1.53, respectively.

2.4.2.1 ML-CPSC

The ML detection of \mathbf{d} using the received signal (2.51) is given by

$$\check{\mathbf{d}}_{\text{ML}} = \underset{\mathbf{d}}{\operatorname{argmin}} \|\mathbf{y} - \mathbf{W}^H \boldsymbol{\Omega} \mathbf{W} \mathbf{d}\|^2 \quad (2.52)$$

$$= \underset{\mathbf{d}}{\operatorname{argmin}} (\mathbf{W} \mathbf{y} - \boldsymbol{\Omega} \mathbf{W} \mathbf{d})^H (\mathbf{W} \mathbf{y} - \boldsymbol{\Omega} \mathbf{W} \mathbf{d}). \quad (2.53)$$

It can be seen that, this time, the ML detection does not come down to a symbol-by-symbol detection, but has to be carried out on a block basis. In other words, unlike for OFDM, some performance loss is expected in CPSC systems if a linear receiver followed by symbol-by-symbol decisions is used. However, (2.53) suggests that, in any case, an FFT is a good linear operation to carry out first on the received signal \mathbf{y} .

2.4.2.2 ZF-CPSC

Given the received signal (2.51), the ZF linear receiver is given by $\mathbf{W}^H \boldsymbol{\Omega}^{-1} \mathbf{W}$. The ZF-CPSC scheme is depicted in part (a) of Fig 2.6, where the diagonal matrix $\mathbf{E} = \boldsymbol{\Omega}^{-1}$. When compared with the OFDM scheme in part (a) of Fig. 2.5, we see that ZF-CPSC differs by where the IFFT operation takes place: by moving the IFFT operation from the transmitter side to the receiver side, we switch from OFDM to ZF-CPSC. The ZF estimate is then calculated as

$$\hat{\mathbf{d}}_{\text{ZF}} = \mathbf{W}^H \boldsymbol{\Omega}^{-1} \mathbf{W} \mathbf{y} \quad (2.54)$$

$$= \mathbf{d} + \mathbf{W}^H \boldsymbol{\Omega}^{-1} \mathbf{W} \mathbf{n}. \quad (2.55)$$

Note that ZF-CPSC allows to deal with frequency selective channels with the same global complexity as that of OFDM: one FFT, K scalar multiplications, and one IFFT are needed. The only difference is that the complexity related to the IFFT operation is moved to the receiver side. This might be convenient in an uplink scenario for instance, where the complexity might be less of an issue at the base station than at each terminal.

2.4.2.3 MMSE-CPSC

The minimum mean square error (MMSE) linear receiver associated with the received signal (2.51) can also be easily calculated, and is given by

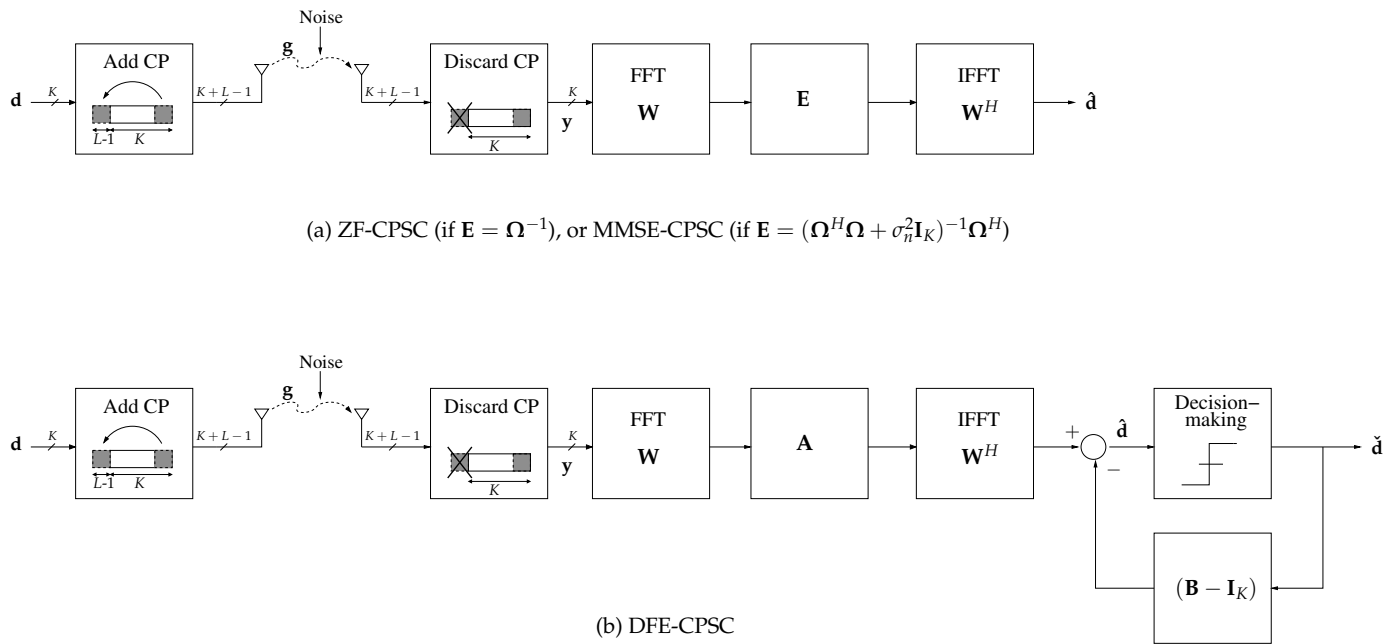


Figure 2.6 CPSC: block diagrams

$\mathbf{W}^H(\mathbf{\Omega}^H\mathbf{\Omega} + \sigma_n^2\mathbf{I}_K)^{-1}\mathbf{\Omega}^H\mathbf{W}$. The MMSE-CPSC scheme is thus also the one in part (a) of Fig 2.6, where $\mathbf{E} = (\mathbf{\Omega}^H\mathbf{\Omega} + \sigma_n^2\mathbf{I}_K)^{-1}\mathbf{\Omega}^H$ this time. In other words, the MMSE equalization is basically not different from the ZF equalization: in both cases the equalization is implemented by scalar multiplications in the frequency domain. The only difference between MMSE and ZF is the values of the scalar multiplications (the value of the diagonal matrix \mathbf{E}). The MMSE estimate is then calculated as

$$\hat{\mathbf{d}}_{\text{MMSE}} = \mathbf{W}^H(\mathbf{\Omega}^H\mathbf{\Omega} + \sigma_n^2\mathbf{I}_K)^{-1}\mathbf{\Omega}^H\mathbf{W} \mathbf{y} \quad (2.56)$$

$$\begin{aligned} &= \mathbf{d} - \sigma_n^2\mathbf{W}^H(\mathbf{\Omega}^H\mathbf{\Omega} + \sigma_n^2\mathbf{I}_K)^{-1}\mathbf{W} \mathbf{d} \\ &\quad + \mathbf{W}^H(\mathbf{\Omega}^H\mathbf{\Omega} + \sigma_n^2\mathbf{I}_K)^{-1}\mathbf{\Omega}^H\mathbf{W} \mathbf{n}. \end{aligned} \quad (2.57)$$

This time, the symbol-by-symbol detection on the MMSE estimate (2.57), will be both perturbed by noise (last term in (2.57)) and intersymbol interference (ISI) (second term in (2.57)). This is a well-known behaviour of an MMSE receiver: it does not entirely cancel the ISI in order to further minimize the mean square error (MSE).

2.4.2.4 DFE-CPSC

The linear MMSE receiver described in the previous subsection was shown to not completely remove the ISI. Therefore, the addition of a feedback component to the detection step might induce a further performance improvement, at the expense of some extra complexity [50]. A decision feedback equalizer (DFE) is thus considered. It is depicted in part (b) of Fig 2.6. The matrices \mathbf{A} and $(\mathbf{B} - \mathbf{I}_K)$ implement the forward and feedback parts of the DFE, respectively. Note that the forward part is held in the frequency domain, while the feedback takes place in the time domain. For causality reasons, the matrix \mathbf{B} must be a unit lower triangular matrix, i.e. a lower triangular matrix with ones on its diagonal.

The matricial formalism has to be well understood. Once the vector \mathbf{y} has been entirely received, the forward filter (in the frequency domain) computes $\mathbf{W}^H\mathbf{A} \mathbf{W} \mathbf{y}$ once for all. However, the decision-making has to be understood sequentially. the decision on the first symbol \check{d}_0 is made using the first entry of $\mathbf{W}^H\mathbf{A} \mathbf{W} \mathbf{y}$. The decision on the second symbol \check{d}_1 is then made using the

second entry of $\mathbf{W}^H \mathbf{A} \mathbf{W} \mathbf{y}$ corrected by $[\mathbf{B}]_{1,0} \check{d}_0$, and so on⁵. From that, we understand why the matrix \mathbf{B} has to be unit lower triangular: the correction on a given symbol estimate can only be constructed from decisions on preceding symbols.

The matrices \mathbf{A} and \mathbf{B} can be designed in order to minimize the MSE, see Appendix 2.A for details. The result is

$$\mathbf{A} = \mathbf{W} \mathbf{B} \mathbf{W}^H (\mathbf{\Omega}^H \mathbf{\Omega} + \sigma_n^2 \mathbf{I}_K)^{-1} \mathbf{\Omega}^H \quad (2.58)$$

$$\mathbf{B} = \mathbf{L}^{-1}. \quad (2.59)$$

The matrix \mathbf{L} is defined by the following Cholesky decomposition

$$\mathbf{W}^H (\mathbf{\Omega}^H \mathbf{\Omega} + \sigma_n^2 \mathbf{I}_K)^{-1} \mathbf{W} = \mathbf{L} \mathbf{D} \mathbf{L}^H \quad (2.60)$$

where \mathbf{L} is a unit lower triangular matrix, and \mathbf{D} is a positive diagonal matrix. Note that if we set $\mathbf{B} = \mathbf{I}_K$, the feedback part is removed and the expression (2.58) reduces to the linear MMSE receiver of previous subsection, which is consistent. With the filters (2.58) and (2.59), and neglecting the error propagation effect in the feedback part, it is shown in Appendix 2.A that the resulting error covariance matrix is diagonal and precisely equal to $\sigma_n^2 \mathbf{D}$. Note that since the matrix (2.60) is a circulant, it turns out that the diagonal entries of \mathbf{D} are with decreasing values. The fact that the error variance associated with a given symbol decreases as its position in the block increases, is a direct consequence of how the feedback part of the DFE is working. For instance, the last symbol of the block has the lowest error variance, since the interference from all other $K - 1$ symbols of the block can ideally be removed before it is detected.

Comment: the reader might be surprised that we referred to (2.60) as a Cholesky decomposition. In fact, the "true" Cholesky decomposition of a positive definite Hermitian matrix \mathbf{H} is

$$\mathbf{H} = \mathbf{T} \mathbf{T}^H, \quad (2.61)$$

⁵In this thesis, the following convention is used: the first element of a vector is at index 0. Similarly, the top left entry of a matrix is at indices $\{0,0\}$. For example, $[\mathbf{B}]_{1,0}$ denotes the second row and first column entry of matrix \mathbf{B} .

where \mathbf{T} is a lower triangular matrix with diagonal entries not necessarily equal to one. Obviously, the decomposition in (2.60) of the type

$$\mathbf{H} = \mathbf{LDL}^H \quad (2.62)$$

with \mathbf{L} a unit lower triangular matrix, and \mathbf{D} a positive diagonal matrix, is related to (2.61) by $\mathbf{T} = \mathbf{LD}^{1/2}$. In this thesis, and in particular in the context of DFE equalizers, we will exclusively use the decomposition (2.62). For this reason and for conciseness, we will abusively refer to (2.62) as a Cholesky decomposition. Note, however, that (2.62) is sometimes simply referred as a "LDL^T decomposition" [51].

2.5 Multi-antenna dimension

Nowadays, we do not need to convince the reader anymore that multiple input multiple output (MIMO) channels, using multiple antennas both at the transmitter and receiver sides, allow a performance enhancement in wireless communication systems. In short, MIMO enables to increase the reliability of the transmission (by transmitting multiple versions of the same signal), or to increase the rate at which the information is sent (by multiplexing independent data over the transmit antennas) [52, 53]. Actually, it was recently shown in [54] that there is a theoretical trade-off between these two opposite strategies, referred to as diversity-multiplexing trade-off. In any case, some additional signal processing at the transmitter/receiver side is the price to pay to take advantage of MIMO channels.

In this section, the focus is set on MIMO cyclic prefixed block transmission, i.e. the addition of a spatial dimension to the single input single output (SISO) systems which have been presented in Sections 2.3 and 2.4. In particular, by adding multiple transmit and receive antennas to part (a) of Fig. 2.3, we end up with the scheme depicted in Fig. 2.7. The number of transmit and receive antennas are respectively denoted by M_t and M_r . Note that the addition (resp. suppression) of the CP is implemented separately at each transmit (resp. receive) antenna. Some extra notations are needed to cope with the spatial dimension, let us introduce them:

- \mathbf{s}_t : the $K \times 1$ symbol block transmitted on antenna t .

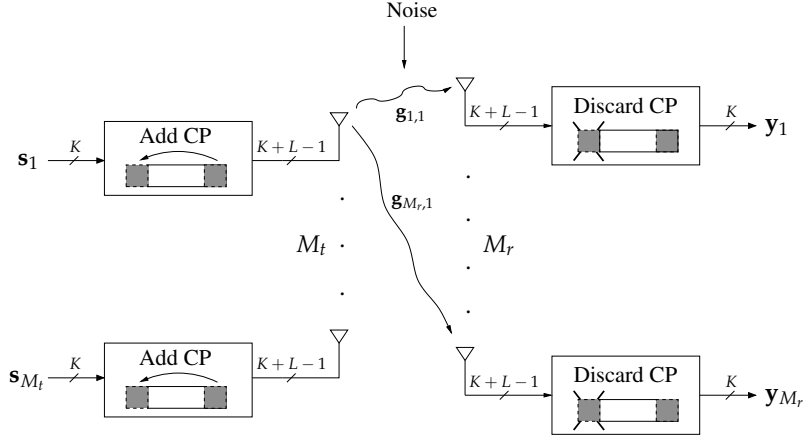


Figure 2.7 MIMO cyclic prefixed block transmission: block diagram.

- \mathbf{y}_r : the $K \times 1$ received block on antenna r (after discarding the CP).
- $\mathbf{g}_{r,t}$: the $L \times 1$ channel impulse response between transmit antenna t and receive antenna r .

with $t = 1, \dots, M_t$ and $r = 1, \dots, M_r$. In this section, L should be understood as the number of taps of the longest channel impulse response of the MIMO frequency selective channel⁶. The M_t (resp. M_r) transmitted (resp. received) blocks can be stacked into a larger $M_t K \times 1$ (resp. $M_r K \times 1$) vector $\mathbf{s} = [\mathbf{s}_1^T, \dots, \mathbf{s}_{M_t}^T]^T$ (resp. $\mathbf{y} = [\mathbf{y}_1^T, \dots, \mathbf{y}_{M_r}^T]^T$). The global received signal model is then

$$\mathbf{y} = \begin{bmatrix} \mathbf{G}_{c_{1,1}} & \cdots & \mathbf{G}_{c_{1,M_t}} \\ \vdots & \ddots & \vdots \\ \mathbf{G}_{c_{M_r,1}} & \cdots & \mathbf{G}_{c_{M_r,M_t}} \end{bmatrix} \mathbf{s} + \mathbf{n} \quad (2.63)$$

where $\mathbf{G}_{c_{r,t}}$ is a $K \times K$ circulant matrix whose first column is given by $\mathbf{g}_{r,t}$ appended by $K - L$ zeros as in (2.22), and \mathbf{n} is the stacked noise vector $\mathbf{n} = [\mathbf{n}_1^T, \dots, \mathbf{n}_{M_r}^T]^T$. The model (2.63) is nothing more than the extension of (2.21): it expresses the signal at each receive antenna as the sum of the

⁶The MIMO frequency selective channel is fully characterized by $M_t M_r$ channel impulse responses.

contributions of all transmit antennas. Remembering the property (2.25), i.e. $\mathbf{G}_{c_r,t} = \mathbf{W}^H \boldsymbol{\Omega}_{r,t} \mathbf{W}$, we rewrite

$$\begin{aligned} \mathbf{y} &= \begin{bmatrix} \mathbf{W}^H & & \\ & \ddots & \\ & & \mathbf{W}^H \end{bmatrix} \begin{bmatrix} \boldsymbol{\Omega}_{1,1} & \dots & \boldsymbol{\Omega}_{1,M_t} \\ \vdots & \ddots & \vdots \\ \boldsymbol{\Omega}_{M_r,1} & \dots & \boldsymbol{\Omega}_{M_r,M_t} \end{bmatrix} \begin{bmatrix} \mathbf{W} & & \\ & \ddots & \\ & & \mathbf{W} \end{bmatrix} \mathbf{s} + \mathbf{n} \\ &\triangleq \boldsymbol{\mathcal{W}}_{M_r}^H \boldsymbol{\Omega}_b \boldsymbol{\mathcal{W}}_{M_t} \mathbf{s} + \mathbf{n} \end{aligned} \quad (2.64)$$

where $\boldsymbol{\Omega}_b$ is composed of $M_t M_r$ diagonal submatrices of size $K \times K$, and $\boldsymbol{\mathcal{W}}_{M_t}$ (resp. $\boldsymbol{\mathcal{W}}_{M_r}^H$) is a block diagonal matrix with M_t (resp. M_r) times the $K \times K$ FFT matrix \mathbf{W} (resp. IFFT \mathbf{W}^H) on its diagonal.

In a very similar way as in Section 2.4, the scheme in Fig. 2.7 will reduce to a multi or single-carrier system, depending on the linear signal processing operation at the transmitter side. Let us thus consider that the vector \mathbf{s} is a precoded version of a $M_t K \times 1$ data symbol vector \mathbf{d}

$$\mathbf{s} = \mathbf{P} \mathbf{d} \quad (2.65)$$

$$\mathbf{d} = [\mathbf{d}_1^T, \dots, \mathbf{d}_{M_t}^T]^T \quad (2.66)$$

where \mathbf{d}_t is the $K \times 1$ data symbol block associated with transmit antenna t . Special choices of the $M_t K \times M_t K$ precoding matrix \mathbf{P} are being described in the next two subsections.

2.5.1 MIMO OFDM

A first natural choice for the precoding matrix is $\mathbf{P} = \boldsymbol{\mathcal{W}}_{M_t}^H$, which means that a size- K IFFT is implemented at each transmit antenna leading to a multi-carrier system. Symmetrically, at the receiver side, a size- K FFT operation is executed at each receive antenna. At this point, the signal is given by

$$\mathbf{y}' = \boldsymbol{\mathcal{W}}_{M_r} \mathbf{y} \quad (2.67)$$

$$= \boldsymbol{\Omega}_b \boldsymbol{\mathcal{W}}_{M_t} \mathbf{s} + \boldsymbol{\mathcal{W}}_{M_r} \mathbf{n} \quad (2.68)$$

$$= \boldsymbol{\Omega}_b \mathbf{d} + \mathbf{n}'. \quad (2.69)$$

Remembering the structure of $\boldsymbol{\Omega}_b$, we see that \mathbf{y}' is still affected by ISI: the symbols transmitted on the same given subcarrier but on different antennas

are interfering with each other. Put differently, thanks to the (I)FFT operations we got rid of the temporal ISI, but we still have to deal with the spatial ISI. Restricting ourself to linear signal processing, let us consider two different approaches for reducing/canceling this spatial ISI.

2.5.1.1 MIMO MMSE-OFDM

Assuming first that the channel is known at the receiver side but not at the transmitter side, a MMSE linear receiver can be carried out on the signal (2.69). This MMSE linear receiver is given by $(\mathbf{\Omega}_b^H \mathbf{\Omega}_b + \sigma_n^2 \mathbf{I}_{M_t K})^{-1} \mathbf{\Omega}_b^H$. The complete system is depicted in Fig. 2.8, where $\mathbf{E} = (\mathbf{\Omega}_b^H \mathbf{\Omega}_b + \sigma_n^2 \mathbf{I}_{M_t K})^{-1} \mathbf{\Omega}_b^H$. The corresponding MMSE estimate is

$$\hat{\mathbf{d}}_{\text{MMSE}} = (\mathbf{\Omega}_b^H \mathbf{\Omega}_b + \sigma_n^2 \mathbf{I}_{M_t K})^{-1} \mathbf{\Omega}_b^H \mathbf{y}' \quad (2.70)$$

$$\begin{aligned} &= \mathbf{d} - \sigma_n^2 (\mathbf{\Omega}_b^H \mathbf{\Omega}_b + \sigma_n^2 \mathbf{I}_{M_t K})^{-1} \mathbf{d} \\ &\quad + (\mathbf{\Omega}_b^H \mathbf{\Omega}_b + \sigma_n^2 \mathbf{I}_{M_t K})^{-1} \mathbf{\Omega}_b^H \mathbf{n}' \end{aligned} \quad (2.71)$$

which is affected by noise and remaining ISI, as expected.

2.5.1.2 Discrete matrix multitone (DMMT)

Assume now that the channel is known at both the transmitter and receiver sides. In this case, channel adaptive linear precoding can be used to remove the spatial ISI. For notation/derivation simplicity, let us assume in this subsection that $M_t = M_r = M$. Remembering the structure of the matrix $\mathbf{\Omega}_b$ in (2.64), there exists a permutation matrix $\mathbf{\Pi}$ such that $\mathbf{\Pi}^T \mathbf{\Omega}_b \mathbf{\Pi}$ is a block diagonal matrix. More precisely, $\mathbf{\Pi}^T \mathbf{\Omega}_b \mathbf{\Pi}$ has K blocks of size $M \times M$ on its diagonal. Each of these blocks is actually the MIMO channel on a given subcarrier, i.e. a MIMO flat fading channel. Then the following singular value decomposition (SVD)

$$\mathbf{\Pi}^T \mathbf{\Omega}_b \mathbf{\Pi} = \mathbf{U} \mathbf{\Lambda} \mathbf{V}^H \quad (2.72)$$

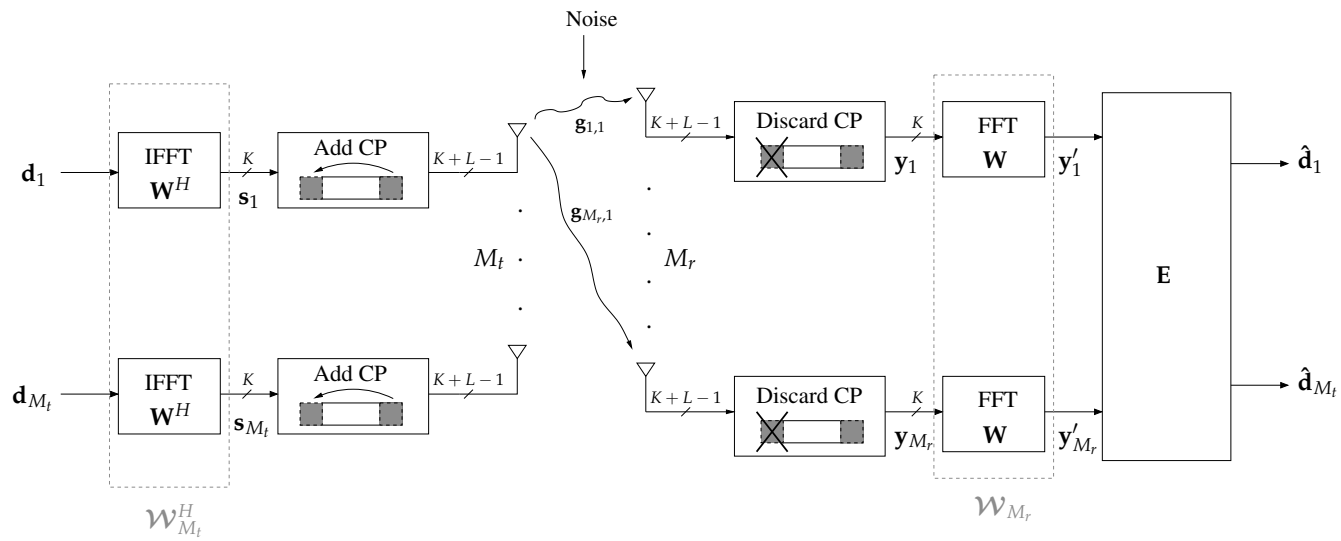


Figure 2.8 MIMO MMSE-OFDM: block diagram, with $\mathbf{E} = (\mathbf{\Omega}_b^H \mathbf{\Omega}_b + \sigma_n^2 \mathbf{I}_{M_r K})^{-1} \mathbf{\Omega}_b^H$.

is such that $\mathbf{\Lambda}$ is a $MK \times MK$ diagonal matrix, and \mathbf{U} and \mathbf{V} are also block diagonal matrices with K blocks of size $M \times M$

$$\mathbf{U} = \begin{bmatrix} \mathbf{U}^{(0)} & & \\ & \ddots & \\ & & \mathbf{U}^{(K-1)} \end{bmatrix} \quad (2.73)$$

$$\mathbf{V} = \begin{bmatrix} \mathbf{V}^{(0)} & & \\ & \ddots & \\ & & \mathbf{V}^{(K-1)} \end{bmatrix}. \quad (2.74)$$

Since $\mathbf{\Pi\Pi}^T = \mathbf{I}_{MK}$, we can rewrite (2.72) as

$$\mathbf{\Omega}_b = \mathbf{\Pi U \Lambda V}^H \mathbf{\Pi}^T. \quad (2.75)$$

From (2.69) and (2.75), we deduce that the channel can be diagonalized (i.e. the spatial ISI can be removed) if:

- At the transmitter side (before the IFFT operations at each antenna), the data symbol vector \mathbf{d} is pre-processed by the matrix $\mathbf{\Pi V}$. Put differently, the M symbols which are to be transmitted on the k th subcarrier (denoted by the $M \times 1$ vector $\mathbf{d}^{(k)}$), are first precoded by $\mathbf{V}^{(k)}$, and then spread over the M transmit antennas (effect of $\mathbf{\Pi}$).
- At the receiver side (after the FFT operations at each antenna), the received signal is post-processed by $\mathbf{U}^H \mathbf{\Pi}^T$. In other words, the M signals received on the k th subcarrier on the M receive antennas, are brought together (effect of $\mathbf{\Pi}^T$) and then affected by $\mathbf{U}^{(k)H}$.

This diagonalization technique of the MIMO multi-carrier channel was introduced in [55], and called "discrete matrix multitone" (DMMT). The output signal is given by $\mathbf{\Lambda d} + \mathbf{n}''$, where \mathbf{n}'' has the same statistical properties as \mathbf{n} (since all pre/post-processing matrices involved are unitary), and $\mathbf{d} = [\mathbf{d}^{(0)T}, \dots, \mathbf{d}^{(K-1)T}]^T$. The ZF linear receiver is optimal on such output signal, and the estimate is

$$\hat{\mathbf{d}}_{\text{ZF}} = \mathbf{d} + \mathbf{\Lambda}^{-1} \mathbf{n}'' \quad (2.76)$$

The complete DMMT scheme is given in Fig. 2.9. Remember that DMMT implies the channel to be perfectly known at the transmitter side.

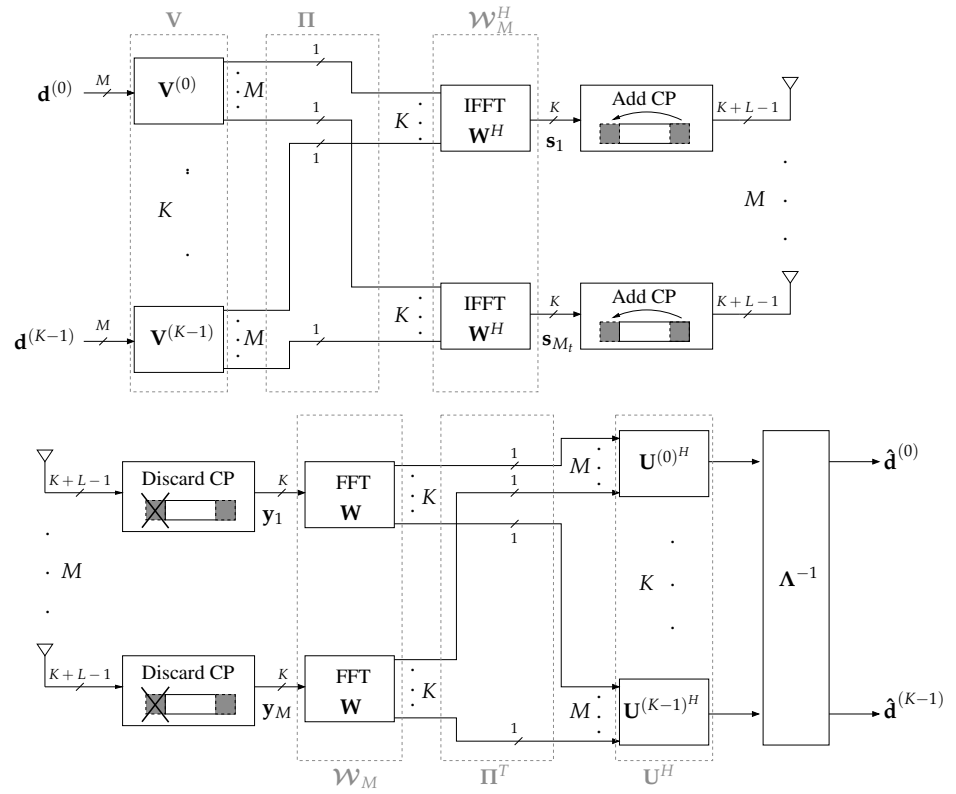


Figure 2.9 DMMT: block diagram.

2.5.2 MIMO DFE-CPSC

Another natural choice for the precoding matrix is $\mathbf{P} = \mathbf{I}_{M_t K}$, i.e. the case of no precoding actually. In this case, the received signal (2.64) becomes

$$\mathbf{y} = \mathcal{W}_{M_r}^H \Omega_b \mathcal{W}_{M_t} \mathbf{d} + \mathbf{n} \quad (2.77)$$

which is to be compared with the SISO signal model (2.51). Just like for (2.51) (see Subsection 2.4.2), different receivers (ML, linear ZF/MMSE, DFE) can be considered to implement the detection on the received signal (2.77). However, for conciseness, only the derivation of the DFE receiver will be presented here. The system is depicted in Fig. 2.10. The derivation of the DFE (minimizing the MSE) is very similar to that of the SISO case (see Subsection 2.4.2.4 and Appendix 2.A). After calculations, we get

$$\mathbf{A} = \mathcal{W}_{M_t} \mathbf{B} \mathbf{\Pi}^T \mathcal{W}_{M_t}^H (\Omega_b^H \Omega_b + \sigma_n^2 \mathbf{I}_{M_t K})^{-1} \Omega_b^H \quad (2.78)$$

$$\mathbf{B} = \mathbf{L}^{-1} \quad (2.79)$$

where the unit lower triangular matrix \mathbf{L} is given by the following Cholesky decomposition

$$\mathbf{\Pi}^T \mathcal{W}_{M_t}^H (\Omega_b^H \Omega_b + \sigma_n^2 \mathbf{I}_{M_t K})^{-1} \mathcal{W}_{M_t} \mathbf{\Pi} = \mathbf{L} \mathbf{D} \mathbf{L}^H \quad (2.80)$$

and the resulting error covariance matrix is diagonal and precisely given by $\sigma_n^2 \mathbf{D}$.

2.6 Conclusions

The goal of this chapter was to introduce the material that will be used in the rest of the thesis.

First, we reminded how the multipath wireless channel translates into a multi-tap system model. Second, the notion of cyclic prefixed block transmission was introduced as a efficient way to deal with wireless channels. It was then shown how a cyclic prefixed block transmission comes down to an OFDM or CPSC system, depending on the linear operation at the transmitter side. For both systems, different receivers were considered and derived, either nonlinear (ML, DFE) or linear (linear ZF, MMSE). Interestingly, for OFDM all

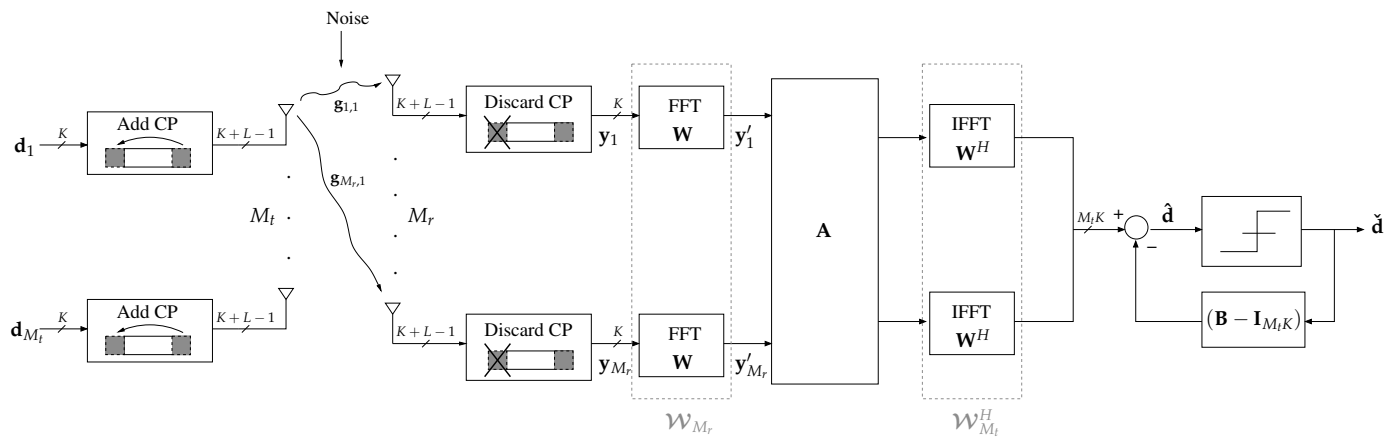


Figure 2.10 MIMO DFE-CPSC: block diagram.

these receivers coincide, unlike for CPSC. Finally, a multi-antenna scenario was explored for both OFDM and CPSC.

We also pointed out the two main advantages of CPSC with respect to OFDM: First, it does not suffer from the PAPR problem. Second, its complexity is mostly moved to the receiver side, which is convenient in an uplink scenario.

In the next chapters, further performance comparisons between OFDM and CPSC will be derived, and that in terms of different figures of merit or criteria.

Appendix 2.A Derivation of the MMSE DFE for CPSC

Based on the scheme reproduced in part (b) of Fig 2.6, this appendix is dedicated to deriving the expressions (2.58) and (2.59).

The data vector estimate $\hat{\mathbf{d}}$ in part (b) of Fig 2.6 is given by

$$\hat{\mathbf{d}} = \mathbf{W}^H \mathbf{A} \mathbf{W} \mathbf{y} - (\mathbf{B} - \mathbf{I}_K) \check{\mathbf{d}} \quad (2.81)$$

where $\check{\mathbf{d}}$ are the decisions made on the data symbols \mathbf{d} , and \mathbf{y} is the received vector (2.51). As we are looking for the expressions of \mathbf{A} and \mathbf{B} that minimize the MSE, we will apply the orthogonality principle which states that the error should be orthogonal to the received signal

$$\mathbb{E}[\boldsymbol{\epsilon} \mathbf{y}^H] = \mathbf{0} \quad (2.82)$$

where the error vector is defined as $\boldsymbol{\epsilon} \triangleq \hat{\mathbf{d}} - \mathbf{d}$. If perfect decision-making is assumed⁷, i.e. $\check{\mathbf{d}} = \mathbf{d}$, we have

$$\boldsymbol{\epsilon} = \mathbf{W}^H \mathbf{A} \mathbf{W} \mathbf{y} - \mathbf{B} \mathbf{d} \quad (2.83)$$

such that (2.82) gives

$$\mathbf{A} = \mathbf{W} \mathbf{B} \mathbb{E}[\mathbf{d} \mathbf{y}^H] \mathbb{E}[\mathbf{y} \mathbf{y}^H]^{-1} \mathbf{W}^H \quad (2.84)$$

$$= \mathbf{W} \mathbf{B} \mathbf{W}^H (\boldsymbol{\Omega}^H \boldsymbol{\Omega} + \sigma_n^2 \mathbf{I}_K)^{-1} \boldsymbol{\Omega}^H \quad (2.85)$$

⁷In other words, if the error propagation effect is neglected.

where the last equality follows from (2.51), and proofs (2.58). Inserting (2.85) and (2.51) into (2.83), we get

$$\begin{aligned}\boldsymbol{\epsilon} &= \mathbf{B} \mathbf{W}^H (\boldsymbol{\Omega}^H \boldsymbol{\Omega} + \sigma_n^2 \mathbf{I}_K)^{-1} \boldsymbol{\Omega}^H \boldsymbol{\Omega} \mathbf{W} \mathbf{d} \\ &+ \mathbf{B} \mathbf{W}^H (\boldsymbol{\Omega}^H \boldsymbol{\Omega} + \sigma_n^2 \mathbf{I}_K)^{-1} \boldsymbol{\Omega}^H \mathbf{W} \mathbf{n} \\ &- \mathbf{B} \mathbf{d}.\end{aligned}\quad (2.86)$$

Furthermore, since $(\boldsymbol{\Omega}^H \boldsymbol{\Omega} + \sigma_n^2 \mathbf{I}_K)^{-1} \boldsymbol{\Omega}^H \boldsymbol{\Omega} = (\mathbf{I}_K - (\boldsymbol{\Omega}^H \boldsymbol{\Omega} + \sigma_n^2 \mathbf{I}_K)^{-1} \sigma_n^2 \mathbf{I}_K)$, the last equation is rewritten as

$$\begin{aligned}\boldsymbol{\epsilon} &= -\sigma_n^2 \mathbf{B} \mathbf{W}^H (\boldsymbol{\Omega}^H \boldsymbol{\Omega} + \sigma_n^2 \mathbf{I}_K)^{-1} \mathbf{W} \mathbf{d} \\ &+ \mathbf{B} \mathbf{W}^H (\boldsymbol{\Omega}^H \boldsymbol{\Omega} + \sigma_n^2 \mathbf{I}_K)^{-1} \boldsymbol{\Omega}^H \mathbf{W} \mathbf{n}\end{aligned}\quad (2.87)$$

$$= \mathbf{B} \mathbf{W}^H (\boldsymbol{\Omega}^H \boldsymbol{\Omega} + \sigma_n^2 \mathbf{I}_K)^{-1} (\boldsymbol{\Omega}^H \mathbf{W} \mathbf{n} - \sigma_n^2 \mathbf{W} \mathbf{d}).\quad (2.88)$$

The error covariance matrix is then easily calculated as

$$\mathbf{R}_{\boldsymbol{\epsilon}\boldsymbol{\epsilon}} = \sigma_n^2 \mathbf{B} \mathbf{W}^H (\boldsymbol{\Omega}^H \boldsymbol{\Omega} + \sigma_n^2 \mathbf{I}_K)^{-1} \mathbf{W} \mathbf{B}^H.\quad (2.89)$$

Let us then remind the Cholesky decomposition in (2.60): $\mathbf{W}^H (\boldsymbol{\Omega}^H \boldsymbol{\Omega} + \sigma_n^2 \mathbf{I}_K)^{-1} \mathbf{W} = \mathbf{L} \mathbf{D} \mathbf{L}^H$, where \mathbf{L} is a unit lower triangular matrix, and \mathbf{D} is a positive diagonal matrix. We are interested in minimizing the total MSE on the block, i.e. the trace of the error covariance matrix. From (2.60) and (2.89), this trace is expressed as

$$\text{trace}(\mathbf{R}_{\boldsymbol{\epsilon}\boldsymbol{\epsilon}}) = \sigma_n^2 \text{trace}(\mathbf{B} \mathbf{L} \mathbf{D} \mathbf{L}^H \mathbf{B}^H)\quad (2.90)$$

$$= \sigma_n^2 \text{trace}(\tilde{\mathbf{B}} \mathbf{D} \tilde{\mathbf{B}}^H)\quad (2.91)$$

where $\tilde{\mathbf{B}} \triangleq \mathbf{B} \mathbf{L}$ is also a unit lower triangular matrix. By the cyclic property of the trace operator, we write

$$\text{trace}(\mathbf{R}_{\boldsymbol{\epsilon}\boldsymbol{\epsilon}}) = \sigma_n^2 \text{trace}(\tilde{\mathbf{B}} \mathbf{D} \tilde{\mathbf{B}}^H)\quad (2.92)$$

$$= \sigma_n^2 \text{trace}(\tilde{\mathbf{B}}^H \tilde{\mathbf{B}} \mathbf{D})\quad (2.93)$$

$$\geq \sigma_n^2 \text{trace}(\mathbf{D})\quad (2.94)$$

where the last inequality is justified by the fact that the diagonal elements of $\tilde{\mathbf{B}}^H \tilde{\mathbf{B}}$ are greater or equal to one. The equality in (2.94) is reached if $\tilde{\mathbf{B}} = \mathbf{I}_K$. Being interested in minimizing the trace of the error covariance matrix, we should thus impose $\tilde{\mathbf{B}} = \mathbf{I}_K$, or equivalently

$$\mathbf{B} = \mathbf{L}^{-1}\quad (2.95)$$

which demonstrates (2.59). The feedback filter (2.95) is such that the error covariance matrix is diagonal

$$\mathbf{R}_{\epsilon\epsilon} = \sigma_n^2 \mathbf{D}. \quad (2.96)$$

Let us close this appendix with the following remark. From the Hadamard's inequality [56], we have

$$\prod_{k=0}^{K-1} [\mathbf{R}_{\epsilon\epsilon}]_{k,k} \geq \det(\mathbf{R}_{\epsilon\epsilon}). \quad (2.97)$$

The equality in (2.97) is reached if and only if $\mathbf{R}_{\epsilon\epsilon}$ is diagonal. From that, it can be stated that the solution (2.95) both minimizes the trace and the product of the diagonal elements of the error covariance matrix. Put differently, both the geometrical and arithmetic means of the error variances are minimized.

Bit Error Rate and Diversity

3

The content of this chapter has been published in [23].

3.1 Introduction

Having perfect and instantaneous knowledge of the channel at the receiver side is certainly not straightforward, but can be almost achieved using efficient channel estimation algorithms. In this thesis, the receiver will be assumed to have perfect channel state information (CSI), unless otherwise stated. However, having perfect CSI at the transmitter side (CSIT) additionally implies the presence of a perfect feedback link (i.e. error and delay free), which is clearly unrealistic.

In this chapter, let us assume that there is no CSIT. In such situation, no adaptive resource (bit, power) allocation is possible at the transmitter side. The goal is then to evaluate the bit error rate (BER) achieved by the cyclic prefix block transmission schemes presented in Chapter 2 (i.e. OFDM or CPSC), and compare them. In order for the comparison to be fair, the bit rate should of course be equal for both schemes.

A first natural question to answer is that of how OFDM and CPSC compete with each other in terms of BER for a given channel realization, i.e. instantaneous BER. Obviously, the different CPSC receivers should be distinguished in the comparison. This is the context of Section 3.2, which is based in part on the results in [21,22].

A second step, which is critical in wireless communication, is to integrate the variability (or fading) of the channel in the comparison. Put differently, the focus is set this time on the average BER, which is nothing more than the average of the instantaneous BER on the channel statistic. A performance indicator directly related to the average BER is the diversity order extracted by the system. In fact, it is well-known that the transmission over fading channels can have its average BER significantly reduced if a diversity technique is used. It consists of transmitting the signal through multiple links which fade independently, so that the communication will be reliable unless all the links fade simultaneously. Different sources of diversity can be identified:

- *Time diversity.* Channels in different coherence time periods experience independent fades. This diversity can be exploited by simple repetition coding, or by using more sophisticated codes along with interleaving [57,58].
- *Spatial diversity.* With multiple transmit and/or receive antennas sufficiently separated from each other, a set of channels which fade independently can be created and taken advantage of, see e.g. [59–62].
- *Multipath diversity.* The wireless channel introduced in Chapter 2 inherently provides a multi-tap transmission, whose taps ideally fade independently.
- *Multi-user diversity.* The fading statistics of the channels of different users might be independent, such that allocating the resource among the different users enhances the performance [63–65].

In this thesis, the focus is set on the multipath diversity. The purpose of Section 3.3 is to evaluate the average BER of the OFDM and CPSC systems (distinguishing the different possible receivers), and to analyze to which extent these schemes exploit the multipath diversity. This subject has actually been investigated for ML-CPSC in [66], and then corrected in [67]. The final conclusion there was that ML-CPSC is unable to extract any multipath diversity. In Section 3.3, we do not question this result, but we still moderate it and prove that the multipath diversity can still be exploited by CPSC under some realistic hypotheses. In particular, the influence of the block size and that of the use of suboptimal receivers on the diversity extraction is investigated.

3.2 Instantaneous bit error rate

In this section, we momentarily neglect the time variation of the channel, and focus on one given channel realization. This is what the word "instantaneous" refers to. The objective is first to derive the instantaneous BER (i.e. BER for a given channel realization) expression for the schemes presented in Chapter 2, and second to compare them.

3.2.1 OFDM

In Subsection 2.4.1, it was shown that, for the OFDM modulation, the ML and linear ZF receivers coincide. The associated data vector estimate was given by (2.39). At this point, the BER expression associated with the decision-making on the estimate (2.39) can be calculated easily. In (2.39), the noise covariance matrix is $\sigma_n^2 \mathbf{\Omega}^{-1,H} \mathbf{\Omega}^{-1}$. In other words, focusing on the k th data symbol d_k transmitted on the k th subcarrier, the noise affecting its estimate (2.39) has variance $\sigma_n^2 / |\omega_k|^2$. For conciseness, let us define the following notations

$$\mathbf{h} = [h_0, h_1, \dots, h_{K-1}]^T \quad (3.1)$$

$$h_k = |\omega_k|^2, \quad (3.2)$$

i.e. \mathbf{h} is the vector of the squared norm of the channel gains in the frequency domain. The instantaneous signal to noise ratio (SNR) on subcarrier k is thus given by

$$\text{SNR}_k^{\text{OFDM}} = \frac{h_k}{\sigma_n^2} \quad (3.3)$$

$$= \gamma h_k \quad (3.4)$$

with $\gamma = 1/\sigma_n^2$ denoting the average SNR. As commented in the first words of this chapter, the channel is assumed to be unknown at the transmitter side. Therefore, no adaptive bit loading can be carried out, and the same constellation is used on all subcarriers. Without loss of generality, let us assume that binary phase shift keying (BPSK) modulation is used. The instantaneous BER on the symbol d_k associated with the decision-making on (2.39) is then given by [68]

$$\text{BER}_k^{\text{OFDM}}(\mathbf{h}, \gamma) = Q\left(\sqrt{2 \gamma h_k}\right) \quad (3.5)$$

where $Q(\cdot)$ denotes the Gaussian Q-function¹. The instantaneous character is expressed by the explicit dependency on \mathbf{h} in (3.5). One can also be interested in the mean instantaneous BER on the block of K symbols

$$\overline{\text{BER}}^{\text{OFDM}}(\mathbf{h}, \gamma) = \frac{1}{K} \sum_{k=0}^{K-1} Q\left(\sqrt{2\gamma h_k}\right). \quad (3.6)$$

Throughout this thesis, the overlined acronym $\overline{\text{BER}}$ will be used to refer to the mean bit error rate on the block. Finally, note that using instead a MMSE linear receiver for OFDM would not have any effect on the BER: the only difference with respect to ZF would be the scaling of the estimate by a positive real factor, which would not affect the symbol-by-symbol decision-making.

3.2.2 ZF-CPSC

In Subsection 2.4.2.2, the ZF linear receiver for CPSC was derived and the data vector estimate was given by (2.55). The noise term in (2.55) has a covariance matrix equal to $\sigma_n^2 \mathbf{W}^H \mathbf{\Omega}^{-1} \mathbf{\Omega}^{-1,H} \mathbf{W}$, which is a circulant matrix. This means that the noise variance is equal for all K symbols of the block (since a circulant matrix has a constant diagonal), and is calculated as

$$(\sigma_n^2)_{\text{ZF}}^{\text{CPSC}} = \frac{1}{K} \text{trace}\left(\sigma_n^2 \mathbf{W}^H \mathbf{\Omega}^{-1} \mathbf{\Omega}^{-1,H} \mathbf{W}\right) \quad (3.7)$$

$$= \frac{1}{K} \sum_{k=0}^{K-1} \frac{1}{\gamma h_k}, \quad (3.8)$$

while the instantaneous SNR is

$$\text{SNR}_{\text{ZF}}^{\text{CPSC}} = \frac{1}{\frac{1}{K} \sum_{k=0}^{K-1} \frac{1}{\gamma h_k}}. \quad (3.9)$$

The instantaneous BER is thus equal for all K symbols of the block, such that the mean instantaneous BER is

$$\overline{\text{BER}}_{\text{ZF}}^{\text{CPSC}}(\mathbf{h}, \gamma) = Q\left(\sqrt{\frac{2}{\frac{1}{K} \sum_{k=0}^{K-1} \frac{1}{\gamma h_k}}}\right). \quad (3.10)$$

¹ $Q(\alpha) = \frac{1}{\sqrt{2\pi}} \int_{\alpha}^{\infty} e^{-u^2/2} du$

3.2.3 MMSE-CPSC

In Subsection 2.4.2.3, the MMSE linear receiver for CPSC was derived and the data vector estimate was given by (2.57). As mentioned then, the symbol-by-symbol detection on (2.57) is both perturbed by noise and ISI. It turns out that the covariance matrices of both these perturbations have a constant diagonal (they are actually circulant again). As a consequence, the MSE and thus the BER is once again equal for all K symbols of the block. In particular, the MSE on each individual symbol of the block is given by

$$\text{MSE} = \frac{\sigma_n^2}{K} \text{trace} \left(\mathbf{W}^H (\mathbf{\Omega}^H \mathbf{\Omega} + \sigma_n^2 \mathbf{I}_K)^{-1} \mathbf{W} \right) \quad (3.11)$$

$$= \frac{1}{K} \sum_{k=0}^{K-1} \frac{1}{\gamma h_k + 1}. \quad (3.12)$$

Next, the unbiased signal to interference plus noise ratio (SINR) is given by $\frac{1}{\text{MSE}} - 1$:

$$\text{SINR}_{\text{MMSE}}^{\text{CPSC}} = \frac{1}{\frac{1}{K} \sum_{k=0}^{K-1} \frac{1}{\gamma h_k + 1}} - 1. \quad (3.13)$$

And finally, if the Gaussian approximation is used for the ISI, the mean instantaneous BER can be approximated by

$$\overline{\text{BER}}_{\text{MMSE}}^{\text{CPSC}}(\mathbf{h}, \gamma) \cong Q \left(\sqrt{2 \left(\frac{1}{\frac{1}{K} \sum_{k=0}^{K-1} \frac{1}{\gamma h_k + 1}} - 1 \right)} \right). \quad (3.14)$$

Generally speaking, the greater the value of K , the more valid the Gaussian approximation of the ISI will be. However, we will come back later on the validity on this approximation in specific conditions.

3.2.4 DFE-CPSC

In Subsection 2.4.2.4, the DFE receiver for CPSC was presented (the complete mathematical derivation being included in Appendix 2.A). It was shown that, if the error propagation effect in the feedback part is neglected, the resulting error covariance matrix is diagonal and equal to $\sigma_n^2 \mathbf{D}$, with \mathbf{D} defined in (2.60). In a similar way as for the MMSE linear receiver, the unbiased SINR for the k th symbol of the block is given by

$$(\text{SINR}_k)_{\text{DFE}}^{\text{CPSC}} = \frac{\gamma}{[\mathbf{D}]_{k,k}} - 1. \quad (3.15)$$

Again, if the Gaussian approximation is used for the remaining ISI, the mean instantaneous BER can be approximated by

$$\overline{\text{BER}}_{\text{DFE}}^{\text{CPSC}}(\mathbf{h}, \gamma) \cong \frac{1}{K} \sum_{k=0}^{K-1} Q \left(\sqrt{2 \left(\frac{\gamma}{[\mathbf{D}]_{k,k}} - 1 \right)} \right). \quad (3.16)$$

3.2.5 Instantaneous BER comparison

Using Jensen's inequality, the instantaneous BER presented in the preceding subsections for OFDM and CPSC with linear receivers are easily compared to each other, as summarized in the following two propositions. Note that Proposition 3.1 has been published in [21, 22]. However, in order to have a complete overview of the subject, we found it interesting to incorporate this result here.

Proposition 3.1.

If $\gamma \geq 3/(2 \min_k h_k)$ then $\overline{\text{BER}}_{\text{ZF}}^{\text{CPSC}}(\mathbf{h}, \gamma) \leq \overline{\text{BER}}^{\text{OFDM}}(\mathbf{h}, \gamma)$.
 If $\gamma \leq 3/(2 \max_k h_k)$ then $\overline{\text{BER}}^{\text{OFDM}}(\mathbf{h}, \gamma) \leq \overline{\text{BER}}_{\text{ZF}}^{\text{CPSC}}(\mathbf{h}, \gamma)$.

Proof. Since $Q(\sqrt{2/x})$ is a convex function as long as $x \in [0, 2/3]$, Jensen's inequality gives

$$\overline{\text{BER}}_{\text{ZF}}^{\text{CPSC}}(\mathbf{h}, \gamma) = Q \left(\sqrt{\frac{2}{\frac{1}{K} \sum_{k=0}^{K-1} \frac{1}{\gamma h_k}}} \right) \quad (3.17)$$

$$\leq \frac{1}{K} \sum_{k=0}^{K-1} Q \left(\sqrt{\frac{2}{\frac{1}{\gamma h_k}}} \right) \quad (3.18)$$

$$= \overline{\text{BER}}^{\text{OFDM}}(\mathbf{h}, \gamma) \quad (3.19)$$

as long as $\frac{1}{\gamma h_k} \leq \frac{2}{3} \forall k \in \{0, \dots, K-1\}$, i.e. if $\gamma \geq 3/(2 \min_k h_k)$. The second part of the proposition is proved in a similar manner, using the fact that $Q(\sqrt{2/x})$ is a concave function for $x \in [2/3, \infty]$. \square

Proposition 3.2.

$$(i) \quad \overline{\text{BER}}_{\text{MMSE}}^{\text{CPSC}}(\mathbf{h}, \gamma) \leq \overline{\text{BER}}^{\text{OFDM}}(\mathbf{h}, \gamma) \quad (3.20)$$

$$(ii) \quad \overline{\text{BER}}_{\text{MMSE}}^{\text{CPSC}}(\mathbf{h}, \gamma) \leq \overline{\text{BER}}_{\text{ZF}}^{\text{CPSC}}(\mathbf{h}, \gamma) \quad (3.21)$$

Proof.

- (i) Since $Q(\sqrt{2(\frac{1}{x} - 1)})$ is a convex function for $x \in [0, 1]$, Jensen's inequality gives

$$\overline{\text{BER}}_{\text{MMSE}}^{\text{CPSC}}(\mathbf{h}, \gamma) = Q\left(\sqrt{2\left(\frac{1}{\frac{1}{K}\sum_{k=0}^{K-1}\frac{1}{\gamma h_k+1}} - 1\right)}\right) \quad (3.22)$$

$$\leq \frac{1}{K} \sum_{k=0}^{K-1} Q\left(\sqrt{2\left(\frac{1}{\gamma h_k+1} - 1\right)}\right) \quad (3.23)$$

$$= \overline{\text{BER}}^{\text{OFDM}}(\mathbf{h}, \gamma). \quad (3.24)$$

- (ii) This part of the proposition will be proved if we proof that

$$\text{SNR}_{\text{ZF}}^{\text{CPSC}} \leq \text{SINR}_{\text{MMSE}}^{\text{CPSC}} \quad (3.25)$$

which, reorganizing (3.9) and (3.13), can be rewritten as

$$\frac{1}{\frac{1}{K}\sum_{k=0}^{K-1}\frac{1}{\gamma h_k}} + 1 \leq \frac{1}{\frac{1}{K}\sum_{k=0}^{K-1}\frac{1}{\gamma h_k+1}}, \quad (3.26)$$

or

$$H(\gamma\mathbf{h}) + H(\mathbf{1}) \leq H(\gamma\mathbf{h} + \mathbf{1}) \quad (3.27)$$

where $H(\mathbf{x})$ denotes the harmonic mean of the entries of vector \mathbf{x} , and $\mathbf{1}$ refers to the all-ones column vector. Note also that, in (3.27), we used the fact that $H(\mathbf{1}) = 1$. Finally (3.27) is proved by the subadditivity of the harmonic mean function [69]

$$H(\mathbf{x}) + H(\mathbf{x}') \leq H(\mathbf{x} + \mathbf{x}') \quad (3.28)$$

for any vectors \mathbf{x} and \mathbf{x}' with positive real entries.

□

Let us illustrate Propositions 3.1 and 3.2. Suppose $K = 64$ and $L = 4$. The two channel realizations whose frequency responses \mathbf{h} are given in Fig. 3.1, are considered. These two channel realizations have equal energy, but the frequency response of the channel realization B is in deep fade at some frequency

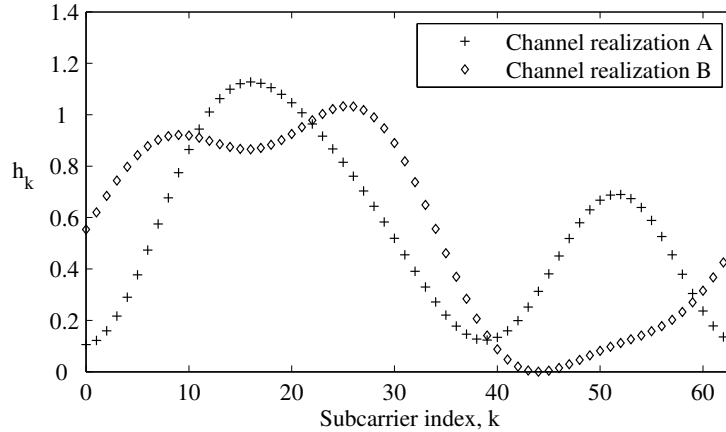


Figure 3.1 Frequency response \mathbf{h} of the two considered channel realizations.

index (see h_{44}). The instantaneous BER curves for channel realizations A and B are given in the upper and lower part of Fig. 3.2, respectively. We see that, for both channel realizations, MMSE-CPSC outperforms both ZF-CPSC and OFDM at all SNRs. This illustrates Proposition 3.2. The property given in Proposition 3.1 can also be observed: for both channel realizations, OFDM outperforms ZF-CPSC at low SNR, while ZF-CPSC outperforms OFDM at high SNR. However, the SNR at which the OFDM and ZF-CPSC curves cross, depends strongly on the channel realization: it happens at approximately 6dB for channel realization A, and at 22dB for channel realization B. This difference in behavior was expected because of the deep fade observed in channel realization B, such that $3/(2 \min_k h_k)$ (see Proposition 3.1) has a much greater value for channel realization B than for channel realization A.

Finally, the instantaneous BER of DFE-CPSC (3.16) is such that the following proposition holds, as expected.

Proposition 3.3. $\overline{\text{BER}}_{\text{DFE}}^{\text{CPSC}}(\mathbf{h}, \gamma) \leq \overline{\text{BER}}_{\text{MMSE}}^{\text{CPSC}}(\mathbf{h}, \gamma)$

Proof. The proposition compares the expressions (3.14) and (3.16). The proposition is then a direct consequence of the two following properties of the Cholesky decomposition (2.60): First, the diagonal entries of \mathbf{D} are with de-

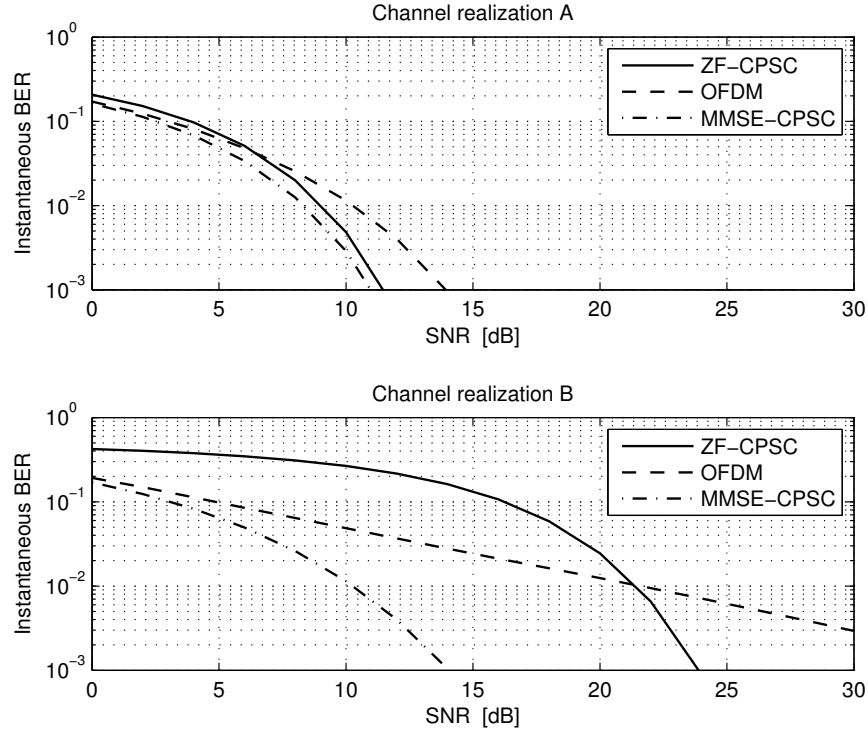


Figure 3.2 Instantaneous BER for channel realizations A (upper figure) and B (lower figure). Comparison between OFDM, ZF-CPSC and MMSE-CPSC.

creasing values, i.e.

$$[\mathbf{D}]_{0,0} \geq [\mathbf{D}]_{1,1} \geq \cdots \geq [\mathbf{D}]_{K-1,K-1}, \quad (3.29)$$

and, second,

$$\sigma_n^2 [\mathbf{D}]_{0,0} = \frac{1}{K} \sum_{k=0}^{K-1} \frac{1}{\gamma h_k + 1}. \quad (3.30)$$

Note that the properties (3.29) and (3.30) will be proved in more detail in the next chapter. \square

The reader should notice that Proposition 3.3 holds only if the potential error propagation effect in the DFE is neglected.

Let us conclude this section by summarizing its main results. In terms of instantaneous BER, here is how the different schemes compare to each other:

- DFE-CPSC outperforms all schemes.
- MMSE-CPSC outperforms ZF-CPSC and OFDM.
- ZF-CPSC outperforms OFDM at high SNR, but is outperformed at low SNR. The transition occurs at a SNR value which highly depends on the channel realization.

Remember that we assume in this chapter that there is no CSIT, such that the power cannot be adaptively allocated. A reader interested in the same comparison with power allocation, can refer to [70]. The authors prove that OFDM with a well-chosen power allocation can outperform ZF-CPSC in terms of instantaneous BER, and that even at high SNR.

3.3 Average BER and diversity

This section goes one step further and takes into account the fluctuation (or fading) of the wireless channel. In particular, the figure of merit analyzed in this section is the average BER, i.e. the average of the instantaneous BER over the channel statistic.

It is well known that the transmission over fading channels can see its performance (in terms of average BER, for instance) significantly improved if a diversity technique is used. It consists of transmitting the signal through multiple links which fade independently. The frequency selective channel (2.20) inherently provides such independent multipath transmission, known as multipath diversity. The objective of this section is to analyze to which extent the transmission techniques of Section 2.4 are able to extract the multipath diversity. The maximum diversity order is equal to L , i.e. the number of taps in (2.20). The diversity order extracted by a transmission technique at a given SNR can be evaluated by looking at the slope of the average BER vs SNR curve on a log-log scale.

3.3.1 OFDM

This subsection is dedicated to reiterating the following well-known result.

Proposition 3.4. *The OFDM modulation does not extract any multipath diversity².*

Proof. Taking into account the channel impulse response taps statistic (2.14), the h_k in (3.2) also have a chi-square distribution with pdf

$$T_{h_k}(h_k) = e^{-h_k}. \quad (3.31)$$

The average BER of an OFDM transmission is calculated by integrating each term of the BER expression (3.6) on the pdf (3.31), and has the following exact closed-form expression

$$\overline{\text{BER}}^{\text{OFDM}}(\gamma) = \text{E} \left[\overline{\text{BER}}^{\text{OFDM}}(\mathbf{h}, \gamma) \right] \quad (3.32)$$

$$= \frac{1}{K} \sum_{k=0}^{K-1} \int_0^{\infty} Q(\sqrt{2\gamma h_k}) e^{-h_k} dh_k \quad (3.33)$$

$$= \frac{1}{2} \left(1 - \sqrt{\frac{\gamma}{\gamma+1}} \right), \quad (3.34)$$

see Appendix 3.A.1 for a detailed derivation. At moderate to high SNR γ , the last equality becomes $\overline{\text{BER}}^{\text{OFDM}}(\gamma) \cong 1/(4\gamma)$: the slope of the BER versus SNR curve on a log-log scale is thus equal to minus one, independently of the value of L . This concludes the proof. \square

Note that this result is independent of the receiver used (ML, linear ZF, or MMSE), since all these receivers are equivalent for OFDM, as we commented earlier. However, we will see in the three following subsections that the average performance of a CPSC transmission will depend much on the receiver used.

²Remember that we refer to OFDM without any precoding or adaptive resource allocation: each subcarrier is assigned the transmission of one and only one data symbol, and the same constellation is used for all data symbols.

3.3.2 ML-CPSC

As commented in Subsection 2.4.2, CPSC differs from OFDM by the absence of the IFFT operation at the transmitter. Put differently, CPSC can be seen as OFDM precoded by an FFT. It is interesting to analyze whether or not this difference allows to extract some diversity, unlike in OFDM. In order to not let the suboptimality of linear receivers affect the result, let us first focus on the optimal ML receiver. This problem has been investigated in [66] and [67]. First, the authors of [66] erroneously stated that ML-CPSC was able to collect the full multipath diversity, if the block size K was large enough. This result was then corrected in [67], where the authors showed that ML-CPSC is unable to collect any diversity. This last result is not contested here, but rather moderated: we show that the block size has indeed an influence, and that some diversity can be extracted by ML-CPSC for the range of BER typically used in practice.

As introduced in Subsection 2.4.2.1, the ML receiver for CPSC has to be carried out on a block basis, and basically has to exhaustively search for the symbol block \mathbf{d} which minimizes the distance (2.53). In practice however, the costly exhaustive search can be replaced by the sphere decoding (SD) algorithm [71–74]. The exact BER analysis is difficult, if not impossible. Alternatively, we will rely on the pairwise error probability (PEP) analysis, which is often used in diversity analysis [59]. Suppose that the vector \mathbf{d} is transmitted, and let us focus on the probability that another vector \mathbf{d}' (with $\mathbf{d}' \neq \mathbf{d}$) be erroneously decoded. The PEP conditioned on the channel is

$$P(\mathbf{d} \rightarrow \mathbf{d}' | \mathbf{g}, \gamma) = Q \left(\sqrt{\frac{\gamma \|\mathbf{G}_c(\mathbf{d} - \mathbf{d}')\|^2}{2}} \right). \quad (3.35)$$

The vector $\mathbf{G}_c(\mathbf{d} - \mathbf{d}')$ can equivalently be written as

$$\mathbf{G}_c(\mathbf{d} - \mathbf{d}') = \mathbf{W}^H \boldsymbol{\Omega} \mathbf{W}(\mathbf{d} - \mathbf{d}') \quad (3.36)$$

$$= \mathbf{W}^H \mathbf{D}_e \mathbf{V} \mathbf{g} \quad (3.37)$$

where $\mathbf{D}_e = \text{diag}(\mathbf{W}\mathbf{e})$, the error vector is defined as $\mathbf{e} = \mathbf{d} - \mathbf{d}'$, and the $K \times L$ matrix \mathbf{V} is the L first columns of $\sqrt{K}\mathbf{W}$. The squared norm in (3.35) can then be developed as

$$\|\mathbf{G}_c(\mathbf{d} - \mathbf{d}')\|^2 = \mathbf{g}^H \mathbf{V}^H \mathbf{D}_e^H \mathbf{D}_e \mathbf{V} \mathbf{g}. \quad (3.38)$$

Since $\mathbf{V}^H \mathbf{D}_e^H \mathbf{D}_e \mathbf{V}$ is a $L \times L$ Hermitian matrix, it can be decomposed as $\mathbf{V}^H \mathbf{D}_e^H \mathbf{D}_e \mathbf{V} = \mathbf{U}^H \mathbf{\Lambda} \mathbf{U}$, with \mathbf{U} a unitary matrix and with $\mathbf{\Lambda} = \text{diag}([\lambda_0, \dots, \lambda_{L-1}]^T)$. Denoting $\tilde{\mathbf{g}} = \mathbf{U} \mathbf{g}$, we find

$$\|\mathbf{G}_c(\mathbf{d} - \mathbf{d}')\|^2 = \mathbf{g}^H \mathbf{U}^H \mathbf{\Lambda} \mathbf{U} \mathbf{g} \quad (3.39)$$

$$= \tilde{\mathbf{g}}^H \mathbf{\Lambda} \tilde{\mathbf{g}} \quad (3.40)$$

$$= \sum_{l=0}^{L-1} \lambda_l |\tilde{g}_l|^2. \quad (3.41)$$

Note that, since \mathbf{U} is a unitary matrix, the modified channel taps $\tilde{\mathbf{g}} = \mathbf{U} \mathbf{g}$ have the same statistical properties (2.14) as \mathbf{g} . The PEP (3.35) can be rewritten as

$$P(\mathbf{d} \rightarrow \mathbf{d}' | \mathbf{g}, \gamma) = Q \left(\sqrt{\frac{\gamma \sum_{l=0}^{L-1} \lambda_l |\tilde{g}_l|^2}{2}} \right). \quad (3.42)$$

The fact that L independent modified channel taps \tilde{g}_l are contributing to the PEP (3.42) confirms that the highest diversity order we can get, is equal to L . However this maximum diversity order is achieved if and only if all λ_l are non null, and this for all vectors \mathbf{d} and \mathbf{d}' . In particular, the number of non null λ_l is given by $\min\{\text{rank}(\mathbf{D}_e), L\}$. The authors of [67] pointed out that the rank of \mathbf{D}_e is equal to one for some error vectors \mathbf{e} . From that, they stated that the diversity order achieved by ML-CPSC is thus equal to one. However, let us moderate this statement: the only thing that we can conclude at this point is that, at infinite SNR, the BER curve of ML-CPSC will have a slope equal to minus one. In other words, the asymptotical (i.e. at infinite SNR) diversity order of CPSC is equal to one. On the other hand, we state the following.

Proposition 3.5. *The events responsible for the asymptotical diversity order one of ML-CPSC translate into a diversity one lower bound on the average BER. The value of this lower bound is exponentially decreasing with the block size K .*

Proof. For ease of presentation, let us keep on assuming that BPSK symbols are used. The four error vectors \mathbf{e}_i which yield a rank one matrix \mathbf{D}_e are given in Table 3.1, together with the corresponding vectors \mathbf{d}_i and \mathbf{d}'_i ($i = 1, \dots, 4$). For these four vectors³, there is only one non null λ_l . Let us denote by l^*

³The block size K is assumed to be even. It is the case in practice since K is chosen to be a power of two in order to allow an efficient implementation of the (I)FFT operations, as commented earlier. Note however, that if K is odd, the last two rows of Table 3.1 no longer hold.

i	\mathbf{e}_i	\mathbf{d}_i	\mathbf{d}'_i
1	$[2, 2, 2, 2, \dots]^T$	$[1, 1, 1, 1, \dots]^T$	$[-1, -1, -1, -1, \dots]^T$
2	$[-2, -2, -2, -2, \dots]^T$	$[-1, -1, -1, -1, \dots]^T$	$[1, 1, 1, 1, \dots]^T$
3	$[2, -2, 2, -2, \dots]^T$	$[1, -1, 1, -1, \dots]^T$	$[-1, 1, -1, 1, \dots]^T$
4	$[-2, 2, -2, 2, \dots]^T$	$[-1, 1, -1, 1, \dots]^T$	$[1, -1, 1, -1, \dots]^T$

Table 3.1 ML-CPSC: error vectors responsible for the asymptotical diversity order one.

the corresponding index, such that $\lambda_l = 0$ if $l \neq l^*$. One can calculate that $\lambda_{l^*} = 4KL$. As a consequence, for these vectors responsible for the asymptotical diversity order one, the PEP (3.42) becomes

$$P(\mathbf{d}_i \rightarrow \mathbf{d}'_i | \mathbf{g}, \gamma) = Q\left(\sqrt{\gamma 2KL |\tilde{g}_{l^*}|^2}\right) \quad \text{for } i = 1, \dots, 4. \quad (3.43)$$

Averaging the last expression over the channel statistic, using the chi-square pdf (2.14), we get

$$P(\mathbf{d}_i \rightarrow \mathbf{d}'_i | \gamma) = \int_0^\infty Q\left(\sqrt{\gamma 2KLx}\right) L e^{-Lx} dx \quad (3.44)$$

$$= \int_0^\infty Q\left(\sqrt{\gamma 2Ky}\right) e^{-y} dy \quad (3.45)$$

$$= \frac{1}{2} \left(1 - \sqrt{\frac{\gamma K}{\gamma K + 1}}\right), \quad (3.46)$$

see Appendix 3.A.2 for a detailed derivation. Taking into account that the probability of transmitting a given vector \mathbf{d}_i is equal to $1/2^K$, we have the following lower bound for the average BER of ML-CPSC

$$\overline{\text{BER}}_{\text{ML}}^{\text{CPSC}}(\gamma) = \text{E} \left[\overline{\text{BER}}_{\text{ML}}^{\text{CPSC}}(\mathbf{g}, \gamma) \right] \quad (3.47)$$

$$\geq \sum_{i=1}^4 \frac{1}{2^K} P(\mathbf{d}_i \rightarrow \mathbf{d}'_i | \gamma) \quad (3.48)$$

$$= \frac{1}{2^{K-1}} \left(1 - \sqrt{\frac{\gamma K}{\gamma K + 1}}\right) \quad (3.49)$$

where the inequality sign is justified by the fact that, in (3.48), we are summing only four specific error vectors out of the set of all possible error vectors.

At moderate to high SNR, the last expression (3.49) is approximately equal to $1/(2^K K \gamma)$ and has slope minus one on a log-log scale, as expected. We see that the expression (3.49) acts as a diversity one lower bound (i.e. a lower bound with slope minus one) on the average BER, and that its value decreases exponentially with K , which concludes the proof. \square

Proposition 3.5 is now illustrated through simulations. The ML receiver was implemented using the SD algorithm [71]. Let us first consider a block of size $K = 8$. Fig. 3.3 shows the average BER for a two taps ($L = 2$) and a three taps ($L = 3$) channel impulse response. The diversity one lower bound (3.49) is also drawn. We see that whatever the value of L , at high SNR the average BER tends to be exactly equal to (3.49), which confirms that the asymptotical diversity order of ML-CPSC is equal to one. However, looking at the $L = 2$ curve, we see that the curve is actually reaching a slope equal to minus two (which is the maximum diversity order) before it tends to the diversity one lower bound. On the other hand, the $L = 3$ curve does not quite reach a slope equal to minus three before it tends to the diversity one lower bound.

Let us now double the block size and assume that $K = 16$. Fig. 3.4 shows once again the average BER for a two taps ($L = 2$) and a three taps ($L = 3$) channel impulse response, and the diversity one lower bound (3.49). We see that this diversity one lower bound has decreased significantly with respect to the case $K = 8$ (redrawn in grey in Fig. 3.4). This illustrates Proposition 3.5. As a consequence, this time, the diversity one events do not affect the performance, except for very low BER values. In particular, for $K = 16$ in Fig. 3.4, the full diversity (slope minus two and three, for $L = 2$ and $L = 3$, respectively) appears to be extracted for the range of BER typically used in practice⁴. We summarize this in the following observation.

Observation 3.6. *For reasonably large values of K , the events responsible for the asymptotical diversity order one of ML-CPSC do not affect the performance for the range of BER values typically used in practice. As a consequence, for reasonably large values of K , the multipath diversity can be extracted by ML-CPSC for the range of BER values typically used in practice.*

⁴Remember that we are talking here about uncoded BER. In practical systems, the actual BER will be further reduced by using error correcting codes on top of the systems considered here. Note that Chapter 5 will take into account the presence of error correction mechanisms.

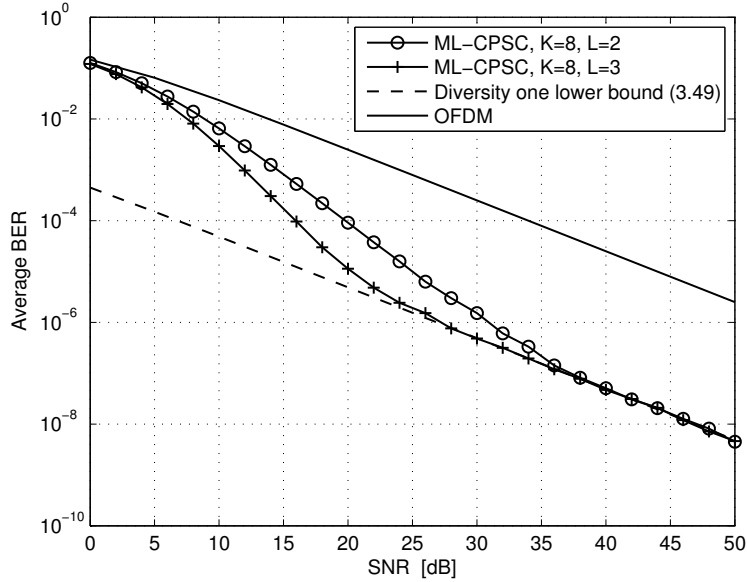


Figure 3.3 ML-CPSC: illustration of the diversity one lower bound (3.49) on the average BER, for $K = 8$ and two values of L .

The average BER (3.34) for OFDM was also given in Fig. 3.3 and 3.4. We see that OFDM is significantly outperformed by ML-CPSC. This is a direct consequence of Proposition 3.4 and Observation 3.6.

3.3.3 ZF-CPSC

With the optimal ML receiver, a CPSC system is able to extract some diversity under the conditions of Observation 3.6. In practice, however, for complexity issues we would be interested in using suboptimal linear receivers. In this subsection, the performance (in terms of diversity) of the ZF linear receiver is studied. The following proposition holds.

Proposition 3.7. *The use of a ZF linear receiver in a CPSC system prevents the extraction of any multipath diversity.*

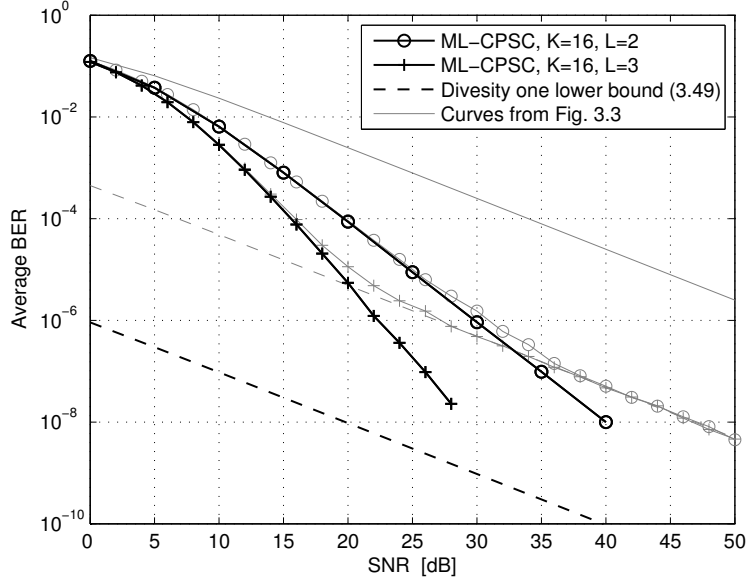


Figure 3.4 ML-CPSC: illustration of the diversity one lower bound (3.49) on the average BER, for $K = 16$ and two values of L .

Proof. Let us focus on the derivation of a lower bound on the average BER of ZF-CPSC. We start from the following obvious inequality on the instantaneous BER (3.10)

$$\overline{\text{BER}}_{\text{ZF}}^{\text{CPSC}}(\mathbf{h}, \gamma) = Q\left(\sqrt{\frac{2}{\frac{1}{K} \sum_{k=0}^{K-1} \frac{1}{\gamma h_k}}}\right) \quad (3.50)$$

$$\geq Q\left(\sqrt{\frac{2\gamma}{\frac{1}{K} \max_k \left(\frac{1}{h_k}\right)}}\right) \quad (3.51)$$

$$= Q\left(\sqrt{2\gamma K \min_k (h_k)}\right). \quad (3.52)$$

For a given value of K , the maximum achievable diversity gain corresponds to the case where $L = K$. Let us assume this situation⁵. In such a case, the

⁵Remember however that the situation $L = K$ is not the one encountered in practical systems: K is usually chosen to be much greater than L to limit the bandwidth efficiency loss induced by the addition of the CP, as explained in Section 2.3.

random variables h_0, \dots, h_{K-1} are uncorrelated, and the pdf of the random variable $x = K \min_k (h_k)$ can be shown (see Appendix 3.B) to be $T_x(x) = e^{-x}$. Averaging the inequality (3.52) over the channel, we get

$$\overline{\text{BER}}_{\text{ZF}}^{\text{CPSC}}(\gamma) = \text{E} \left[\overline{\text{BER}}_{\text{ZF}}^{\text{CPSC}}(\mathbf{h}, \gamma) \right] \quad (3.53)$$

$$\geq \int_0^\infty Q(\sqrt{2\gamma x}) e^{-x} dx \quad (3.54)$$

$$= \frac{1}{2} \left(1 - \sqrt{\frac{\gamma}{\gamma+1}} \right) \quad (3.55)$$

$$= \overline{\text{BER}}^{\text{OFDM}}(\gamma), \quad (3.56)$$

since the integral (3.54) is just the same as the one in (3.33). Combining the inequality (3.56) with Proposition 3.4 concludes the proof. \square

Note that Proposition 3.7 can also be understood using Proposition 3.1. It is well known that the average BER is mainly influenced by the bad channel realizations (i.e., here, realizations with a frequency gain close to zero). For these realizations, Proposition 3.1 states that the inequality $\overline{\text{BER}}_{\text{ZF}}^{\text{CPSC}}(\mathbf{h}, \gamma) \leq \overline{\text{BER}}^{\text{OFDM}}(\mathbf{h}, \gamma)$ holds only for an infinite SNR γ .

Let us illustrate this result through simulations. Fig. 3.5 compares the simulated average BER of OFDM and ZF-CPSC. The block size was $K = 64$, and two extreme values for the channel impulse response length were considered: $L = 2$ and $L = 64$. For both values of L , we see that the inequality (3.56) holds, and as a consequence so does Proposition 3.7.

The result in Proposition 3.7 is rather a negative one. However, the reader can easily identify the actual intuitive reason for that: having only one of the h_k be in deep fade is enough to have the argument of the Q-function in (3.10) tend to zero. In more mathematical terms, the SNR in (3.10) is determined by the harmonic mean of the h_k . And the harmonic mean of a set of positive real numbers is known to be mainly influenced by the lowest values in the set, as illustrated by an every day life example in Appendix 3.C.

3.3.4 MMSE-CPSC

As it was just mentioned, the bad performance of the ZF receiver for CPSC comes from the fact that having only one of the h_k be in deep fade is enough

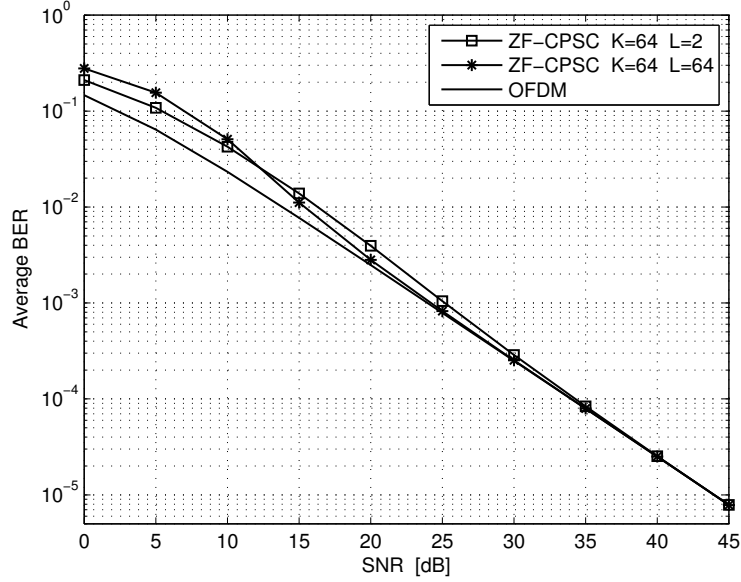


Figure 3.5 Average BER comparison between OFDM and ZF-CPSC, for $K = 64$ and $L = 2$ or 64 .

to have the BER (3.10) tend to one half. A first look at the argument of the Q-function in (3.14) suggests that the MMSE linear receiver might be correcting that flaw. In particular the following proposition holds.

Proposition 3.8. *The diversity one lower bound associated with the average of the instantaneous BER (3.14) is exponentially decreasing with the block size K .*

Proof. In a similar way as in (3.52), the following lower bound can be created for the instantaneous BER (3.14) of MMSE-CPSC

$$\overline{\text{BER}}_{\text{MMSE}}^{\text{CPSC}}(\mathbf{h}, \gamma) \geq Q \left(\sqrt{2(K-1) + 2\gamma K \min_k(h_k)} \right). \quad (3.57)$$

Let us suppose again that $L = K$, so that the variables h_0, \dots, h_{K-1} are uncorrelated. The diversity one lower bound of MMSE-CPSC is obtained by averaging the quantity at the right side of (3.57) over the channel statistic, which

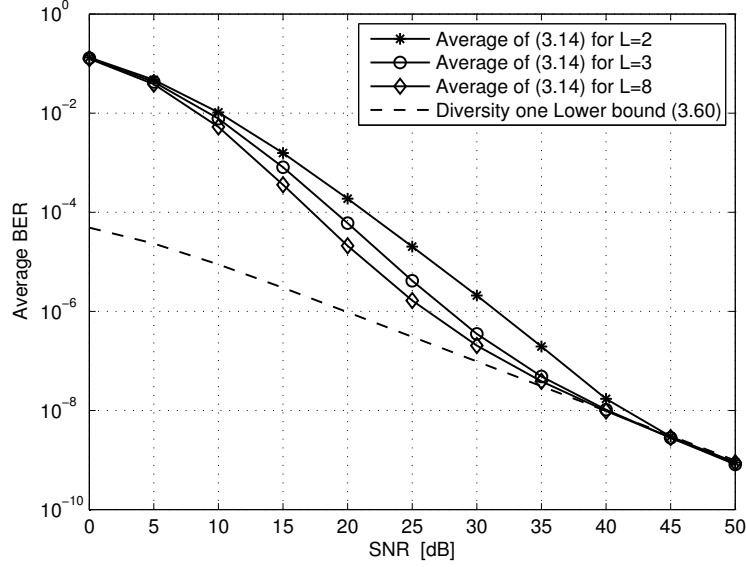


Figure 3.6 MMSE-CPSC: illustration of the diversity one lower bound (3.60) on the average of the instantaneous BER (3.14), for $K = 8$ and different values of L .

gives the following approximated result

$$\overline{\text{BER}}_{\text{MMSE}}^{\text{CPSC}}(\gamma) = \text{E} \left[\overline{\text{BER}}_{\text{MMSE}}^{\text{CPSC}}(\mathbf{h}, \gamma) \right] \quad (3.58)$$

$$\geq \text{E} \left[Q \left(\sqrt{2(K-1) + 2\gamma K \min_k(h_k)} \right) \right] \quad (3.59)$$

$$\cong \frac{1}{\sqrt{4\pi(K-1)}} e^{-(K-1)} \frac{1}{\gamma+1}, \quad (3.60)$$

see Appendix 3.A.3 for a detailed derivation. The diversity one lower bound (3.60) is exponentially decreasing with K . This concludes the proof. \square

Before going further in the analysis of MMSE-CPSC, let us illustrate the last proposition. For $K = 8$, the average (computed numerically) of the expression (3.14) over the channel statistic is given in Fig. 3.6 for different values of L . The expression (3.60) is also depicted in Fig. 3.6. We see that the expression (3.60) is an accurate approximation of the diversity one lower bound of (3.14), and that for any value of L (even though it was derived for $L = K$).

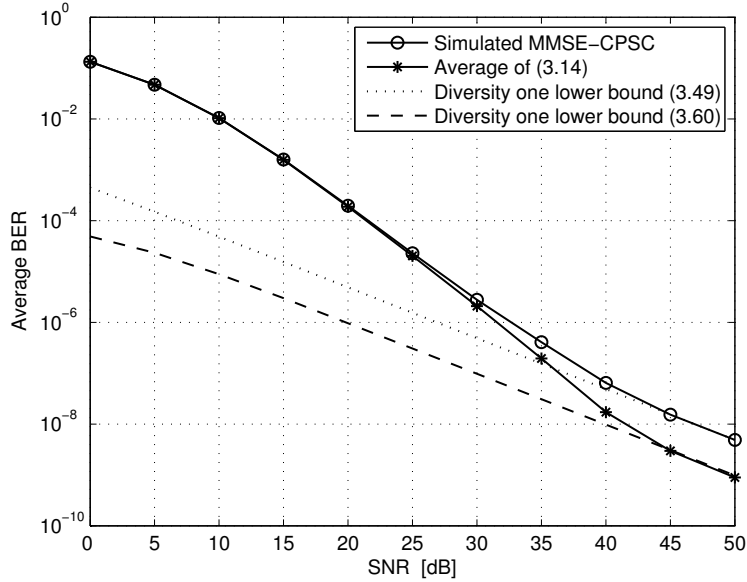


Figure 3.7 MMSE-CPSC: comparison of the simulated average BER with the average of the expression (3.14), for $K = 8$ and $L = 2$.

At this point, an important comment has to be made. It is obvious that MMSE-CPSC will never outperform ML-CPSC. However, it turns out that the diversity one lower bound (3.60) associated with the average of (3.14) is lower than the diversity one lower bound (3.49) of ML-CPSC. The explanation is quite simple: for the vectors in Table 3.1 responsible for the asymptotical diversity order one of ML-CPSC, the Gaussian assumption for the ISI associated with the MMSE receiver no longer holds. In other words, for those vectors, the expression (3.14) is not valid. However, the fact that (3.60) is lower than (3.49) is a good news: first, it suggests that the MMSE receiver might be able to reach the same diversity one lower bound as the ML receiver. And second, since this last lower bound is exponentially decreasing with K , it suggests that MMSE-CPSC might also be able to extract the multipath diversity for the range of BER typically used in practice, and for sufficiently large values of K . Let us verify these two comments by simulations:

- Let us suppose that $K = 8$ and $L = 2$. Fig. 3.7 shows the average of the approximated BER (3.14) over the channel statistic (computed numerically), the simulated average BER of MMSE-CPSC, along with both lower bounds (3.49) and (3.60). It can be seen that, at first, the average of (3.14) fits very well the true (simulated) MMSE-CPSC average BER. At higher SNR, we see that the simulated average BER obviously does not cross the diversity one lower bound (3.49) of ML-CPSC, but more interestingly tends to equal this bound. In that sense, the MMSE receiver can be seen as optimal (in terms of average BER) at high SNR for CPSC (since it reaches the same performance as the ML detection).
- Let us now increase the block size to a more realistic value: $K = 64$. The simulated average BER is drawn in Fig. 3.8, for $L = 2$ and 3. For such value of K , thanks to Propositions 3.5 and 3.8, both diversity one lower bounds (3.49) and (3.60) take very low values, such that they are not even included in Fig. 3.8. As a consequence, these bounds do not have any influence on the performance of MMSE-CPSC for the range of BER values considered in Fig. 3.8. In particular, it can be seen that the full diversity (slope minus two and three, for $L = 2$ and 3, respectively) is reached.

The main result of this subsection is summarized in the following observation.

Observation 3.9. *For sufficiently large values of K , the multipath diversity can be extracted by MMSE-CPSC for the range of BER values typically used in practice.*

3.4 Conclusions

This Chapter first derived the expressions of the instantaneous BER for the OFDM and CPSC schemes introduced in Chapter 2. After that, OFDM and CPSC were compared in terms in BER, for a fixed bit rate and without CSIT.

In terms of instantaneous BER, the best-performing scheme is DFE-CPSC (if the error propagation effect is neglected), followed by MMSE-CPSC. The worst-performing schemes are OFDM and ZF-CPSC. The comparison between these last two schemes is very much interesting: there exists a SNR

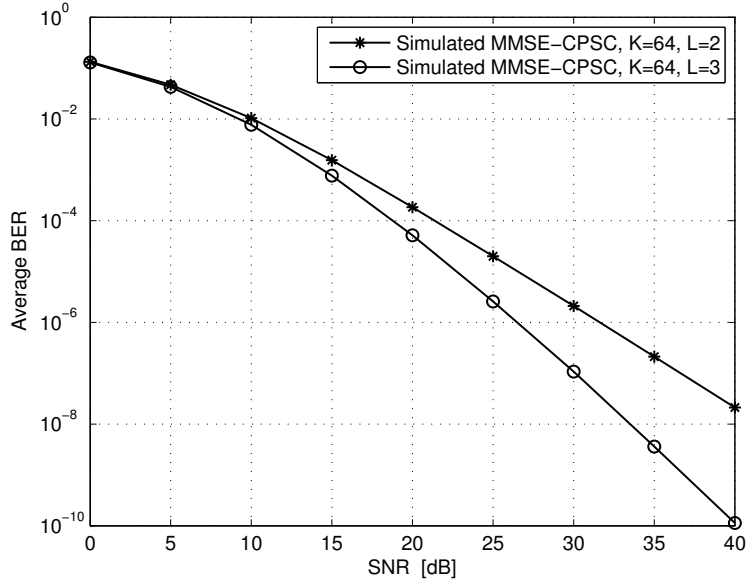


Figure 3.8 MMSE-CPSC: simulated average BER for $K = 64$ and $L = 2$ or 3 .

value below which OFDM outperforms ZF-CPSC, and above which ZF-CPSC outperforms OFDM. The value of this transition SNR depends much on the channel realization, and can tend to infinity for channels presenting a null gain at some frequency index.

In the context of digital wireless communications, it was important to go one step further, and to integrate the fading of the channel in the analysis. The figure of merit was then the average BER. In particular, a performance indicator directly related to the average BER is the diversity order extracted by the system. The following properties were shown in this chapter.

- The OFDM modulation does not extract any multipath diversity.
- For reasonably large values of K , the multipath diversity can be extracted by ML-CPSC for the range of BER values typically used in practice.

- The use of a ZF linear receiver in a CPSC system prevents the extraction of any multipath diversity.
- For sufficiently large values of K , the multipath diversity can be extracted by MMSE-CPSC for the range of BER values typically used in practice.

As a conclusion, in terms of average BER, the MMSE linear receiver achieves the best performance/complexity trade-off in a CPSC system. It generates a major average BER improvement with respect to OFDM.

Appendix 3.A Detailed calculations

3.A.1 Derivation of (3.34)

Even though the result of Proposition 3.4 is well known (see e.g. [31]), the reader might be interested in finding here its detailed demonstration. With the definition of the Gaussian Q-function, the integral (3.33) is rewritten as

$$\frac{1}{\sqrt{2\pi}} \int_0^\infty \left(\int_{\sqrt{2\gamma x}}^\infty e^{-\frac{y^2}{2}} dy \right) e^{-x} dx. \quad (3.61)$$

By using the substitution $z = \frac{y^2}{2\gamma x}$, we rewrite (3.61) as

$$\frac{1}{\sqrt{2\pi}} \int_0^\infty \left(\int_1^\infty e^{-\gamma x z} \frac{dz}{\sqrt{z}} \frac{\sqrt{\gamma x}}{\sqrt{2}} \right) e^{-x} dx \quad (3.62)$$

$$= \frac{1}{\sqrt{\pi}} \int_1^\infty \left(\int_0^\infty e^{-x(\gamma z+1)} \frac{\sqrt{x}}{2} dx \right) \sqrt{\gamma} \frac{dz}{\sqrt{z}}. \quad (3.63)$$

The integral in parentheses in (3.63) can be calculated as

$$\int_0^\infty e^{-x(\gamma z+1)} \frac{\sqrt{x}}{2} dx = \int_0^\infty e^{-w^2(\gamma z+1)} w^2 dw \quad (3.64)$$

$$= \frac{\sqrt{\pi}/2}{2(\gamma z+1)^{3/2}}, \quad (3.65)$$

where (3.64) comes from the substitution $w = \sqrt{x}$, and (3.65) can be deduced from most tables of definite integrals. Consequently, (3.63) becomes

$$\frac{1}{2} \int_1^\infty \frac{\sqrt{\gamma}}{2(\gamma z + 1)^{3/2}} \frac{1}{\sqrt{z}} dz = \frac{1}{2} \int_\gamma^\infty \frac{1}{2(v+1)^{3/2}} \frac{1}{\sqrt{v}} dv \quad (3.66)$$

$$= \frac{1}{2} \left[\frac{\sqrt{v}}{\sqrt{v+1}} \right]_\gamma^\infty \quad (3.67)$$

$$= \frac{1}{2} \left(1 - \sqrt{\frac{\gamma}{\gamma+1}} \right) \quad (3.68)$$

where the substitution $v = \gamma z$ has been used in (3.66). Finally, (3.68) proofs (3.34).

3.A.2 Derivation of (3.46)

The integral (3.45) is equal to the one in (3.33) where γ is replaced by $K\gamma$. Substituting γ by $K\gamma$ in (3.34) gives (3.46).

3.A.3 Derivation of (3.60)

In this subsection, we provide the detailed derivation of (3.60). With the definition of the Gaussian Q-function and by denoting $x = K \min_k (h_k)$ (whose pdf is given by $T_x(x) = e^{-x}$, see Appendix 3.B), the integral (3.59) is rewritten as

$$\frac{1}{\sqrt{2\pi}} \int_0^\infty \left(\int_{\sqrt{2(K-1)+2\gamma x}}^\infty e^{-\frac{y^2}{2}} dy \right) e^{-x} dx \quad (3.69)$$

Let us focus first on the integral in parentheses, we successively calculate:

$$\int_{\sqrt{2(K-1)+2\gamma x}}^\infty e^{-\frac{y^2}{2}} dy = \int_{\sqrt{2\gamma x}}^\infty e^{-\frac{z^2}{2}} e^{-(K-1)} \frac{z}{\sqrt{z^2 + 2(K-1)}} dz \quad (3.70)$$

$$\cong \int_{\sqrt{2\gamma x}}^\infty e^{-\frac{z^2}{2}} e^{-(K-1)} \frac{z}{\sqrt{2(K-1)}} dz \quad (3.71)$$

$$\cong \frac{e^{-(K-1)}}{\sqrt{2(K-1)}} \left[-e^{-\frac{z^2}{2}} \right]_{\sqrt{2\gamma x}}^\infty \quad (3.72)$$

$$\cong \frac{e^{-(K-1)}}{\sqrt{2(K-1)}} e^{-\gamma x} . \quad (3.73)$$

In (3.70), the substitution $z^2 = y^2 - 2(K-1)$ has been used. The approximation (3.71) is justified by the fact that the smallest values of z will contribute

most to the integral such that $\sqrt{z^2 + 2(K-1)} \cong \sqrt{2(K-1)}$. Consequently (3.69) approximatively becomes

$$\begin{aligned} \frac{1}{\sqrt{2\pi}} \frac{e^{-(K-1)}}{\sqrt{2(K-1)}} \int_0^\infty e^{-x(\gamma+1)} dx &= \frac{1}{\sqrt{2\pi}} \frac{e^{-(K-1)}}{\sqrt{2(K-1)}} \frac{1}{\gamma+1} \left[-e^{-x(\gamma+1)} \right]_0^\infty \\ &= \frac{e^{-(K-1)}}{\sqrt{4\pi(K-1)}} \frac{1}{\gamma+1} \end{aligned} \quad (3.74)$$

which proofs (3.60).

Appendix 3.B Derivation of the pdf of $x = K \min_k (h_k)$

Let us first compute the cumulative distribution function (cdf) $F_y(y)$ of the variable $y = \min_k (h_k)$:

$$F_y(y) = \text{Prob} (\text{at least one } h_k \text{ smaller than } y) \quad (3.75)$$

$$= 1 - \text{Prob} (\text{all } h_k \text{ greater than } y) \quad (3.76)$$

$$= 1 - (1 - F_h(y))^K \quad (3.77)$$

where the last equality holds only if the h_k are uncorrelated, i.e. if $L = K$. Taking the derivative with respect to y , the last relation can be written in terms of pdf

$$T_y(y) = K (1 - F_h(y))^{K-1} T_h(y). \quad (3.78)$$

Inserting the pdf (3.31) into (3.78) gives

$$T_y(y) = K e^{-Ky}. \quad (3.79)$$

And finally taking into account that $x = K \min_k (h_k) = Ky$, we have

$$T_x(x) = \frac{1}{K} T_y\left(\frac{x}{K}\right) = e^{-x}. \quad (3.80)$$

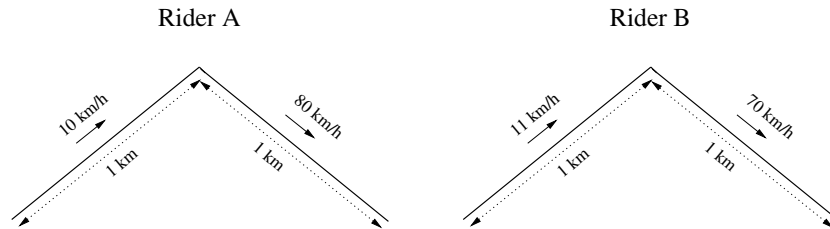


Figure 3.9 Tour de France.

Appendix 3.C The harmonic mean - an every day life example

The harmonic mean of the positive real entries of a vector $\mathbf{x} = [x_0, x_1, \dots, x_{K-1}]^T$ is defined as

$$H(\mathbf{x}) = \frac{1}{\frac{1}{K} \sum_{k=0}^{K-1} \frac{1}{x_k}}. \quad (3.81)$$

At the end of Subsection 3.3.3, it was said that the harmonic mean of a set of positive real values was mainly influenced by the lowest values in the set. Let us illustrate this statement by an every day life example, and consider the situation in Fig. 3.9: two bicycle riders at the "Tour de France" are climbing and then descending a mountain. Both the climb and the descent are assumed to be 1km long. The rider A has a climbing speed of 10km/h, while its descending speed is 80km/h. On the other hand, the rider B is a little better at climbing with a 11km/h speed, but is however much worse at descending with only a 70km/h speed. The riders average speed for this 2km ride are, respectively,

$$\text{Rider A: } \frac{2\text{km}}{\frac{1\text{km}}{10\text{km/h}} + \frac{1\text{km}}{80\text{km/h}}} = \frac{1}{\frac{1}{2} \left(\frac{1}{10} + \frac{1}{80} \right)} \text{ km/h} = 17.8\text{km/h} \quad (3.82)$$

$$\text{Rider B: } \frac{2\text{km}}{\frac{1\text{km}}{11\text{km/h}} + \frac{1\text{km}}{70\text{km/h}}} = \frac{1}{\frac{1}{2} \left(\frac{1}{11} + \frac{1}{70} \right)} \text{ km/h} = 19.0\text{km/h} \quad (3.83)$$

which are nothing else than the harmonic mean of their climbing and descending speeds. With this every day life example, we want to illustrate that the

harmonic mean is much more influenced by the low values than by the high ones: even though it is much slower at descending, the rider B will win this race thanks to its 1km/h increase in the climbing speed with respect to the rider A. As a consequence, the best climber is quite naturally expected to win the "Tour de France", not the best descender!

Achievable Bit Rate

4

The content of this chapter has been published in part in [25].

4.1 Introduction

In Chapter 3, it was assumed that there was no CSI at the transmitter side (CSIT). Let us now consider the opposite: the channel is assumed to be perfectly known at both the transmitter and receiver sides. This knowledge allows the use of adaptive transmit signal processing. By adaptive transmit signal processing, we mean any strategy that instantaneously adjusts how the information is sent, to the instantaneous channel state. In this chapter, however, we will restrict ourselves to using the CSIT to adaptively allocate the bits to the different transmitted symbols of a block. Note that the terminology "bit loading" is often used.

The OFDM and CPSC systems were compared in Chapter 3 in terms of achievable BER for a given bit rate. In a dual fashion, this chapter is dedicated to comparing the achievable bit rate for a given target BER. Note that all the derivations will be done for one given channel realization. That is, the variability of the channel will not be integrated in the discussion. The results of this chapter extend the work in [24], where the achievable bit rates of OFDM and CPSC were compared for the SISO case and for the high SNR regime. Our contribution is twofold: it extends the comparison to any SNR value, and to the MIMO case.

The remainder of this chapter is organized as follows. Before entering the core of the problem and for ease of presentation, Section 4.2 starts by presenting and deriving the mathematical properties which will be used in this chapter. In particular, the majorization theory [75] will be extensively used. Next, the mathematical formulation of the achievable bit rate for a given target BER is reiterated in Section 4.3. Finally, Section 4.4 analytically compares OFDM and CPSC (with the different possible receivers) in terms of achievable bit rate, and that both for the SISO and MIMO cases.

4.2 Mathematical preliminaries

This section is devoted to first briefly reminding the basics of the majorization theory, and second to deriving some relations between the Cholesky and the eigenvalue decompositions of a positive definite Hermitian matrix (both without and with the circulant property).

4.2.1 Majorization theory

All the material of this subsection can be found in [75], to which the reader should refer for further details and proofs.

The basic idea behind the majorization theory is to quantify the imprecise notion that the component of a vector \mathbf{x} are "less spread out" or "more nearly equal" than the components of another vector \mathbf{y} , and to develop properties associated with this notion. In particular, this elegant theory is based on the following definition.

Definition 4.1. (1.A.1 in [75]) For $\mathbf{x}, \mathbf{y} \in \mathbb{R}^K$, \mathbf{y} is said to majorize \mathbf{x} , and is denoted by $\mathbf{x} \prec \mathbf{y}$, if

$$\sum_{i=0}^{N-1} x_{[i]} \leq \sum_{i=0}^{N-1} y_{[i]}, \quad N = 1, \dots, K-1 \quad (4.1)$$

$$\sum_{i=0}^{K-1} x_{[i]} = \sum_{i=0}^{K-1} y_{[i]} \quad (4.2)$$

where $x_{[0]} \geq x_{[1]} \geq \dots \geq x_{[K-1]}$ denote the components of \mathbf{x} in decreasing order.

Equivalently, $\mathbf{x} \prec \mathbf{y}$, if

$$\sum_{i=0}^{N-1} x_{(i)} \geq \sum_{i=0}^{N-1} y_{(i)}, \quad N = 1, \dots, K-1 \quad (4.3)$$

$$\sum_{i=0}^{K-1} x_{(i)} = \sum_{i=0}^{K-1} y_{(i)} \quad (4.4)$$

where $x_{(0)} \leq x_{(1)} \leq \dots \leq x_{(K-1)}$ denote the components of \mathbf{x} in increasing order.

On the basis of this definition, we can immediately develop the following straightforward property which will be used later in this chapter.

Property 4.2. For any $\mathbf{x}, \mathbf{y} \in \mathbb{R}^K$,

$$\mathbf{x} \prec \mathbf{y} \quad \Rightarrow \quad -\mathbf{x} \prec -\mathbf{y} \quad (4.5)$$

Proof. Starting from (4.1), we deduce that $\sum_{i=0}^{N-1} -x_{[i]} \geq \sum_{i=0}^{N-1} -y_{[i]}$, for any $N \in \{1, \dots, K-1\}$. Then realizing that $-x_{[i]} = (-x)_{(i)}$ and $-y_{[i]} = (-y)_{(i)}$, we write

$$\sum_{i=0}^{N-1} (-x)_{(i)} \geq \sum_{i=0}^{N-1} (-y)_{(i)}, \quad N = 1, \dots, K-1. \quad (4.6)$$

Also, obviously,

$$\sum_{i=0}^{K-1} (-x)_{(i)} = -\sum_{i=0}^{K-1} x_{(i)} = -\sum_{i=0}^{K-1} y_{(i)} = \sum_{i=0}^{K-1} (-y)_{(i)}. \quad (4.7)$$

On the basis of the definitions (4.3)-(4.4) of majorization, we deduce from (4.6)-(4.7) that $-\mathbf{x} \prec -\mathbf{y}$. \square

Another crucial notion in the majorization theory is that of Schur-convex functions. It is defined as follows.

Definition 4.3. (3.A.1 in [75]) A real-valued function ϕ defined on a set $\mathcal{A} \subset \mathbb{R}^K$ is said to be Schur-convex on \mathcal{A} if

$$\mathbf{x} \prec \mathbf{y} \quad \text{on } \mathcal{A} \quad \Rightarrow \quad \phi(\mathbf{x}) \leq \phi(\mathbf{y}). \quad (4.8)$$

In the sequel, we will need the following two propositions, which give sufficient conditions for a function to be Schur-convex.

Proposition 4.4. (3.C.1 in [75]) *If $\mathcal{I} \subset \mathbb{R}$ is an interval and $g : \mathcal{I} \rightarrow \mathbb{R}$ is convex, then*

$$\phi(\mathbf{x}) = \sum_{k=0}^{K-1} g(x_k) \quad (4.9)$$

is Schur-convex on \mathcal{I}^K . Consequently, $\mathbf{x} \prec \mathbf{y}$ on \mathcal{I}^K implies $\phi(\mathbf{x}) \leq \phi(\mathbf{y})$.

Proof. The proof can be found in [75]. □

Proposition 4.5. (3.H.2 in [75]) *Let $\mathcal{D} = \{\mathbf{x} : x_0 \geq x_1 \geq \dots \geq x_{K-1}\}$, and let $\phi(\mathbf{x}) = \sum_{k=0}^{K-1} g_k(x_k)$, $\mathbf{x} \in \mathcal{D}$, where each $g_k : \mathbb{R} \rightarrow \mathbb{R}$ is differentiable. Then ϕ is Schur-convex on \mathcal{D} if and only if*

$$g'_k(a) \geq g'_{k+1}(b) \quad \text{whenever } a \geq b, \quad k = 0, \dots, K-2. \quad (4.10)$$

Proof. The proof can be found in [75]. □

4.2.2 Relation between the Cholesky and eigenvalue decompositions

This subsection presents/derives various properties, first for any positive definite Hermitian matrix, and then for such matrices with, besides, the circulant property.

4.2.2.1 For any positive definite Hermitian matrix

Any positive definite Hermitian matrix \mathbf{H} is equivalently defined by its eigenvalue and Cholesky decompositions, which are respectively given by

$$\mathbf{H} = \mathbf{V}\mathbf{\Lambda}\mathbf{V}^H \quad (4.11)$$

$$\mathbf{H} = \mathbf{L}\mathbf{D}\mathbf{L}^H \quad (4.12)$$

where both matrices $\mathbf{\Lambda}$ and \mathbf{D} are diagonal, \mathbf{V} is a unitary matrix, and \mathbf{L} is a unit lower triangular matrix. Obviously there must be some relation between the diagonal elements of the matrices $\mathbf{\Lambda}$ and \mathbf{D} . First, the product of these

elements is equal for both matrices, as described in the following proposition.

Proposition 4.6. *Let \mathbf{H} be a $K \times K$ Hermitian positive definite matrix whose eigenvalue and Cholesky decompositions are respectively given by $\mathbf{H} = \mathbf{V}\mathbf{\Lambda}\mathbf{V}^H$ and $\mathbf{H} = \mathbf{L}\mathbf{D}\mathbf{L}^H$. Then, the diagonal matrices $\mathbf{\Lambda} = \text{diag}(\lambda)$ and $\mathbf{D} = \text{diag}(\delta)$ are such that the following relations hold*

$$(i) \quad \prod_{k=0}^{K-1} \lambda_k = \prod_{k=0}^{K-1} \delta_k \quad (4.13)$$

$$(ii) \quad \prod_{k=0}^{K-1} \frac{1}{\lambda_k} = \prod_{k=0}^{K-1} \frac{1}{\delta_k}. \quad (4.14)$$

Proof. Let us proof these relations successively:

(i) We easily establish the equality

$$\prod_{k=0}^{K-1} \lambda_k = \det(\mathbf{\Lambda}) \quad (4.15)$$

$$= \det(\mathbf{V}\mathbf{\Lambda}\mathbf{V}^H) \quad (4.16)$$

$$= \det(\mathbf{L}\mathbf{D}\mathbf{L}^H) \quad (4.17)$$

$$= \det(\mathbf{D}) \quad (4.18)$$

$$= \prod_{k=0}^{K-1} \delta_k. \quad (4.19)$$

The equality (4.16) is due to the multiplicative property of the determinant (for square matrices), together with the unitary property of \mathbf{V} . Similarly, the equality (4.18) follows from the multiplicative property of the determinant again, together with the fact that \mathbf{L} (resp. \mathbf{L}^H) is a unit lower (resp. upper) triangular matrix such that its determinant is equal to 1.

(ii) In a very similar way, we have

$$\prod_{k=0}^{K-1} \frac{1}{\lambda_k} = \det(\mathbf{\Lambda}^{-1}) \quad (4.20)$$

$$= \det(\mathbf{V}\mathbf{\Lambda}^{-1}\mathbf{V}^H) \quad (4.21)$$

$$= \det(\mathbf{H}^{-1}) \quad (4.22)$$

$$= \det(\mathbf{L}^{H,-1} \mathbf{D}^{-1} \mathbf{L}^{-1}) \quad (4.23)$$

$$= \det(\mathbf{D}^{-1}) \quad (4.24)$$

$$= \prod_{k=0}^{K-1} \frac{1}{\delta_k} \quad (4.25)$$

where, besides the properties already mentioned in the proof of part (i), we have used the multiplicative property of the matrix inverse (for square matrices) and the fact that \mathbf{L}^{-1} (resp. $\mathbf{L}^{H,-1}$) is also a unit lower (resp. upper) triangular matrix such that its determinant is, once more, equal to 1.

□

There is actually a much stronger relation than that of Proposition 4.6 that connects the elements of $\mathbf{\Lambda}$ and \mathbf{D} , as described in the following proposition.

Proposition 4.7. *Under the same conditions as in Proposition 4.6, λ logarithm-majorizes δ , denoted by $\log_2(\delta) \prec \log_2(\lambda)$, i.e.¹*

$$[\log_2(\delta_0), \dots, \log_2(\delta_{K-1})]^T \prec [\log_2(\lambda_0), \dots, \log_2(\lambda_{K-1})]^T \quad (4.26)$$

which is equivalent to

$$\prod_{i=0}^{N-1} \delta_{[i]} \leq \prod_{i=0}^{N-1} \lambda_{[i]}, \quad N = 1, \dots, K-1 \quad (4.27)$$

$$\prod_{i=0}^{K-1} \delta_{[i]} = \prod_{i=0}^{K-1} \lambda_{[i]}. \quad (4.28)$$

In other words, λ majorizes δ in the product sense.

Proof. The proof can be found in [76].

□

Note that the binary logarithm was used in Proposition 4.7, but the proposition remains valid for any other logarithm base. In addition, Proposition 4.7 has the following corollary.

¹When using the notation $\log_2(\mathbf{x})$, we refer to taking the logarithm of each element of the vector \mathbf{x} .

Corollary 4.8. *Under the same conditions as in Proposition 4.6, we have that*

$$[\log_2(\frac{1}{\delta_0}), \dots, \log_2(\frac{1}{\delta_{K-1}})]^T \prec [\log_2(\frac{1}{\lambda_0}), \dots, \log_2(\frac{1}{\lambda_{K-1}})]^T \quad (4.29)$$

i.e.

$$\prod_{i=0}^{N-1} \frac{1}{\delta_{(i)}} \leq \prod_{i=0}^{N-1} \frac{1}{\lambda_{(i)}}, \quad N = 1, \dots, K-1 \quad (4.30)$$

$$\prod_{i=0}^{K-1} \frac{1}{\delta_{(i)}} = \prod_{i=0}^{K-1} \frac{1}{\lambda_{(i)}}. \quad (4.31)$$

Proof. Applying Property 4.2 to (4.26) gives (4.29) □

At this point, we have all we need to cope with the main contribution of this section, which is presented in the following proposition and corollary. As far as we are aware, this result might even be somewhat novel as a pure mathematical contribution.

Proposition 4.9. *Under the same conditions as in Proposition 4.6, and for any $\alpha \geq 0$, the following inequality holds*

$$\sum_{k=0}^{K-1} \log_2(\alpha + \delta_k) \leq \sum_{k=0}^{K-1} \log_2(\alpha + \lambda_k). \quad (4.32)$$

Proof. Consider the function $g(z) = \log_2(\alpha + 2^z)$. It can be easily verified that it is a convex function for $\alpha \geq 0$. Then, by Proposition 4.4, the function $\phi(\mathbf{x}) = \sum_{k=0}^{K-1} \log_2(\alpha + 2^{x_k})$ is Schur-convex. From Proposition 4.7 we know that $\log_2(\delta) \prec \log_2(\lambda)$, which implies by Proposition 4.3 that

$$\phi(\log_2(\delta)) \leq \phi(\log_2(\lambda)) \quad (4.33)$$

or, finally,

$$\sum_{k=0}^{K-1} \log_2(\alpha + 2^{\log_2(\delta_k)}) \leq \sum_{k=0}^{K-1} \log_2(\alpha + 2^{\log_2(\lambda_k)}) \quad (4.34)$$

$$\sum_{k=0}^{K-1} \log_2(\alpha + \delta_k) \leq \sum_{k=0}^{K-1} \log_2(\alpha + \lambda_k). \quad (4.35)$$

□

We have finally opted for a proof of Proposition 4.9 based on the majorization theory. However, before being aware of this elegant theory, we had derived another proof for Proposition 4.9, which can be found in Appendix 4.A.

Corollary 4.10. *Under the same conditions as in Proposition 4.6, and for any $\alpha \geq 0$, the following inequality holds*

$$\sum_{k=0}^{K-1} \log_2\left(\alpha + \frac{1}{\delta_k}\right) \leq \sum_{k=0}^{K-1} \log_2\left(\alpha + \frac{1}{\lambda_k}\right). \quad (4.36)$$

Sketch of Proof. The corollary is easily demonstrated by applying the same proof as the one of Proposition 4.9, starting from Corollary 4.8 (instead of from Proposition 4.7). \square

4.2.2.2 For any positive definite Hermitian circulant matrix

If the positive definite Hermitian matrix is circulant, further properties can be established. They are summarized in the following two propositions.

Proposition 4.11. *Let \mathbf{H}_c be a $K \times K$ positive definite Hermitian circulant matrix whose eigenvalue and Cholesky decompositions are respectively given by $\mathbf{H}_c = \mathbf{W}^H \mathbf{\Lambda} \mathbf{W}$ and $\mathbf{H}_c = \mathbf{L} \mathbf{D} \mathbf{L}^H$, with $\mathbf{\Lambda} = \text{diag}(\lambda)$ and $\mathbf{D} = \text{diag}(\delta)$. The elements of δ are with decreasing values $\delta_0 \geq \delta_1 \geq \dots \geq \delta_{K-1}$, and in particular δ_0 (resp. δ_{K-1}) is equal to the arithmetic (resp. harmonic) mean of the elements of λ*

$$(i) \quad \delta_0 = \frac{1}{K} \sum_{k=0}^{K-1} \lambda_k \quad (4.37)$$

$$(ii) \quad \delta_{K-1} = \frac{1}{\frac{1}{K} \sum_{k=0}^{K-1} \frac{1}{\lambda_k}}. \quad (4.38)$$

Proof.

(i) Quite straightforwardly,

$$\delta_0 = [\mathbf{LDL}^H]_{0,0} \quad (4.39)$$

$$= [\mathbf{W}^H \mathbf{\Lambda} \mathbf{W}]_{0,0} \quad (4.40)$$

$$= \frac{1}{K} \text{trace}(\mathbf{W}^H \mathbf{\Lambda} \mathbf{W}) \quad (4.41)$$

$$= \frac{1}{K} \sum_{k=0}^{K-1} \lambda_k. \quad (4.42)$$

(ii) In a similar way,

$$\frac{1}{\delta_{K-1}} = [\mathbf{D}^{-1}]_{K-1,K-1} \quad (4.43)$$

$$= [\mathbf{L}^{H,-1} \mathbf{D}^{-1} \mathbf{L}^{-1}]_{K-1,K-1} \quad (4.44)$$

$$= [\mathbf{W}^H \mathbf{\Lambda}^{-1} \mathbf{W}]_{K-1,K-1} \quad (4.45)$$

$$= \frac{1}{K} \text{trace}(\mathbf{W}^H \mathbf{\Lambda}^{-1} \mathbf{W}) \quad (4.46)$$

$$= \frac{1}{K} \sum_{k=0}^{K-1} \frac{1}{\lambda_k}. \quad (4.47)$$

□

Finally, Proposition 4.11 has the following corollary.

Corollary 4.12. *Under the same conditions as in Proposition 4.11, The diagonal elements of \mathbf{D} and $\mathbf{\Lambda}$ verify*

$$(i) \quad \sum_{k=0}^{K-1} \delta_k \leq \sum_{k=0}^{K-1} \lambda_k \quad (4.48)$$

$$(ii) \quad \sum_{k=0}^{K-1} \frac{1}{\delta_k} \leq \sum_{k=0}^{K-1} \frac{1}{\lambda_k}. \quad (4.49)$$

Proof. Using equations (4.37) and (4.38), it is quite straightforward to establish (4.48) and (4.49):

$$(i) \quad \sum_{k=0}^{K-1} \delta_k \leq K \delta_0 \quad (4.50)$$

$$= \sum_{k=0}^{K-1} \lambda_k. \quad (4.51)$$

$$(ii) \quad \sum_{k=0}^{K-1} \frac{1}{\delta_k} \leq K \frac{1}{\delta_{K-1}} \quad (4.52)$$

$$= \sum_{k=0}^{K-1} \frac{1}{\lambda_k}. \quad (4.53)$$

□

We are aware that this purely mathematical section was probably not smoothly readable, and that, at this point, the reader does not see clearly the objective pursued. Hopefully, things will become clearer in the remainder of this chapter. After all, this section had to be seen as nothing more than a collection of mathematical results which will be useful next.

4.3 Bit rate formulation

This section reminds the mathematical formulation of the achievable bit rate for a given target BER.

It has been shown that, for commonly used constellations (e.g. QAM), the achievable bit rate under a target BER can be approximated by the same mathematical formulation as the capacity of the Gaussian channel with a SNR reduced by the so called SNR gap [77–79]

$$b = \log_2 \left(1 + \frac{\text{SNR}}{\Gamma} \right) \quad (4.54)$$

where b is the number of bits that can be transmitted per symbol at the target BER, and the SNR gap Γ is a constant ($\Gamma \geq 1$) which is directly related to the target BER: the larger Γ , the lower the BER will be. Note that if $\Gamma = 1$, the expression (4.54) reduces indeed to the well-known formula of the capacity of the Gaussian channel [26].

Obviously, the expression (4.54) for the bit rate inherently assumes the presence of adaptive bit loading. On top of that, it is important to remember that two hypotheses are associated with the use of (4.54):

1. It is assumed in (4.54) that the residual noise plus interference affecting the transmission is Gaussian.
2. For the discrete constellations used in practice (e.g. QAM), the number of bits transmitted per symbol is an integer value. This constraint is obviously relaxed in (4.54): in fact, b in (4.54) continuously spans all real positive values, as the SNR varies from 0 to ∞ .

4.4 Bit rate comparison

This section finally enters the core of the problem treated in this chapter: it compares OFDM with the different variants of CPSC in terms of achievable bit rate. The focus is set successively on SISO and MIMO systems.

4.4.1 SISO

Remember that no adaptive power loading but only bit loading is considered in this chapter. In other words, the power is uniformly allocated to the K symbols of the data block \mathbf{d} . This was also assumed in the scenarios that were studied in Chapters 2 and 3. Consequently, inserting the SNR expressions (3.4), (3.9), (3.13) and (3.15) into (4.54), we straightforwardly get the expressions of the achievable mean bit rate (the mean being taken over all K symbols of the block) for the different schemes:

$$b_{\text{ZF}}^{\text{CPSC}} = \log_2 \left(1 + \frac{1}{\frac{\Gamma}{K} \sum_{k=0}^{K-1} \frac{1}{\gamma h_k}} \right) \quad (4.55)$$

$$b_{\text{MMSE}}^{\text{CPSC}} = \log_2 \left(\left(1 - \frac{1}{\Gamma} \right) + \frac{1}{\frac{\Gamma}{K} \sum_{k=0}^{K-1} \frac{1}{\gamma h_k + 1}} \right) \quad (4.56)$$

$$b_{\text{DFE}}^{\text{CPSC}} = \frac{1}{K} \sum_{k=0}^{K-1} \log_2 \left(\left(1 - \frac{1}{\Gamma} \right) + \frac{\gamma}{\Gamma [\mathbf{D}]_{k,k}} \right) \quad (4.57)$$

$$b^{\text{OFDM}} = \frac{1}{K} \sum_{k=0}^{K-1} \log_2 \left(1 + \frac{\gamma h_k}{\Gamma} \right) . \quad (4.58)$$

with \mathbf{D} defined in (2.60). Quite naturally, and this is precisely the objective of this chapter, we are interested in analytically comparing the achievable bit rate expressions (4.55)-(4.58). This comparison results in the following important proposition.

Proposition 4.13. *At all SNR, the following inequalities hold*

$$b_{ZF}^{CPSC} \stackrel{(i)}{\leq} b_{MMSE}^{CPSC} \stackrel{(ii)}{\leq} b_{DFE}^{CPSC} \stackrel{(iii)}{\leq} b^{OFDM}. \quad (4.59)$$

Proof. The inequality signs (i), (ii), and (iii) in (4.59) will be successively proved

- (i) The inequality is a direct consequence of (3.25) which was proved earlier.
- (ii) The inequality is a direct consequence of (3.29) and (3.30).
- (iii) Let us first reiterate and reorganize the bit rate expressions (4.58)

$$b^{OFDM} = \frac{1}{K} \sum_{k=0}^{K-1} \log_2 \left(1 + \frac{\gamma h_k}{\Gamma} \right) \quad (4.60)$$

$$= \frac{1}{K} \sum_{k=0}^{K-1} \log_2 \left(\left(1 - \frac{1}{\Gamma}\right) + \frac{\gamma h_k + 1}{\Gamma} \right). \quad (4.61)$$

Also, rescaling both sides of the equation (2.60) by a factor $\frac{\Gamma}{\gamma}$, we get

$$\mathbf{W}^H \Gamma (\gamma \boldsymbol{\Omega}^H \boldsymbol{\Omega} + \mathbf{I}_K)^{-1} \mathbf{W} = \mathbf{L} \frac{\Gamma \mathbf{D}}{\gamma} \mathbf{L}^H. \quad (4.62)$$

The left side of (4.62) is an eigenvalue decomposition whose diagonal matrix has $\frac{\Gamma}{\gamma h_k + 1}$ as k th diagonal element. The right side is a Cholesky decomposition whose diagonal matrix has $\frac{\Gamma [\mathbf{D}]_{k,k}}{\gamma}$ as k th element. Consequently, the inequality (4.57) \leq (4.61) is just a direct application of Corollary 4.10 to the matrix (4.62), with $\alpha = 1 - \frac{1}{\Gamma}$.

□

Let us stress that the inequalities in (4.59) are valid at all SNR. But interestingly, at high SNR some equalities hold, as summarized in the following proposition.

Proposition 4.14. *At high SNR, the following relations hold*

$$b_{ZF}^{CPSC} \stackrel{(i)}{=} b_{MMSE}^{CPSC} \leq b_{DFE}^{CPSC} \stackrel{(iii)}{=} b^{OFDM}. \quad (4.63)$$

Proof.

- (i) It is easy to see that expressions (4.55) and (4.56) meet for sufficiently large values of the SNR γ . This is nothing more than an illustration of the following well-known fact: for a given channel realization, the ZF and MMSE linear receivers coincide at high SNR.
- (iii) For large values of γ , the term $(1 - \frac{1}{\Gamma})$ can be neglected in (4.57) and (4.61). The equality is thus demonstrated if we prove that $\prod_{k=0}^{K-1} \frac{\gamma}{\Gamma |\mathbf{D}|_{k,k}} = \prod_{k=0}^{K-1} \frac{\gamma h_{k+1}}{\Gamma}$, which is a direct application of part (ii) of Proposition 4.6 to the matrix (4.62).

□

Proposition 4.14 establishes an important result: at high SNR and when bit loading only is allowed, the DFE receiver allows the CPSC scheme to equal OFDM in terms of achievable bit rate. This result was first presented in [24]. Our contribution here is the extension of this result to all SNR values, as described in Proposition 4.13. For completeness, note that all inequality signs in Propositions 4.13 and 4.14 trivially become equalities if the channel is flat fading, i.e. if $h_0 = h_1 = \dots = h_{K-1}$.

Let us illustrate Propositions 4.14 and 4.13 with a numerical example. Consider $K = 64$, $L = 4$, $\Gamma = 2$, and the channel realization \mathbf{B} of Fig. 3.1. The corresponding achievable bit rates (4.55)-(4.58) versus the SNR γ , are drawn in Fig. 4.1. First, we can observe Proposition 4.14: at high SNR, OFDM and DFE-CPSC perform identically. And so do ZF-CPSC and MMSE-CPSC. Second, a zoom of the low to moderate SNR region is also given in Fig. 4.1 in order to better illustrate Proposition 4.13: at all SNR, ZF-CPSC is outperformed by MMSE-CPSC, which in turn is outperformed by DFE-CPSC, which is finally outperformed by OFDM. However, we can see that the gap between DFE-CPSC and OFDM is much smaller than that between any other two strategies.

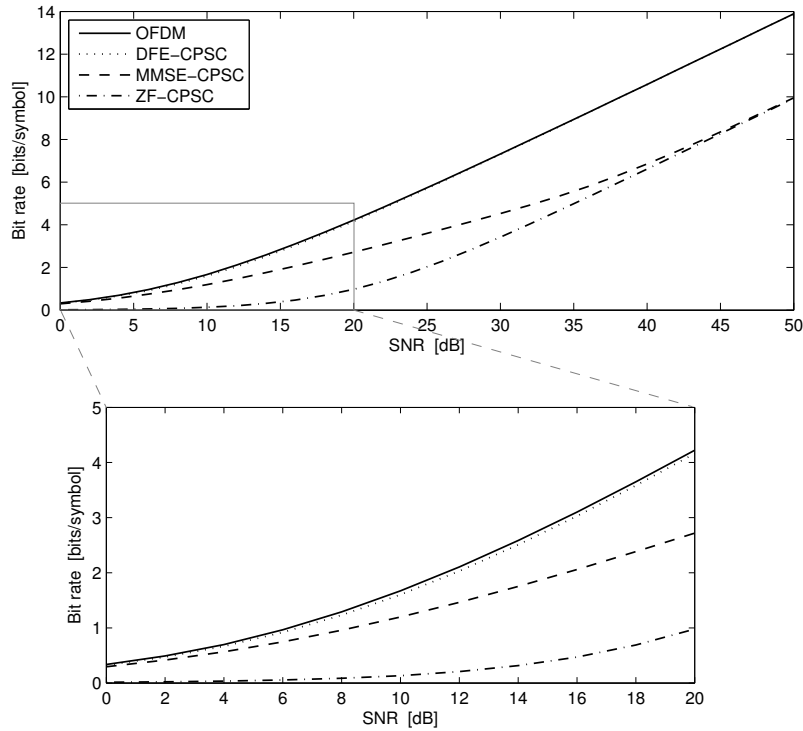


Figure 4.1 Achievable bit rates (4.55)-(4.58) for channel realization B in Fig. 3.1, for $K = 64$, $L = 4$ and $\Gamma = 2$.

4.4.2 MIMO

Last subsection showed that, in the SISO case, OFDM and DFE-CPSC achieve equal bit rate at high SNR. The goal here is to extend that result to the MIMO case. The content of this subsection was published in [25].

Let us restrict ourselves to comparing the three following schemes which were introduced in Chapter 2: MIMO MMSE-OFDM, DMMT and MIMO DFE-CPSC. From what has been presented in Subsections 2.5.1 and 2.5.2, we can derive the expressions of the achievable bit rate for these three schemes.

- MIMO MMSE-OFDM: the error covariance matrix associated with the estimate (2.71) is equal to $(\gamma \mathbf{\Omega}_b^H \mathbf{\Omega}_b + \mathbf{I}_{M_t K})^{-1}$. The unbiased SINRs can be deduced from the diagonal elements of this matrix, and introduced in (4.54) to get

$$b_{\text{MMSE}}^{\text{MIMO-OFDM}} = \frac{1}{M_t K} \sum_{k=0}^{M_t K-1} \log_2 \left(\left(1 - \frac{1}{\Gamma}\right) + \frac{1}{\Gamma [(\gamma \mathbf{\Omega}_b^H \mathbf{\Omega}_b + \mathbf{I}_{M_t K})^{-1}]_{k,k}} \right) \quad (4.64)$$

- DMMT: the estimate (2.76) is ISI free and its error covariance matrix is $\sigma_n^2 \mathbf{\Lambda}^{-1} \mathbf{\Lambda}^{-1,H}$, with $\mathbf{\Lambda}$ defined in (2.72). The corresponding mean achievable bit rate expression is

$$b^{\text{DMMT}} = \frac{1}{M_t K} \sum_{k=0}^{M_t K-1} \log_2 \left(1 + \frac{\gamma [\mathbf{\Lambda}^H \mathbf{\Lambda}]_{k,k}}{\Gamma} \right) \quad (4.65)$$

$$= \frac{1}{M_t K} \sum_{k=0}^{M_t K-1} \log_2 \left(\left(1 - \frac{1}{\Gamma}\right) + \frac{[\gamma \mathbf{\Lambda}^H \mathbf{\Lambda} + \mathbf{I}_{M_t K}]_{k,k}}{\Gamma} \right) \quad (4.66)$$

- MIMO DFE-CPSC: the error covariance matrix associated with this scheme is given by $\sigma_n^2 \mathbf{D}$, with \mathbf{D} defined in (2.80). The achievable mean bit rate is then

$$b_{\text{DFE}}^{\text{MIMO-CPSC}} = \frac{1}{M_t K} \sum_{k=0}^{M_t K-1} \log_2 \left(\left(1 - \frac{1}{\Gamma}\right) + \frac{\gamma}{\Gamma [\mathbf{D}]_{k,k}} \right) \quad (4.67)$$

We will focus only on the bit rate comparison at high SNR. The following proposition holds.

Proposition 4.15. *At high SNR, the following relations hold*

$$b_{\text{MMSE}}^{\text{MIMO-OFDM}} \leq b_{\text{DFE}}^{\text{MIMO-CPSC}} = b^{\text{DMMT}}. \quad (4.68)$$

Proof. At high SNR, the contribution of the term $(1 - \frac{1}{\Gamma})$ inside the logarithm can be neglected in (4.64), (4.66) and (4.67). We then successively calculate

■

$$b_{\text{MMSE}}^{\text{MIMO-OFDM}} \cong \frac{-1}{M_t K} \log_2 \left(\prod_{k=0}^{M_t K - 1} \Gamma \left[(\gamma \mathbf{\Omega}_b^H \mathbf{\Omega}_b + \mathbf{I}_{M_t K})^{-1} \right]_{k,k} \right) \quad (4.69)$$

$$\leq \frac{-1}{M_t K} \log_2 \left(\det \left(\Gamma (\gamma \mathbf{\Omega}_b^H \mathbf{\Omega}_b + \mathbf{I}_{M_t K})^{-1} \right) \right) \quad (4.70)$$

$$= \frac{1}{M_t K} \log_2 \left(\det \left(\frac{\gamma \mathbf{\Omega}_b^H \mathbf{\Omega}_b + \mathbf{I}_{M_t K}}{\Gamma} \right) \right) \quad (4.71)$$

where the inequality sign comes from Hadamard's inequality [56].

■

$$b^{\text{DMMT}} \cong \frac{1}{M_t K} \log_2 \left(\det \left(\frac{\gamma \mathbf{\Lambda}^H \mathbf{\Lambda} + \mathbf{I}_{M_t K}}{\Gamma} \right) \right) \quad (4.72)$$

$$= \frac{1}{M_t K} \log_2 \left(\det \left(\frac{\gamma \mathbf{\Omega}_b^H \mathbf{\Omega}_b + \mathbf{I}_{M_t K}}{\Gamma} \right) \right) \quad (4.73)$$

where the equality (4.73) is easily proved using (2.72) (and the unitary property of the matrices $\mathbf{\Pi}$, \mathbf{U} and \mathbf{V} therein).

■

$$b_{\text{DFE}}^{\text{MIMO-CPSC}} \cong \frac{1}{M_t K} \log_2 \left(\det \left(\frac{\gamma}{\Gamma} \mathbf{D}^{-1} \right) \right) \quad (4.74)$$

$$= \frac{1}{M_t K} \log_2 \left(\det \left(\frac{\gamma}{\Gamma} \mathbf{L}^{H,-1} \mathbf{D}^{-1} \mathbf{L}^{-1} \right) \right) \quad (4.75)$$

$$= \frac{1}{M_t K} \log_2 \left(\det \left(\frac{\gamma \mathbf{\Omega}_b^H \mathbf{\Omega}_b + \mathbf{I}_{M_t K}}{\Gamma} \right) \right) \quad (4.76)$$

where (2.80) was used. In particular the unit lower triangular characteristic of \mathbf{L} was used in (4.75), and the unitary property of $\mathbf{\Pi}$ and \mathbf{W}_{M_t} (see (2.80)) were used in (4.76).

The property (4.68) is then demonstrated by comparing inequality (4.71) with equalities (4.73) and (4.76). \square

4.5 Conclusions

This chapter was dedicated again to the theoretical comparison between OFDM and CPSC. However, in contrast with Chapter 3, a target BER was

assumed to be given, and the comparison of the different schemes was done in terms of achievable bit rate. Another difference with previous chapter is that the channel was assumed to be known at the transmitter side. Moreover, we assumed that this knowledge was used to adaptively allocate the bits among the different symbols of the data block, but not for power loading.

First, the focus was set on SISO systems. In [24], it was proved that DFE-CPSC and OFDM achieve identical bit rates at high SNR, which is a strong result. Here, thanks to the majorization theory, we were able to generalize this result to any SNR value. We analytically proved that, in terms of achievable bit rate and at all SNR, the best performing scheme is OFDM, followed by DFE-CPSC, then MMSE-CPSC, and finally ZF-CPSC.

Second, the result in [24] was extended to a MIMO system. Focusing on the high SNR region, we analytically proved that MIMO DFE-CPSC outperforms MIMO MMSE-OFDM. This result is interesting but not surprising: the DFE receiver does a better job than the MMSE receiver at mitigating the spatial interference. However, if spatial precoding is added on a tone basis, leading to a DMMT scheme, both the temporal and spatial interferences are removed. But, surprisingly again, we have demonstrated that MIMO DFE-CPSC and DMMT perform identically at high SNR.

Additionally, we can mention the purely mathematical results of Propositions 4.9 and 4.10, which might hopefully be useful in other contexts.

The main limitation of the results of this chapter is probably related to the hypotheses associated with the use of (4.54). In particular, (4.54) expresses the bit rate (in bits/symbol) as a real number, which is obviously not realistic: in practice, the symbols are chosen within a discrete constellation. That is, an integer number of bits is transmitted on each data symbol. Note that this discrete constraint will be taken into account in the next chapter, in a slightly different context however. Another important limitation which has to be pointed out is the following: the bit rate expressions (4.55)-(4.58) were obtained by using the expression (4.54) at each position k of the data block. It means that the same target BER is imposed for all symbols of the block. Nevertheless, one could be interested by the achievable bit rate for a target mean BER, i.e. with a constraint on the mean of the BER on the block.

Appendix 4.A An alternative proof for Proposition 4.9

Proving (4.32) is equivalent to demonstrating that

$$\prod_{k=0}^{K-1} (\alpha + \delta_k) \leq \prod_{k=0}^{K-1} (\alpha + \lambda_k). \quad (4.77)$$

Starting from the right-hand side of the inequality (4.77), the following relations can be successively built

$$\prod_{k=0}^{K-1} (\alpha + \lambda_k) = \det(\alpha \mathbf{I}_K + \mathbf{\Lambda}) \quad (4.78)$$

$$= \det(\alpha \mathbf{I}_K + \mathbf{V}\mathbf{\Lambda}\mathbf{V}^H) \quad (4.79)$$

$$= \det(\alpha \mathbf{I}_K + \mathbf{L}\mathbf{D}\mathbf{L}^H) \quad (4.80)$$

$$= \det(\alpha \mathbf{L}^{-1} \mathbf{L}^{H,-1} + \mathbf{D}) \quad (4.81)$$

$$\geq \det(\alpha \mathbf{I}_K + \mathbf{D}) \quad (4.82)$$

$$= \prod_{k=0}^{K-1} (\alpha + \delta_k). \quad (4.83)$$

The equality (4.79) and (4.81) follow again from properties already mentioned in the proof of Proposition 4.6. The inequality (4.82), however, is not obvious. Let us thus conclude this proof by establishing this key inequality. Reorganizing the expressions, this inequality will be demonstrated if we prove that

$$\det(\mathbf{L}^{-1} \mathbf{L}^{H,-1} + \alpha^{-1} \mathbf{D}) \geq \det(\mathbf{I}_K + \alpha^{-1} \mathbf{D}). \quad (4.84)$$

We denote by \mathcal{S} any subset of $\{0, \dots, K-1\}$, and rewrite the right part of (4.84) as

$$\det(\mathbf{I}_K + \alpha^{-1} \mathbf{D}) = \prod_{k=0}^{K-1} (1 + \alpha^{-1} \delta_k) \quad (4.85)$$

$$= \sum_{\mathcal{S}} \left(\alpha^{-|\mathcal{S}|} \prod_{k \in \mathcal{S}} \delta_k \right) \quad (4.86)$$

where the last sum extends over all possible subsets \mathcal{S} (including the empty set and the set $\{0, \dots, K-1\}$ itself), and $|\mathcal{S}|$ refers to the cardinality of set \mathcal{S} . Remember also that an empty product is equal to one. On the other hand,

using the diagonal expansion [80] of the determinant, the left part of (4.84) can be rewritten as

$$\det(\mathbf{L}^{-1}\mathbf{L}^{H,-1} + \alpha^{-1}\mathbf{D}) = \sum_{\mathcal{S}} \left(\det(\mathbf{L}^{-1}\mathbf{L}^{H,-1}(\mathcal{S})) \alpha^{-|\mathcal{S}|} \prod_{k \in \mathcal{S}} \delta_k \right) \quad (4.87)$$

where $\mathbf{L}^{-1}\mathbf{L}^{H,-1}(\mathcal{S})$ denotes the principal submatrix of $\mathbf{L}^{-1}\mathbf{L}^{H,-1}$ resulting from deleting the rows and the columns whose indices are in \mathcal{S} . By the way, remember that the determinant of an empty matrix is equal to one. Now, since \mathbf{L}^{-1} (resp. $\mathbf{L}^{H,-1}$) is a unit lower (resp. upper) triangular matrix, any principal submatrix $\mathbf{L}^{-1}\mathbf{L}^{H,-1}(\mathcal{S})$ has a determinant greater or equal to one (see explanation in Appendix 4.B), such that (4.87) \geq (4.86) which proves (4.84) and thus (4.77).

Appendix 4.B About the principal submatrices of a matrix of the type \mathbf{LL}^H

This appendix is dedicated to giving the reader an illustration of the following statement: "any principal submatrix of $\mathbf{Q} = \mathbf{LL}^H$ has a determinant greater or equal to one", with \mathbf{L} a unit lower triangular matrix. This statement was used at the end of the proof in the previous section of this appendix. Let us use an example to illustrate the statement, and consider the following $K \times K$ unit lower triangular matrix, with $K = 3$,

$$\mathbf{L} = \begin{pmatrix} 1 & 0 & 0 \\ L_{1,0} & 1 & 0 \\ L_{2,0} & L_{2,1} & 1 \end{pmatrix}. \quad (4.88)$$

Remember how we defined any principal submatrix: given \mathcal{S} any subset of $\{0, \dots, K-1\}$, $\mathbf{Q}(\mathcal{S})$ denotes the principal submatrix of $\mathbf{Q} = \mathbf{LL}^H$ resulting from deleting the rows and the columns whose indices are in \mathcal{S} . For the example (4.88), let us consider all possible submatrix sizes, i.e. all possible values of the cardinality $|\mathcal{S}|$, and show that the corresponding determinants are all greater or equal to one

- $|\mathcal{S}| = 3$

The subset \mathcal{S} is equal to $\{0, 1, 2\}$ and $\mathbf{Q}(\mathcal{S})$ is an empty matrix whose determinant is equal to one, by definition.

- $|\mathcal{S}| = 2$

$\mathbf{Q}(\mathcal{S})$ is equal to one of the diagonal elements of \mathbf{Q} , which can be proved to be greater or equal to one

$$[\mathbf{Q}]_{k,k} = 1 + \sum_{l < k} |L_{k,l}|^2 \quad (4.89)$$

$$\geq 1 \quad k \in \{0, 1, 2\}. \quad (4.90)$$

- $|\mathcal{S}| = 1$

As an illustration, let us consider $\mathcal{S} = \{0\}$. $\mathbf{Q}(\mathcal{S})$ is a 2×2 matrix, which can be obtained from \mathbf{Q} by left and right multiplying by rectangular binary matrices

$$\begin{aligned} \mathbf{Q}(\{0\}) &= \begin{pmatrix} 0 & 1 & 0 \\ 0 & 0 & 1 \end{pmatrix} \begin{pmatrix} 1 & 0 & 0 \\ L_{1,0} & 1 & 0 \\ L_{2,0} & L_{2,1} & 1 \end{pmatrix} \begin{pmatrix} 1 & L_{1,0}^* & L_{2,0}^* \\ 0 & 1 & L_{2,1}^* \\ 0 & 0 & 1 \end{pmatrix} \begin{pmatrix} 0 & 0 \\ 1 & 0 \\ 0 & 1 \end{pmatrix} \\ &= \begin{pmatrix} L_{1,0} & 1 & 0 \\ L_{2,0} & L_{2,1} & 1 \end{pmatrix} \begin{pmatrix} L_{1,0}^* & L_{2,0}^* \\ 1 & L_{2,1}^* \\ 0 & 1 \end{pmatrix}. \end{aligned} \quad (4.91)$$

For calculating the determinant of the matrix (4.91) which is expressed as the product of two rectangular matrices, the Cauchy-Binet formula [56] can be used. It gives

$$\begin{aligned} \det(\mathbf{Q}(\{0\})) &= \det \begin{pmatrix} L_{1,0} & 1 \\ L_{2,0} & L_{2,1} \end{pmatrix} \det \begin{pmatrix} L_{1,0}^* & L_{2,0}^* \\ 1 & L_{2,1}^* \end{pmatrix} \\ &+ \det \begin{pmatrix} L_{1,0} & 0 \\ L_{2,0} & 1 \end{pmatrix} \det \begin{pmatrix} L_{1,0}^* & L_{2,0}^* \\ 0 & 1 \end{pmatrix} \\ &+ \det \begin{pmatrix} 1 & 0 \\ L_{2,1} & 1 \end{pmatrix} \det \begin{pmatrix} 1 & L_{2,1}^* \\ 0 & 1 \end{pmatrix} \end{aligned} \quad (4.92)$$

$$\begin{aligned} &= \left| \det \begin{pmatrix} L_{1,0} & 1 \\ L_{2,0} & L_{2,1} \end{pmatrix} \right|^2 + \left| \det \begin{pmatrix} L_{1,0} & 0 \\ L_{2,0} & 1 \end{pmatrix} \right|^2 + 1 \\ &\geq 1 \end{aligned} \quad (4.93)$$

where we used the fact that the determinant of a unit lower or upper triangular matrix is equal to one, and that $\det(\mathbf{A}^H) = (\det(\mathbf{A}))^*$. In a very similar way, the reader can check that $\det(\mathbf{Q}(\{1\}))$ and $\det(\mathbf{Q}(\{2\}))$ are greater or equal to one.

- $|\mathcal{S}| = 0$

The subset \mathcal{S} is empty and $\mathbf{Q}(\mathcal{S})$ is \mathbf{Q} itself, whose determinant is equal to one: $\det(\mathbf{Q}) = \det(\mathbf{L}) \det(\mathbf{L}^H) = 1$.

In this section of the appendix, we only presented the case $K = 3$. However, the reader can easily verify that the statement is true for any value of K : in fact, when calculating the determinant of a submatrix using the Cauchy-Binet formula like in (4.92), there will always be a term in the sum equal to one (because involving determinants of unit triangular matrices), and that for any value of K .

The Goodput Criterion: a Practical Trade-Off

5

This chapter is essentially a reproduction of the journal paper [27], with additional details. Parts of this chapter have also been published in [28] and [29].

Achieving the best trade-off possible between the amount of time needed for executing a task and the quality of the result, is something that is very often encountered in practical situations. It goes from daily life situations (house cleaning, cooking, ...) to professional activities (manufacturing a product, treating a patient in a hospital, ...). In this chapter, we investigate the use of such trade-off as objective function in the optimization of digital wireless communications systems.

5.1 Introduction

This chapter assumes again that the channel is perfectly known at the transmitter and receiver sides. However, this time, we consider that both the bits and power can be adaptively allocated. Moreover, with respect to what has been presented up to here, a different figure of merit or criterion is considered.

The problem of allocating resource among a set of parallel frequency-flat subchannels is often encountered in transmitter design, both in wired and wireless transmissions. For instance, let us mention three well-known examples which involve the transmission over a set of parallel subchannels:

- *Multi-carrier modulation.* As described in detail in Chapter 2, the OFDM modulation copes efficiently with frequency selective channels, and divides the spectrum into orthogonal narrowband subcarriers, each of which constitutes a parallel frequency-flat subchannel.
- *Multi-antenna communication.* In MIMO channels, where multiple antennas are used both at the transmitter and receiver, the left and right singular vectors of the MIMO matrix can be used for pre/decoding (as described in Subsection 2.5.1.2). The outcome is a set of parallel frequency-flat subchannels [52,55].
- *Time varying flat fading channels.* When the gain of a SISO flat fading channel is varying with time, the communication over successive time slots can be seen as a transmission over a collection of parallel (correlated) subchannels [81].

It has long been proved that the mutual information of a set of parallel subchannels with Gaussian inputs is maximized by allocating the power according to the waterfilling solution [26]. Also, it was reminded in Section 4.3 that, for commonly used constellations, the bit rate under a target BER has the same mathematical formulation as the above mentioned mutual information maximization where the SNR is reduced by the so-called SNR gap [77]. Several algorithms were further proposed to modify the waterfilling solution in order to take into account the fact that the constellations sizes are, in practice, constrained to be integer [82,83].

In communication systems which are power-constrained, two main optimization strategies are commonly used in the literature: the minimization of the BER under a bit rate constraint (see Chapter 3), or the maximization of the bit rate under a BER constraint (see Chapter 4). These strategies are appropriate for applications like speech or video transmissions which do not require a null BER because of the user's limited sensitivity. However, some applications like data file transmission require that all bits be transmitted correctly. For this kind of applications, the user is only interested in one quantity: the number of information bits delivered without error to the user by unit of time, or goodput. The real challenge in such systems is to come to the best trade-off between the bit rate and BER criteria, and this is exactly what the goodput criterion expresses. However, for this system-based criterion to make sense, it

has to take into account the presence of error-correction and frame retransmission mechanisms in the system: in other words, the goodput criterion has to be cross-layer oriented. In [84], the goodput was used as criterion to dynamically select the best physical layer mode for IEEE 801.11a wireless LANs. This has been extended to a multi-user environment in [85]. In [86], it was proposed to adaptively choose the transmission mode (modulation and coding levels) to maximize the spectral efficiency (defined similarly to the goodput) of a wireless link with truncated automatic repeat request (ARQ) protocol. All these works [84–86] have shown that the performance of a communication system can be improved if the physical layer is designed while taking into account the error-correction and frame retransmission mechanisms used in the system. However, these works have assumed transmission modes with uniform bit and power allocations.

Our contribution here addresses the problem of allocating bits and power among a set of parallel subchannels in order to maximize the goodput. This chapter starts basically with the reproduction of [27], with additional details and with the focus strictly on the OFDM modulation. A frame-oriented transmission with convolutional coding, hard Viterbi decoding, and ARQ retransmission protocol is considered. Different bit and power allocation algorithms will be proposed. It will be shown that allocating the power in such a way that the BER is equal on all used subcarriers is near-optimal. The discrete constellation constraint will then be relaxed in order to enable further analytical results. In particular, we will prove that the waterfilling solution is near-optimal (in terms of goodput maximization) if and only if the SNR gap value is chosen as shown in this chapter. In addition to that, a comparison between OFDM and CPSC in terms of goodput will be given.

The rest of the chapter is organized as follows. We start in Section 5.2 by describing the communication system considered in this chapter. Section 5.3 reiterates the waterfilling solution, and Section 5.4 mathematically formulates the goodput maximization problem. Different bit and power allocation strategies for solving the discrete problem are described in Section 5.5. Under some hypotheses and relaxing the discrete constellation constraint, further analytical results are derived in Section 5.6, while a comparison with the waterfilling solution is given in Section 5.7. Simulation results are given in Section 5.8. Finally, a goodput comparison between OFDM and CPSC is given in Section 5.9.

5.2 System model: OFDM with error-correction and retransmission mechanism

The communication system considered in this chapter is depicted in Fig. 5.1, where a distinction is made between the physical and data link layers. In this section, this communication system is described and modeled.

The data link layer deals with frames. Each frame contains a given number (N_f) of information bits. At the transmitter side, the frames which are ready to be transmitted are queued in a buffer. At the receiver side, the frames that are received without any error are also buffered before being delivered in correct order to the user¹. However, when a received frame is detected in error, it has to be retransmitted. We consider that the transmission and retransmission of frames are controlled by an ARQ protocol (see Fig. 5.1). In particular, three basic types of ARQ are considered in this work: stop-and-wait (SAW), go-back-N (GBN), and selective-repeat (SR) ARQ. The reader should refer to [87] for a detailed discussion of these three types of ARQ. However, let us briefly describe each of them:

- *Stop-and-wait*. The transmitter sends one frame at a time and waits for an acknowledgment for that frame before transmitting again. If a negative acknowledgment (NAK) is received, the same frame is sent again. If positive acknowledgment (ACK) is received, the next frame is sent.
- *Go-back-N*. The transmitter sends frames continuously: N frames are sent during a round-trip time, which is defined as the time interval between the transmission of a frame and the reception of an acknowledgment for that frame. When a NAK is received for a frame, the transmitter sends that frame again as well as the $N - 1$ succeeding frames. At the receiver side, when a frame is detected in error, the receiver sends a NAK to the transmitter, and discards that frame as well as the $N - 1$ subsequently received frames.

¹We assume that the receiver is able to perfectly distinguish error-free frames from others. In other words, even though it is not described in the system model, this chapter assumes perfect cyclic redundancy check.

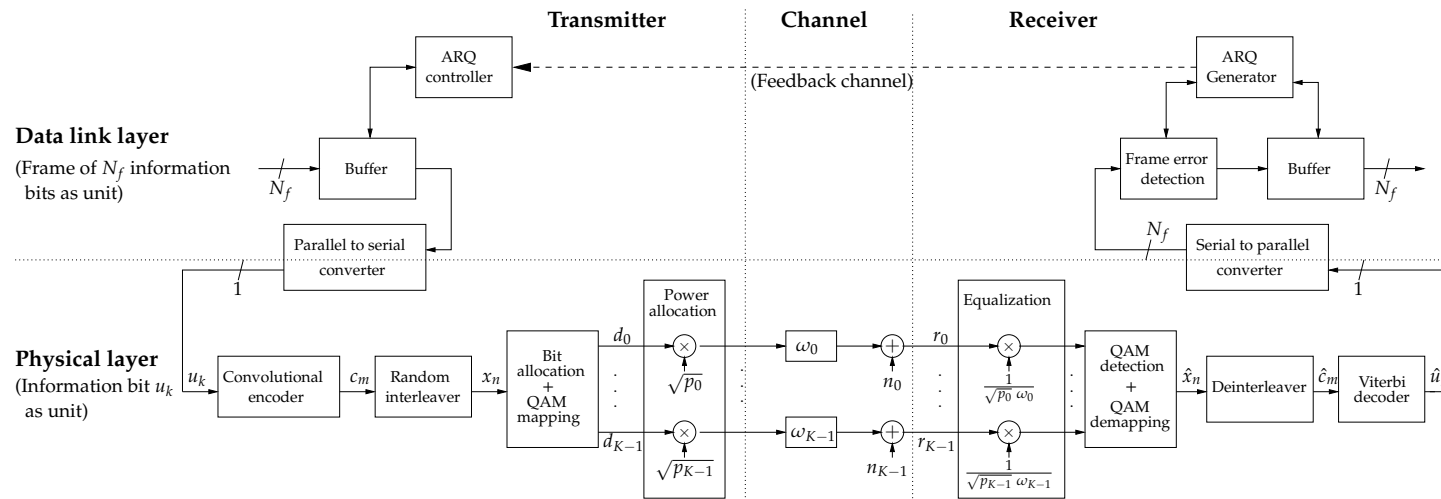


Figure 5.1 Structure of the communication system: physical and data link layers.

- *Selective-repeat.* The frames are also transmitted continuously. However, the transmitter only retransmits the frame for which a NAK was received. A sufficiently large buffer must be provided at the receiver side to deliver the frames in correct order to the user.

Note that this work considers both the presence of an ARQ frame retransmission protocol and an error-correction mechanism (see next paragraph) within each frame. This combination is often referred as a hybrid ARQ scheme [87].

At the transmitter side, the N_f information bits contained in a frame which has to be transmitted, are passed to the physical layer for transmission. There, the information bits u_n are first convolutionally encoded and randomly interleaved (Fig. 5.1). The resulting coded bits x_n are then transmitted. This operation will be described in the next paragraph. At the receiver side, first, hard-decisions are made on the received signal to produce decisions \hat{x}_n on the coded bits. The bits \hat{x}_n are then deinterleaved and Viterbi decoded. Finally, the detected information bits \hat{u}_n are reorganized in frames of N_f bits, and passed to the data link layer. Depending on how the bits are transmitted through the channel, the BER associated with the hard-decision on the coded bits might generally not be equal for all coded bits in a frame. However, in the theoretical analysis of this chapter, we will assume an ideal (de)interleaver. With this assumption, the superchannel seen by the Viterbi decoder may be viewed as a memoryless binary symmetric channel with transition probability given by the mean BER associated with the hard-decision making on the coded bits of a frame, denoted by $\bar{\rho}$. As a consequence, the probability that a frame is Viterbi decoded without any error is a function of this mean BER $\bar{\rho}$. As in [86], a negative exponential will be used in this chapter to approximate the frame success rate (FSR)²:

$$FSR(\bar{\rho}) = b \exp \left(- \left(a_v \bar{\rho}^v + \dots + a_2 \bar{\rho}^2 + a_1 \bar{\rho} \right) \right) \quad (5.1)$$

where $b, a_v, \dots, a_2, a_1, v$ are constants which have to be designed such that (5.1) fits the true FSR curve. These constants depend on the convolutional code used, and on the frame length N_f . Note that, in [28], we used the lower bound given in [88] (based on the union bound) for the FSR. However, in this chapter

²Throughout this chapter, the acronym BER will stand for the uncoded bit error rate, while FSR will denote the frame success rate after Viterbi decoding.

5.2 System model: OFDM with error-correction and retransmission mechanism 99

we will use the approximation (5.1) in order to enable the establishment of analytical results.

Let us now describe the transmission in itself. As said earlier, in the context of this thesis, the focus is set on an OFDM transmission. In Subsection 2.4.1, it was shown that the OFDM transmission is equivalent to the scheme drawn in part (b) of Fig. 2.5, where the frequency selective channel is converted into a set of parallel frequency-flat subcarriers. As shown in Fig. 5.1, we consider here that the power and the bits are allocated to these subcarriers. This allocation is adaptive, in the sense that it depends on the channel state on each subcarrier. The coded bits x_n are spread over the set of subcarriers, and mapped to constellation symbols d_k which are then multiplied by a power allocation factor and transmitted. The allocation strategy has to determine the constellation size and the power assigned to each subcarrier. Denoting as before the number of subcarriers by K , we have the following model for the received signal on the k th subcarrier:

$$r_k = \sqrt{p_k} \omega_k d_k + n_k \quad k = 0, \dots, K-1 \quad (5.2)$$

where p_k is the power allocated to the k th subcarrier, and we remind that ω_k is the complex channel gain on the k th subcarrier. Recall also the definition $h_k \triangleq |\omega_k|^2$, introduced in (3.2). We suppose here, without loss of generality, that the subcarriers are sorted such that $h_0 \geq \dots \geq h_{K-1}$. As before, the noise samples n_k are assumed to be i.i.d. circularly symmetric complex Gaussian random variables with zero mean and variance σ_n^2 . Finally, d_k is the symbol transmitted on the k th subcarrier. We consider square QAM symbols with unit variance. We will denote by m_k the number of bits per symbol in the constellation used on the k th subcarrier. As stated earlier, after equalization hard-decision is made on the received signal, followed by QAM demapping in order to recover the coded bits. Let us denote by ρ_k the BER on the k th subcarrier, associated with this hard-decision making. The approximate BER expression given in [89] for square QAM constellations with Gray bit mapping will be used:

$$\rho_k = c_1 \exp\left(-\frac{c_2 h_k p_k}{(2^{m_k} - 1)\sigma_n^2}\right) \quad (5.3)$$

with $c_1 = 0.2$, and $c_2 = 1.6$. Note that, unlike in Chapter 3, we opt here for an approximative expression for the BER. This will enable to go deeper in the analytical developments.

The transmission of the N_f information bits of a frame will typically involve several consecutive transmission periods over the set of subcarriers. We suppose that the channel remains constant over the time needed for transmitting a frame. In other words, the developments done in this chapter are valid for static channels and for channels with slow fading. In this case, the mean BER $\bar{\rho}$ introduced in (5.1) is given by the BER (5.3) averaged over the K subcarriers, taking into account the number of bits assigned to each subcarrier:

$$\bar{\rho} = \frac{1}{\sum_{i=0}^{K-1} m_i} \sum_{k=0}^{K-1} m_k c_1 \exp\left(-\frac{c_2 h_k p_k}{(2^{m_k} - 1)\sigma_n^2}\right). \quad (5.4)$$

The problem treated in this work is that of allocating the bits (m_k) and the power (p_k) among the K subcarriers. Note that typical bit and power allocation strategies might decide not to transmit on some subcarriers that are in deep fade. Let us then denote by K' the number of subcarriers used for transmission, i.e. with a non null positive bit allocation, with $K' \leq K$. In the next section, we will reiterate the waterfilling solution.

5.3 The waterfilling solution

It has long been proved that the mutual information of a set of K parallel subchannels is maximized by using Gaussian inputs and by allocating the power among the subchannels according to the waterfilling solution [26]. The expression of this power allocation is derived by solving the following maximization problem

$$\max_{p_k \geq 0} \frac{1}{K} \sum_{k=0}^{K-1} \log_2 \left(1 + p_k \frac{h_k}{\sigma_n^2 \Gamma}\right) \quad (5.5)$$

subject to a power constraint

$$\sum_{k=0}^{K-1} p_k \leq P_T \quad (5.6)$$

where P_T is the total available power for a block. Note that we have included the SNR gap Γ in (5.5), in order to talk in terms of achievable bit rate (and not of mutual information), see Section 4.3. Without loss of generality, we assume that the subcarrier gains are with decreasing order: $h_0 \geq h_1 \geq \dots \geq$

h_{K-1} . The solution to (5.5)-(5.6) is easily derived, and is precisely the so-called waterfilling allocation

$$p_k = \left[\mu - \frac{\sigma_n^2 \Gamma}{h_k} \right]^+ \quad k = 0, \dots, K-1 \quad (5.7)$$

with $[x]^+ \triangleq \max(0, x)$. This solution finds its name in the following interpretation: if water (representing the power) is poured into a container whose bottom has exactly the shape of the $\frac{\sigma_n^2 \Gamma}{h_k}$ curve, then the water will rise to a level equal to μ . For a given subcarrier k' , there are then two possible situations. From (5.7),

- if $\frac{\sigma_n^2 \Gamma}{h_{k'}}$ is above the water level μ , no power is allocated to subcarrier k' .
- otherwise, subcarrier k' receives a power allocation equal to $\mu - \frac{\sigma_n^2 \Gamma}{h_{k'}}$, i.e. proportional to the water height above $\frac{\sigma_n^2 \Gamma}{h_{k'}}$.

In order to satisfy the power constraint (5.6), the water-level μ has to be equal to

$$\mu = \frac{P_T}{K'} + \frac{1}{K'} \sum_{k=0}^{K'-1} \frac{\sigma_n^2 \Gamma}{h_k} \quad (5.8)$$

where K' denotes the number of subcarriers used for transmission by the waterfilling policy (i.e. with a non null bit and power allocation). Note that, strictly speaking, (5.7)-(5.8) can not be seen as a closed-form solution. In fact, the value of K' has to be found iteratively using, for example, the following algorithm.

Algorithm 5.1. *Waterfilling solution: selection of the value of K'*

1. Sort h_k with decreasing order
2. Set $K' = K$
3. Compute $p_{K'-1}$ using (5.7) and (5.8)
4. If $p_{K'-1} \leq 0$, $K' \leftarrow K' - 1$, and go to step 3.
Else, return K' and algorithm finishes

The bit allocation as a function of the power allocation is then given by

$$m_k = \log_2 \left(1 + \frac{p_k h_k}{\sigma_n^2 \Gamma} \right). \quad (5.9)$$

After some algebra on (5.7)-(5.9), the waterfilling policy can be rewritten as:

$$\frac{2^{m_k}}{h_k} = \frac{P_T}{K' \sigma_n^2 \Gamma} + \frac{1}{K'} \sum_{l=0}^{K'-1} \frac{1}{h_l}, \quad (5.10)$$

$$p_k = \frac{(2^{m_k} - 1) \sigma_n^2}{h_k} \frac{P_T}{\sum_{l=0}^{K'-1} \frac{(2^{m_l} - 1) \sigma_n^2}{h_l}}, \quad (5.11)$$

for $k = 0, \dots, K' - 1$. Equation (5.10) suggests that the waterfilling bit allocation is such that the ratio $2^{m_k}/h_k$ is equal for all used subcarriers. Moreover, the waterfilling power allocation (5.11) as a function of the bit allocation equalizes the approximate BER (5.3) on all used subcarriers.

Note that the waterfilling policy is conventionally defined by (5.7)-(5.9). However, in this chapter the equivalent form (5.10)-(5.11) will be used. Let us also mention that several algorithms were proposed to modify the waterfilling solution in order to take into account the fact that the constellations sizes are, in practice, constrained to be integer [82, 83]. It is also worth mentioning the recent work in [90]: the authors introduced the so-called mercury/waterfilling solution, which is the generalization of the waterfilling policy to the case of arbitrary input distributions (not necessarily Gaussian).

A reader familiar with the subject has not learned anything new from this section. However, we would recommend such reader to read Appendix 5.A which tackles an less common issue about the waterfilling solution.

5.4 Problem formulation

When evaluating the performance of the system described in Section 5.2, the most meaningful criterion is the number of information bits delivered without error to the user by unit of time, or goodput. The objective of this chapter is to propose solutions for the allocation of the bits (m_k) and the power (p_k) among the subcarriers in such a way that it maximizes the goodput of the

communication system. In this section, a formulation is given for the goodput, for the three types of ARQ protocols considered here.

The goodput is defined as the number of information bits delivered without error to the user by unit of time. For the frame-oriented transmission considered in this work, a bit is delivered without error to the user if it belongs to an error-free frame. As the unit of time, we will use the transmission time over the set of subcarriers. Let us denote by r the rate of the convolutional code used. We know that there are N_f information bits in a frame, and that $r \sum_{k=0}^{K-1} m_k$ information bits are transmitted at each use of the set of subcarriers. As a consequence, there are $N_f / (r \sum_{k=0}^{K-1} m_k)$ transmissions over the set of subcarriers needed for one frame to be transmitted. Moreover, with SR ARQ, it was shown [87] that the average number of frame transmissions needed for a frame to be successfully transmitted is given by $1/FSR$. For SR ARQ, the goodput (GP) can thus be expressed as

$$GP_{SR} = \frac{N_f}{\frac{N_f}{(r \sum_{k=0}^{K-1} m_k)} \frac{1}{FSR(\bar{\rho})}} = \left(r \sum_{k=0}^{K-1} m_k \right) FSR(\bar{\rho}). \quad (5.12)$$

Note that the last expression in (5.12) gives another interpretation for the goodput. It expresses the goodput as the number of information bits sent at each use of the set of subcarriers, multiplied by the probability that these bits belong to an error-free frame, which makes sense. For GBN ARQ, the average number of transmissions needed for a successful frame transmission is

$$\frac{N - (N - 1) FSR}{FSR}, \quad (5.13)$$

and the associated goodput is given by

$$GP_{GBN} = \frac{N_f}{\frac{N_f}{(r \sum_{k=0}^{K-1} m_k)} \frac{N - (N - 1) FSR(\bar{\rho})}{FSR(\bar{\rho})}} \quad (5.14)$$

$$= \frac{\left(r \sum_{k=0}^{K-1} m_k \right) FSR(\bar{\rho})}{N - (N - 1) FSR(\bar{\rho})}, \quad (5.15)$$

where N denotes the number of frames that are transmitted during a round-trip time. Finally, since the SAW ARQ protocol is similar to SR ARQ except that it only sends one frame per round trip time [87], its goodput is given by

$$GP_{SAW} = \frac{1}{N} GP_{SR}. \quad (5.16)$$

For the time being, let us focus on the SR or SAW ARQ. Adding constraints on the total transmitted power and on the possible constellation sizes, the problem of finding the bit and power allocation which maximizes the goodput of the system can be written as:

$$\max_{m_k, p_k} GP = \left(r \sum_{k=0}^{K-1} m_k \right) FSR(\bar{\rho}) \quad (5.17)$$

subject to

$$\sum_{k=0}^{K-1} p_k \leq P_T \quad (5.18)$$

$$m_k \in \mathcal{M}, \quad k = 0, \dots, K-1 \quad (5.19)$$

where P_T is the total power available for the set of subcarriers, and with $FSR(\bar{\rho})$ and $\bar{\rho}$ respectively given by (5.1) and (5.4). The set \mathcal{M} is defined as the union of the possible constellation sizes (in bits) together with 0 (no transmission). In this work, we consider three possible constellations: 4-QAM, 16-QAM and 64-QAM. We have $\mathcal{M} = \{0, 2, 4, 6\}$.

The presence of the constraint (5.19) in the problem formulation makes it a discrete problem, for which solution strategies will be proposed in Section 5.5. However, under some hypotheses, relaxing the constraint (5.19) will allow further analytical derivations as it will be shown in Section 5.6.

5.5 Discrete problem

The discrete problem (5.17)-(5.19) can be solved in a decoupled manner: first we analyze the power allocation problem for a given bit allocation, and then the bit allocation problem is treated.

5.5.1 Power allocation strategy for a given bit allocation

In this subsection, the bit allocation is assumed to be fixed. In other words, the m_k are no longer considered as variables but as given constants. Let us denote again by K' the number of subcarriers with a non null positive bit allocation. The focus is set on the derivation of power allocation strategies for a given bit allocation. In particular, two different power allocation strategies are proposed in the following.

5.5.1.1 Optimal Power Allocation

For a given bit allocation, i.e. for given m_0, m_1, \dots, m_{K-1} , the first parenthesis in (5.17) is a constant. As a consequence, the optimal power allocation is such that it maximizes the frame success probability $FSR(\bar{\rho})$, and thus minimizes the mean BER $\bar{\rho}$ (since $FSR(\bar{\rho})$ is a decreasing function³ with $\bar{\rho}$). The optimal power allocation problem comes down to the minimization of the mean BER (5.4) subject to the power constraint (5.18). Using Lagrange multipliers, we find the following solution:

$$p_k = \frac{(2^{m_k} - 1)\sigma_n^2}{c_2 h_k} \left[\log \left(\frac{h_k m_k}{(2^{m_k} - 1)\sigma_n^2} \right) - \log(\lambda) \right]^+. \quad (5.20)$$

Remember that $[x]^+$ means $\max(x, 0)$. The Lagrange multiplier λ has to be such that (5.20) satisfies the power constraint (5.18), and is given by

$$\log(\lambda) = \frac{\sum_{i=0}^{K''-1} \frac{(2^{m_i} - 1)\sigma_n^2}{c_2 h_i} \log \left(\frac{h_i m_i}{(2^{m_i} - 1)\sigma_n^2} \right) - P_T}{\sum_{i=0}^{K''-1} \frac{(2^{m_i} - 1)\sigma_n^2}{c_2 h_i}} \quad (5.21)$$

where K'' denotes the number of subcarriers with a non null power allocation. This value has to be found iteratively, in a similar way as in Algorithm 5.1. We will refer to the solution (5.20)-(5.21) using the acronym OPA (Optimal Power Allocation). Note that $K'' \leq K'$. In fact, the OPA might assign a null power allocation to a subcarrier having a non null positive bit allocation.

The first factor in (5.20) tends to equalize the BER (5.3) on all used subcarriers: it allocates more power to the subcarriers with low channel gain and high constellation size. On the other hand, the second factor in (5.20) seems to compensate for that effect and allocate more power to the subcarriers with large channel gain and low constellation size.

5.5.1.2 Equal BER Power Allocation

Like the first factor in the OPA (5.20) suggests, let us focus on a power allocation which would equalize the BER (5.3) on all used subcarriers:

$$\rho_k = \rho, \quad \forall k = 0, \dots, K' - 1. \quad (5.22)$$

³The decreasing character of the expression (5.1) depends on the values of the constants b, a_v, \dots, a_1, v . However, since the expression has to fit a true FSR curve, it is obvious that it should be a decreasing function with $\bar{\rho}$.

Taking into account the power constraint (5.18), the equal BER power allocation is given by:

$$p_k = \frac{(2^{m_k} - 1)\sigma_n^2}{c_2 h_k} \frac{P_T}{\sum_{i=0}^{K'-1} \frac{(2^{m_i} - 1)\sigma_n^2}{c_2 h_i}}, \quad k = 0, \dots, K' - 1. \quad (5.23)$$

The acronym EBPA (Equal BER Power Allocation) will be used to refer to this solution. Note that the power allocation (5.11) of the waterfilling solution is exactly the EBPA. Note also that the EBPA would be the result of a min-max BER strategy (minimization of the worst BER among the subcarriers). Moreover, as previously shown in [91], it is easy to see that the OPA (5.20)-(5.21) comes down to the EBPA (5.23) as the transmit power P_T grows to infinity.

5.5.1.3 An illustrating example

Let us illustrate these two bit allocation strategies with an example. Let us consider again the channel realization A in Fig. 3.1 ($K = 64$). Let us compute the EBPA and OPA for two different given bit allocations:

- In Fig. 5.2, the bit allocation is uniform: 4-QAM is used for all K symbols of the block. We see that the EBPA strictly assigns the power inversely proportionally to the channel, while the OPA has a much different and less straightforward behavior. For the good subcarriers (i.e. with high subcarrier gains), the OPA allocates the power inversely proportionally to the channel. On the contrary, for the bad subcarriers, the OPA has the tendency to allocate less power (and even zero power). We see that, by doing so, the OPA achieves a lower mean BER on the block than the EBPA.
- In Fig. 5.3, the bit allocation is much more adapted to the channel: 4-QAM is used on the good subcarriers, and no bits are transmitted on the bad ones. We see that, this time, both the OPA and EBPA have the same overall behaviors and allocate the power inversely proportionally to the channel. Also, the achieved mean BER is nearly equal for both strategies, this time.

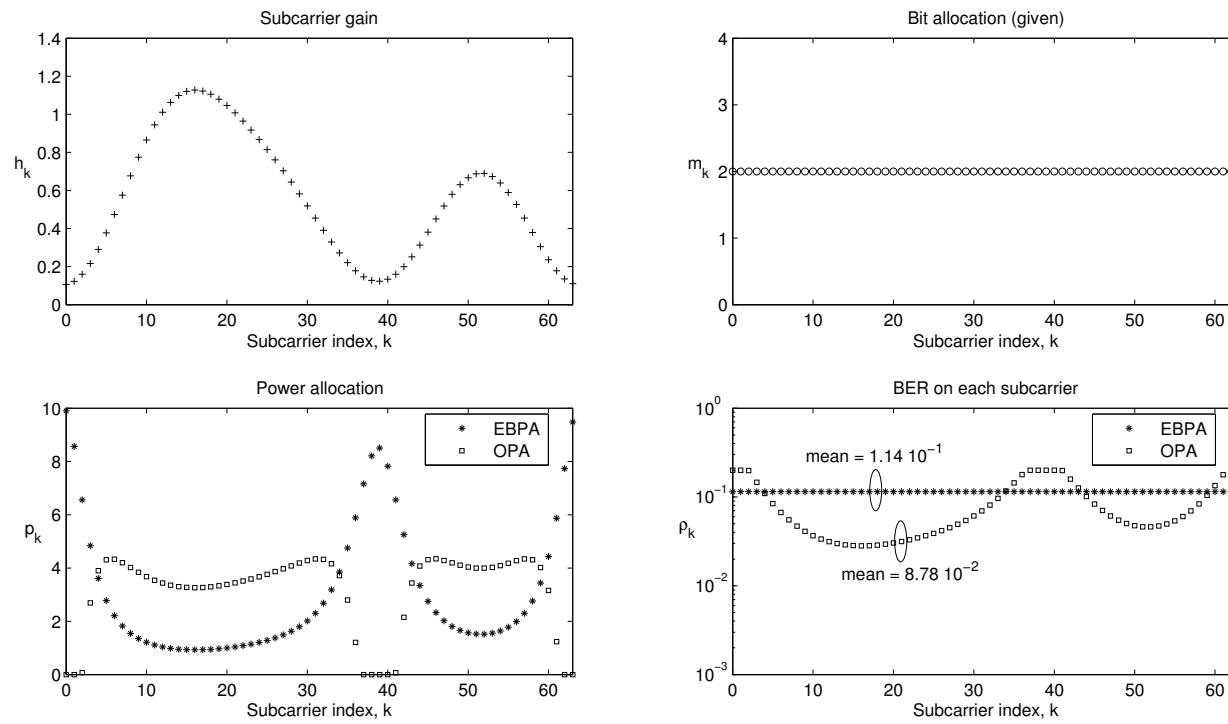


Figure 5.2 The OPA versus the EBPA for the channel realization A in Fig. 3.1, $K = 64$, and $\frac{P_T}{K\sigma_n^2} = 11.4$ dB. Uniform 4-QAM bit allocation.

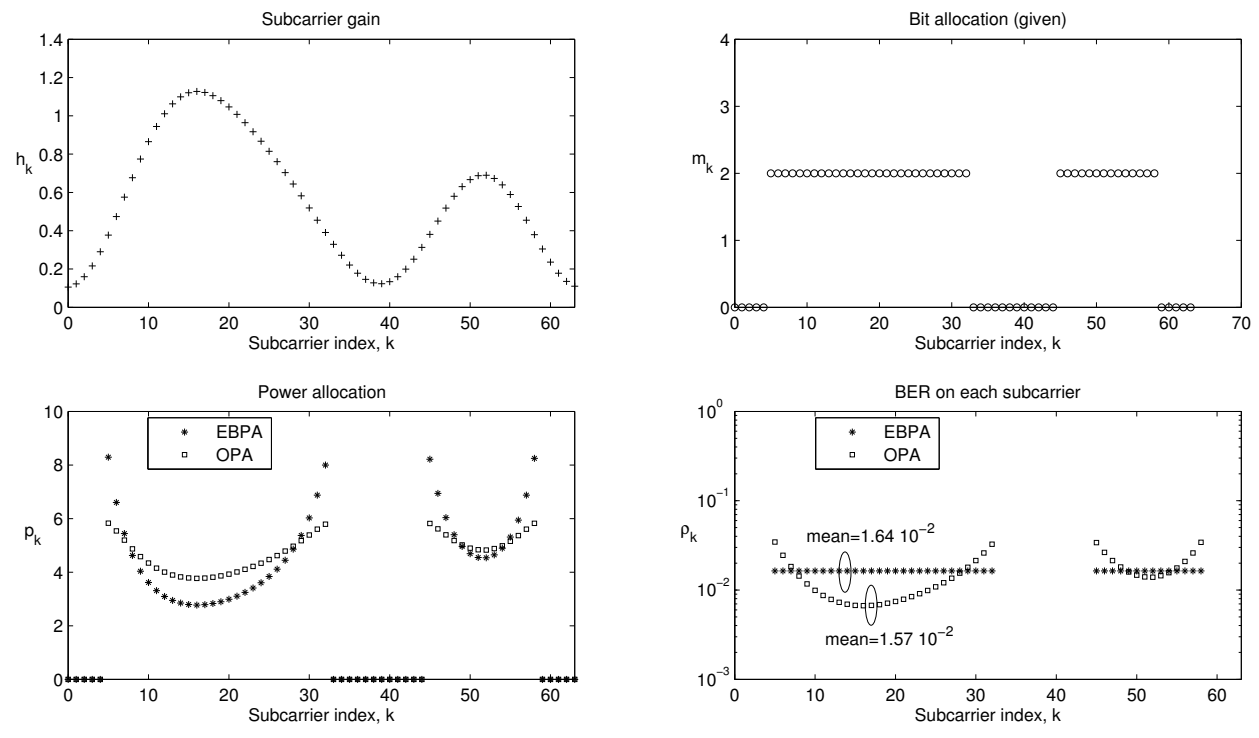


Figure 5.3 The OPA versus the EBPA for channel realization A in Fig. 3.1, $K = 64$, and $\frac{P_T}{K\sigma_n^2} = 11.4$ dB. Bit allocation adapted to the channel.

5.5.2 Bit allocation strategy

In Subsection 5.5.1, two different power allocation strategies for a given bit allocation were derived. Using these results, this subsection is devoted to allocating the bits among the subcarriers.

5.5.2.1 Optimal bit allocation - exhaustive search

Even though very complex, a possible strategy is the exhaustive search among all possible bit allocations. In this work, we assume that 0, 2, 4 or 6 bits can be allocated to each of the K subcarriers: in total, there is 4^K possible bit allocations. The exhaustive search bit allocation (ESBA) consists of, for each of these 4^K bit allocations, computing the chosen power allocation (OPA or EBPA), deducing the mean BER (5.4) and the associated goodput value (5.17), and selecting the bit allocation with the highest goodput value. Note that the exhaustive search with the optimal power allocation (ESBA/OPA) is the optimal bit and power allocation strategy.

5.5.2.2 Greedy Algorithm

In order to reduce the complexity, one alternative is to use a greedy algorithm [92]: It starts with a null bit allocation on each subcarrier, and then proceeds iteratively. At each iteration, the allocation of two more bits on the k th subcarrier is proposed, for each $k \in \{0, \dots, K-1\}$. Thanks to Subsection 5.5.1, we can associate with each of these K proposals, a new power allocation (OPA or EBPA), thus a new mean BER value (5.4), and finally a new goodput value (5.17). We choose the proposal with highest new goodput value, but only if this value is greater than the value that was reached at the previous step (otherwise the algorithm stops). The algorithm can be written as follows:

Algorithm 5.2. *Greedy bit allocation*

1. Set $\mathcal{M} = \{0, 2, 4, 6\}$
2. Set $m_k = 0, \forall k \in \{0, \dots, K-1\}$. Set $GP = 0$.

3. $\forall k \in \{0, \dots, K-1\}$ compute $GP_k(m_k+2)$, the goodput value achieved if the constellation on the k th subcarrier is increased by 2 bits. This is done by first computing the power allocation using (5.20) or (5.23), and then by deducing the goodput value (5.17) using (5.4). If $m_k = 6$, set $GP_k = 0$, since 64-QAM was chosen as the largest constellation size in this work.
4. Select $k^* = \operatorname{argmax}_k GP_k$
5. If $GP_{k^*} > GP$, $GP \leftarrow GP_{k^*}$ and $m_{k^*} \leftarrow m_{k^*} + 2$, and go to step 3. Else, algorithm finishes.

The acronym GABA (Greedy Algorithm Bit Allocation) will be used to refer to this algorithm. Since it does not have to test all possible bit allocations, the GABA reduces the complexity comparing to the ESBA. However, unlike the ESBA, the GABA is not optimal, as it will be shown by simulation in Section 5.8.

5.6 Relaxed problem with EBPA

It turns out that the EBPA is a near-optimal power allocation strategy: in fact, as it will be shown by simulation in Section 5.8, the EBPA barely suffers any loss (in terms of goodput) comparing to the OPA. This section takes advantage of this result and shows that, under the hypothesis of EBPA, some analytical results can be further derived and used for developing efficient allocation strategies (in terms of trade-off between performance and complexity).

Let us thus consider that the power is allocated according to the EBPA (5.23). Inserting (5.23) into (5.4) gives

$$\bar{\rho} = c_1 \exp \left(\frac{-c_2 P_T}{\sigma_n^2 \sum_{i=0}^{K'-1} \frac{(2^{m_i}-1)}{h_i}} \right). \quad (5.24)$$

Suppose for a moment that the constraint (5.19) is relaxed, and that the variables m_k are allowed to take any positive real value. This new problem will be

referred to as the relaxed problem. By doing so, the goodput expression (5.17) can be differentiated with respect to each variable m_k . Equating each of these derivatives to zero, we get, after calculation, that the following equality must hold

$$\frac{2^{m_k}}{h_k} = \frac{\left(\sum_{i=0}^{K'-1} \frac{(2^{m_i}-1)}{h_i}\right)^2}{\left(\sum_{i=0}^{K'-1} m_i\right)(v a_v \bar{\rho}^v + \dots + a_1 \bar{\rho}) \left(\frac{c_2 P_T \ln(2)}{\sigma_n^2}\right)} \quad (5.25)$$

for all $k \in \{0, \dots, K' - 1\}$. Since the expression on the right side of the equality (5.25) is independent of k , we must have that

$$\frac{2^{m_k}}{h_k} = \frac{2^{m_q}}{h_q} \quad \forall k, q \in \{0, \dots, K' - 1\}. \quad (5.26)$$

Using (5.26), the equality (5.25) can be rewritten as a function of m_k only:

$$\begin{aligned} & \frac{2^{m_k}}{h_k} \left(\sum_{i=0}^{K'-1} \log_2 \left(\frac{h_i}{h_k} \right) + K' m_k \right) (v a_v \bar{\rho}^v + \dots + a_1 \bar{\rho}) \\ & \times \left(\frac{c_2 P_T \ln(2)}{\sigma_n^2} \right) - \left(K' \frac{2^{m_k}}{h_k} - \sum_{i=0}^{K'-1} \frac{1}{h_i} \right)^2 = 0 \end{aligned} \quad (5.27)$$

where $\bar{\rho}$ is given by rewriting (5.24) as a function of m_k only, using (5.26). The problem of finding the bit allocation maximizing the goodput under the hypothesis of EBPA and allowing real bit allocations can then be solved by the following procedure:

Algorithm 5.3. *Optimal relaxed bit allocation, assuming EBPA*

1. Sort the subcarriers such that $h_0 \geq \dots \geq h_{K-1}$.
Set $k^* = K - 1$.
2. Solve (5.27) for m_{k^*} . This is a nonlinear equation which has to be solved numerically.
If there is no positive solution for m_{k^*} , then $m_{k^*} = 0$, $k^* \leftarrow k^* - 1$, and go to step 2. Else, go to step 3.
3. Using (5.26), $\forall k \leq k^*$: $m_k = \log_2 \left(\frac{h_k}{h_{k^*}} 2^{m_{k^*}} \right)$.

At this point we are able to find the optimal real bit allocations for the relaxed

goodput maximization problem, and under the assumption of EBPA. In the sequel, details are given on how to use that result to solve the constrained problem (i.e. with constraint (5.19)). In particular, three possible methods are described:

1. *Rounding.* Each real bit allocation m_k ($k = 0, \dots, K - 1$) of the solution to the relaxed problem can be rounded to the nearest element of $\mathcal{M} = \{0, 2, 4, 6\}$. We will use the acronym RRBA (Round Relaxed Bit Allocation) to refer to this bit allocation strategy.
2. *Rounding down and greedy algorithm.* Each real bit allocation m_k of the solution to the relaxed problem can be rounded down to the nearest element of \mathcal{M} , and the greedy algorithm can be run with the result as starting bit allocation. This bit allocation will be referred as RRBA-GABA, the concatenation of the two previously defined acronyms.
3. *Branch-and-bound approach.* As it was explained earlier, the ESBA consists of trying out all 4^K elements of the solution space, and has a complexity that is exponential in the number of subcarriers K . However, being able to solve the relaxed problem, a branch-and-bound approach [93] can be used to find the optimal solution without exploring the whole solution space. This approach uses the following obvious property: the goodput achieved by the optimal real solution to the relaxed problem (which disregards the constraint (5.19)) can never be worse than the goodput associated with any integer solution (which satisfies the constraint (5.19)). The branch-and-bound approach is better explained using the example depicted in Fig. 5.4, where $K = 2$. In this example, the real solution to the relaxed problem is $[m_0, m_1] = [0.96, 2.69]$, and the associated GP is 1.6. Thus we know that the GP achieved by any integer solution will never exceed 1.6. The solution space, represented as a tree, can then be split in two branches⁴ depending on if $m_1 = 2$ or 4. Solving the relaxed problems, with m_1 being fixed to 2 or 4, gives solutions with associated GP equal to 1.5 and 0.8, respectively. We therefore naturally choose to further explore the left branch. The real solution achieving GP=1.5 was given by $[1.35, 2]$. At this point, the left branch can itself

⁴A good heuristic approach is to choose for branching the variable whose value is the closest to an element of \mathcal{M} .

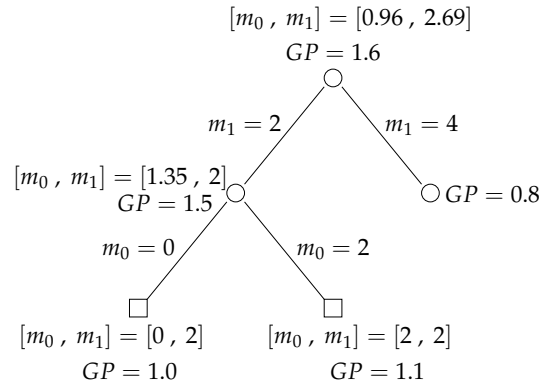


Figure 5.4 Illustration of the branch-and-bound approach.

be split depending on if $m_0 = 0$ or 2 , leading to two possible integer solutions $[0, 2]$ and $[2, 2]$. It turns out that the second solution achieves a GP equal to 1.1 and outperforms the first one. Moreover, since the GP achieved by that solution is greater than 0.8 (which is an upper bound of what can be achieved by any solutions at the right side of the tree), we do not need to further explore the right side of the tree. Note that this the branch-and-bound approach guarantees to find the optimal solution to the constrained problem. The acronym BBBA (Branch-and-Bound Bit Allocation) will be used to refer to this approach.

5.7 Comparison with the waterfilling solution

In this section, the waterfilling and the goodput maximizing solutions are compared to each other. In particular we show how to choose the value of the SNR gap in such a way that the waterfilling solution be near-optimal in terms of goodput.

Let us consider again that the constraint (5.19) is relaxed. On the one hand, in Section 5.3, the equivalent form (5.10)-(5.11) was presented for the waterfilling solution. On the other hand, Section 5.6 was dedicated to the relaxed goodput maximization problem and derived the near-optimal relaxed solu-

tion given by the EBPA (5.23) and the bit allocation satisfying (5.25). Comparing solutions (5.10) and (5.25), we see that both equations suggest that the ratio $2^{m_k}/h_k$ should be equal for all used subcarriers. We can therefore conclude that the waterfilling solution is equal to the near-optimal relaxed solution with EBPA if and only if the SNR gap value Γ is chosen such that quantities at the right-hand side of the equality sign in (5.10) and (5.25) are equal. In doing so, we end up with the following non linear equation in Γ

$$\left(\frac{P_T}{\sigma_n^2 K' \Gamma} + \frac{1}{H(\mathbf{h}, K')} \right) \left[\log_2 \left(G(\mathbf{h}, K') \left(\frac{P_T}{\sigma_n^2 K' \Gamma} + \frac{1}{H(\mathbf{h}, K')} \right) \right) \right] \\ \times (v a_v \bar{\rho}^v + \dots + a_1 \bar{\rho}) c_2 \ln(2) - \frac{P_T}{\sigma_n^2 K' \Gamma^2} = 0 \quad (5.28)$$

where:

- the harmonic and geometric means of the subcarrier gains are respectively defined by

$$H(\mathbf{h}, K') = \frac{K'}{\sum_{l=0}^{K'-1} \frac{1}{h_l}} \quad (5.29)$$

$$G(\mathbf{h}, K') = \left(\prod_{l=0}^{K'-1} h_l \right)^{1/K'}. \quad (5.30)$$

- the mean BER as a function of Γ is given by inserting (5.10) into (5.24): $\bar{\rho} = c_1 \exp(-c_2 \Gamma)$.

For the considered system with SAW/SR ARQ, solving (5.28) yields the value for the SNR gap Γ which is such that the waterfilling solution is near-optimal in terms of goodput. The same mathematical developments can be done for GBN ARQ, i.e. using the goodput expression (5.15). A counterpart of (5.28) for GBN ARQ can be derived, and is given by

$$\frac{\left(\frac{P_T}{\sigma_n^2 K' \Gamma} + \frac{1}{H(\mathbf{h}, K')} \right)}{\left(1 - \left(1 - \frac{1}{N} \right) FSR(\bar{\rho}) \right)} \left[\log_2 \left(G(\mathbf{h}, K') \left(\frac{P_T}{\sigma_n^2 K' \Gamma} + \frac{1}{H(\mathbf{h}, K')} \right) \right) \right] \\ \times (v a_v \bar{\rho}^v + \dots + a_1 \bar{\rho}) c_2 \ln(2) - \frac{P_T}{\sigma_n^2 K' \Gamma^2} = 0. \quad (5.31)$$

Analyzing (5.28) and (5.31), it turns out that this near-optimal SNR gap Γ depends on:

- *the ARQ protocol used.* In case of SAW or SR ARQ, the near-optimal Γ has to solve (5.28), while (5.31) has to be solved in case of GBN ARQ.
- *the available transmit power.* Both (5.28) and (5.31) depend on the ratio P_T/σ_n^2 .
- *the channel realization.* Both (5.28) and (5.31) depend on the harmonic and geometric means of the subcarrier gains.
- *the convolutional code used and the frame length N_f .* Both (5.28) and (5.31) depend on the constants a_v, \dots, a_1, v which in turn depend on the convolutional code used and the frame length.

Let us remember that determining a value for the SNR gap Γ is equivalent to choosing the BER at which the system will be working.

5.8 Simulation results

In this section, the different bit and power allocation strategies are simulated and compared to one another. The analytical result which was derived in the previous section is also illustrated.

Let us consider the following parameters: $N_f = 1024$ or 4096 . Two convolutional codes of rate $r = 1/2$ are considered. Their respective generator polynomials are [5,7] and [133,171], in octal notation. The FSR associated with these two codes, as a function of the mean BER at the input of the Viterbi decoder, is depicted in Fig. 5.5. It shows that the expression (5.1) (with the constants given in Fig. 5.5) approximates very well the simulated FSR. We consider an OFDM system with a seven-tap channel impulse response ($L = 7$). The taps are i.i.d circularly symmetric complex Gaussian random variables with zero mean and variance such that the channel impulse response has unitary mean energy. All curves will present the average goodput as a function of $P_T/(K\sigma_n^2)$, and result from an average over a thousand channel realizations. The average goodput is expressed as the average number of information bits transmitted correctly (i.e. belonging to an error-free frame) per symbol period. Moreover, the bandwidth efficiency loss induced by the CP is taken into account in the curves.

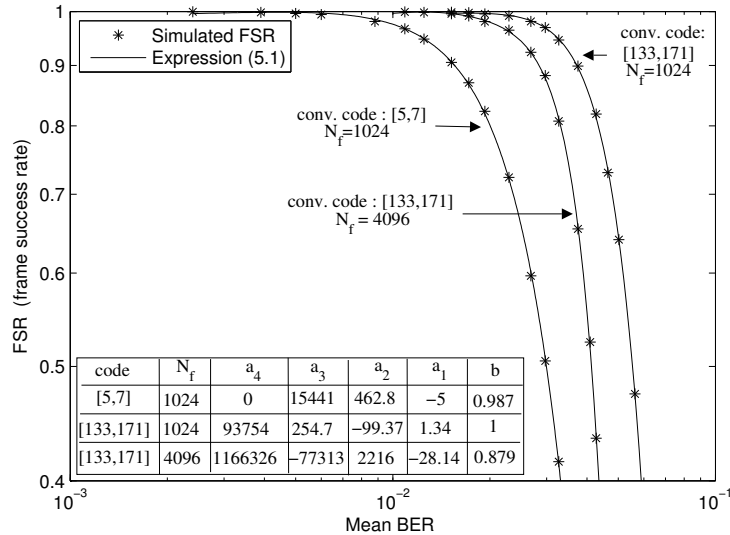


Figure 5.5 Comparison between the simulated and approximated FSR.

We know that the optimal bit and power allocation strategy for the discrete problem (5.17)-(5.19) is the ESBA/OPA. The Fig. 5.6 analyzes the performance degradation if the suboptimal EBPA is used instead of the OPA, with the optimal bit allocation (ESBA) (for $K = 8$, $N_f = 1024$ and convolutional code [133,171]). It turns out that the performance degradation is very small. In other words, using the EBPA rather than the OPA has a very small effect on the achievable goodput. This is what we meant when referring to the near-optimality of the EBPA, in Sections 5.6 and 5.7. Note that this near-optimality of the EBPA is justified by the observation made in the second point of Subsection 5.5.1.3: if the bit allocation is well adapted to the channel, the EBPA does not exhibit a significant loss (in terms of mean BER) with respect to the OPA.

Let us now suppose that the power is allocated using the near-optimal EBPA. It was shown in Section 5.6 that its relatively simple expression (5.23) allowed further analytical derivations. Here we compare the different proposed bit allocation strategies, supposing the EBPA. The BBBA guarantees to find the optimal bit allocation when the EBPA is used. It explains why it out-

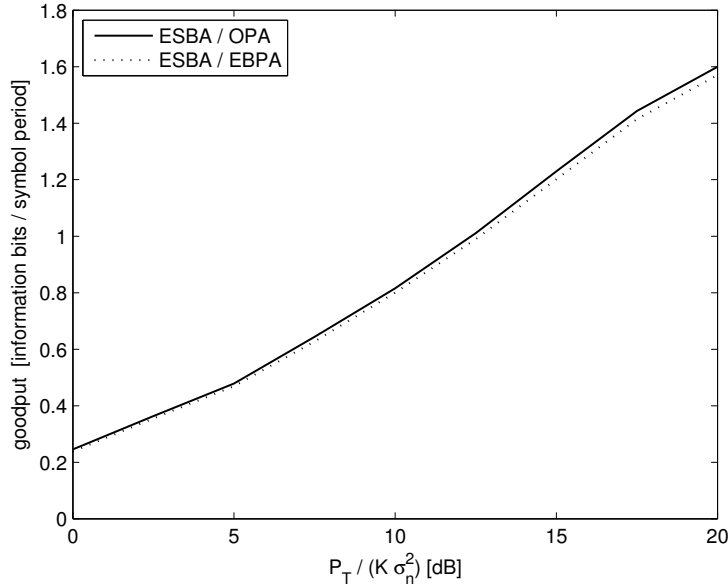


Figure 5.6 Goodput achieved by the ESBA with the OPA, or EBPA. ($K = 8$, $N_f = 1024$, conv. code [133,171], SR ARQ).

performs all the other strategies, see Fig. 5.7 (where $K = 32$, $N_f = 1024$ and convolutional code [133,171]). It also shows that the GABA and RRBA-GABA perform identically (since they only differ in the starting point of the greedy bit allocation), and suffer a non-negligible goodput loss comparing with the BBBA. However, the RRBA strategy suffers a smaller loss than GABA, comparing with the BBBA. Note also that the RRBA significantly reduces the complexity: the RRBA implicates to run only once the Algorithm 5.3, while the BBBA supposes to run it twice as many times as the number of explored nodes in the tree search, and the RRBA-GABA supposes to run the Algorithm 5.3 followed by the greedy Algorithm 5.2. We conclude that the RRBA/EBPA is the strategy achieving the best trade-off between performance and complexity.

Section 5.7 showed how to compute the value of the SNR gap Γ^* which is such that the waterfilling solution be near-optimal in term of goodput. Let us compute Γ^* for different values of the ratio $P_T / (K\sigma_n^2)$ and analyze the influence of the code used, the frame length, the channel realization, and the

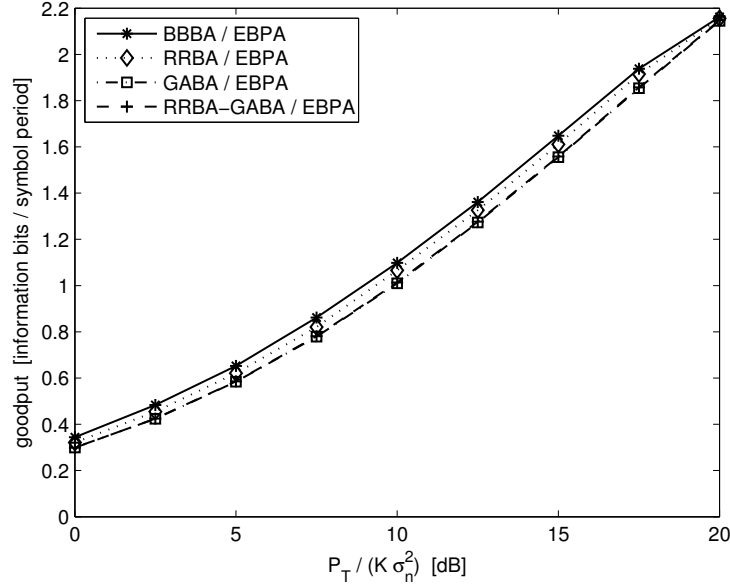


Figure 5.7 Goodput achieved by the different proposed bit allocation strategies, supposing EBPA. ($K = 32$, $N_f = 1024$, conv. code [133,171], SR ARQ).

retransmission protocol considered. We consider two channel realizations which are depicted in Fig. 5.8. The result is given in Table 5.1. We observe that:

1. In all scenarios, the larger the ratio $P_T / (K \sigma_n^2)$, the larger Γ^* will be. In other words, when extra transmit power is available, the BER at which the system is operating should be decreased.
2. The lower the correcting capability of the code used, the larger Γ^* will be (see comparison between [5,7] and [133,171] codes). It is obvious that a lower uncoded BER should be achieved when a less effective code is used. The same comment holds for an increase in the frame length N_f .
3. A larger Γ (and thus a lower BER) should be chosen if GBN ARQ is used instead of SAW/SR ARQ. In fact, a system with GBN ARQ should

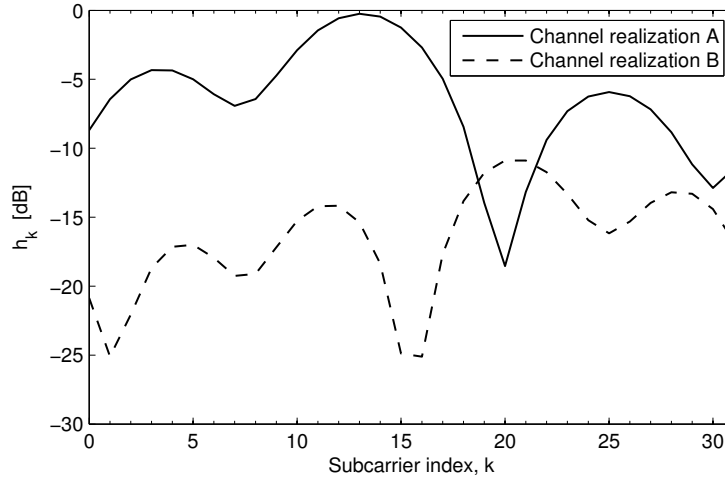


Figure 5.8 Subcarrier gains of the two considered channel realizations.

operate at lower FSR, since each frame error involves the retransmission of not one but N frames.

4. The poorer the channel quality, the lower Γ^* will be. In fact, a poorer channel quality can be seen as a reduction of the available transmit power.

5.9 Goodput comparison between OFDM and CPSC

In the previous sections of this chapter, the goodput optimization of an OFDM system has been considered. This section is devoted to comparing these results to what can be achieved by a CPSC system, in terms of goodput.

Let us consider a ZF-CPSC scheme together with the same error-correction and ARQ retransmission mechanisms as in Fig. 5.1. In a ZF-CPSC scheme, as presented in Subsection 3.2.2, the SNR is equal for all K symbols of the block and is given by (3.9). In the context of this chapter, this means that less degrees of freedom are available for bit and power loading. In fact, in a ZF-CPSC scheme:

Table 5.1 Near-optimal SNR gap for different scenarios.

Near-optimal SNR gap Γ^*				$P_T / (K\sigma_n^2)$		
				0 dB	10 dB	20 dB
Channel realization	ARQ protocol	Conv. Code	N_f			
A	SAW/SR ARQ	[133,171]	1024	1.08	1.15	1.22
A	SAW/SR ARQ	[5,7]	1024	1.62	1.72	1.85
A	SAW/SR ARQ	[133,171]	4096	1.26	1.32	1.41
A	GBN ARQ ($N=5$)	[133,171]	1024	1.29	1.34	1.39
B	SAW/SR ARQ	[133,171]	1024	1.07	1.09	1.14

- No power loading is possible. Each symbol of the block is assigned a power P_T/K .
- The bit allocation will be equal for all symbols of the block: $m_0 = \dots = m_{K-1} = m$.

The resulting mean BER and goodput are respectively given by

$$\bar{\rho}_{ZF}^{\text{CPSC}} = c_1 \exp \left(- \frac{c_2 \frac{P_T}{K\sigma_n^2}}{(2^m - 1) \frac{1}{K} \sum_{k=0}^{K-1} \frac{1}{h_k}} \right) \quad (5.32)$$

$$GP_{ZF}^{\text{CPSC}} = (r K m) FSR(\bar{\rho}_{ZF}^{\text{CPSC}}). \quad (5.33)$$

As a consequence, the only possible adaptive strategy for ZF-CPSC is the choice of the constellation level m , which is common for all symbols of the block. To be more specific, given a channel realization \mathbf{h} and a transmit power value P_T , the goodput (5.32)-(5.33) can be computed for all possible constellation levels ($m \in \{2, 4, 6\}$ in this work). Then, the constellation level m which generates the highest goodput is chosen for transmission. This strategy will be referred to as "adaptive ZF-CPSC" in the following.

Let us consider the same simulations parameters as in Fig. 5.7 ($K = 32$, $L = 7$, $N_f = 1024$, convolutional code [133, 171], SR/SAW ARQ) and compare OFDM (with RRBA/EBPA) and ZF-CPSC in terms of goodput. The result is depicted in Fig. 5.9. Let us analyze it. First, considering ZF-CPSC with a

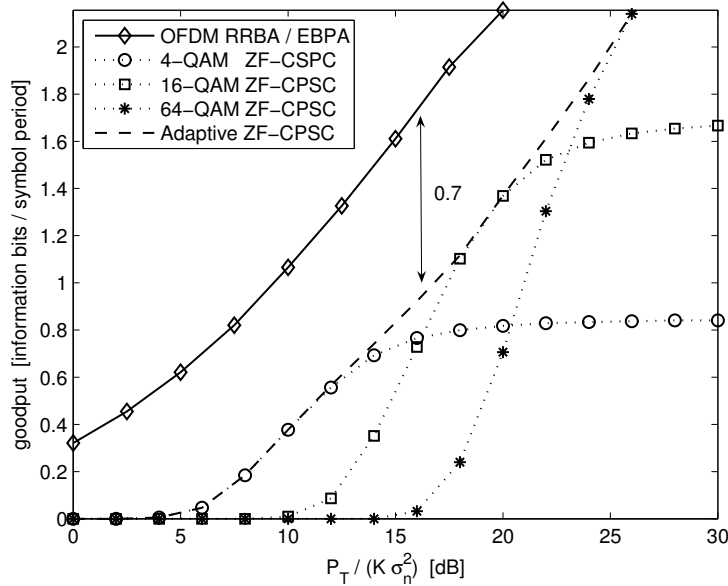


Figure 5.9 Goodput comparison between OFDM and ZF-CPSC ($K = 32$, $L = 7$, $N_f = 1024$, convolutional code [133, 171], SR ARQ).

fixed constellation size (4-QAM, 16-QAM, or 64-QAM), we see that 4-QAM is best for low $\frac{P_T}{K \sigma_n^2}$ values, 64-QAM for high values, and 16-QAM for middle range values, as expected. Second, we see that adaptive ZF-CPSC presents a goodput curve which envelops the curves for fixed constellations, as expected again. In particular, adaptive ZF-CPSC generates a non-negligible goodput gain for the $\frac{P_T}{K \sigma_n^2}$ intervals [12,18] and [20,26] dB. These ranges of $\frac{P_T}{K \sigma_n^2}$ correspond to the transition between the optimality zones of the different constellations. Finally, and most importantly, we see that OFDM with RRBA/EBPA considerably outperforms adaptive ZF-CPSC. The goodput increase is about 0.7 information bits per symbol period, which is obviously significant.

5.10 Conclusions

We have addressed the problem of allocating bits and power in a convolutionally coded adaptive OFDM system with hard Viterbi decoding, and ARQ

retransmission protocol. The objective was to maximize the number of information bits delivered without error to the user by unit of time, or goodput. This criterion has been chosen because it reaches a trade-off between the bit rate and BER criteria, and because it really expresses what a user is specifically looking for in some applications like data file transmission. For three types of ARQ protocols, we presented a formulation of the goodput, under the assumption of channels with slow fading, purely random (de)interleaver, and perfect cyclic redundancy check.

Different strategies were proposed for solving the discrete bit and power allocation problem. Note that, although it is clear that some of the proposed algorithms (e.g. the BBBA) have a high complexity, they were developed mainly for comparison purpose. The main result of this chapter is then the following: it was proved that the waterfilling solution with adequate SNR gap value (or equivalently target BER) is equal to the solution to the relaxed problem with EBPA, which was shown to be near-optimal in terms of goodput while having lower complexity. Note that the near-optimality of the waterfilling solution should not surprise the reader: the goodput expresses a trade-off between the bit rate and BER criteria. Maximizing the goodput can thus be done by jointly maximizing the bit rate for a target BER (a problem whose solution is the waterfilling solution), and tuning the target BER. In this chapter, we showed how to choose this target BER, or equivalently the SNR gap value. We analytically showed how this SNR gap value depends on the convolutional code used, the frame length, the type of ARQ protocol used, the available transmit power, and the harmonic and geometric mean of the subcarrier gains.

In addition, the OFDM and ZF-CPSC systems (with potential bit and power loading) were compared in terms of achievable goodput. It was shown that the OFDM modulation significantly outperforms ZF-CPSC. This is also not a surprise: since the SNR is equal for all symbols of a ZF-CPSC block, less degrees of freedom are available for bit and power loading in such system (with respect to OFDM).

The work presented in this chapter has considered a system with hard-decision Viterbi decoding, which is known to be suboptimal. An extension of this work to a system with soft Viterbi decoding (i.e. based on Euclidean distances) is under investigation [94]. Another interesting direction to pursue

could be the introduction of the coding rate selection into the goodput maximization problem.

Appendix 5.A More on the waterfilling solution

let us now focus on a less common issue related to the waterfilling policy that was presented in Section 5.3: imagine you are given two realizations of the subcarrier gains, say \mathbf{h}^A and \mathbf{h}^B . Knowing that you get to perform waterfilling on \mathbf{h}^A or \mathbf{h}^B , which realization would you choose? In other words, we look for a relation between the elements of \mathbf{h}^A and \mathbf{h}^B such that, after waterfilling, the channel realization B is ensured to outperform realization A (or vice versa) in terms of bit rate. The following answer could come first to the reader's mind: if $\max(\mathbf{h}^B) > \max(\mathbf{h}^A)$, then the channel realization B is going to outperform channel realization A , for very low values of the transmit power P_T . In fact, at very low P_T , only one subcarrier (the one with the highest gain) is likely to be used for transmission ($K' = 1$). Nevertheless, we would be interested in identifying a sufficient condition which would be independent of the value of the transmit power P_T . Obviously, the condition $\min(\mathbf{h}^B) > \max(\mathbf{h}^A)$ is sufficient for realization B to outperform realization A at all values of P_T . However, this last condition is too restrictive and we would like to develop a weaker sufficient condition. This is the purpose of the following proposition.

Proposition 5.4. *Assume two sets of realizations of subcarrier gains $\mathbf{h}^A = [h_0^A, \dots, h_{K-1}^A]^T$ and $\mathbf{h}^B = [h_0^B, \dots, h_{K-1}^B]^T$. If set B logarithm-majorizes set A , i.e. $\log_2(\mathbf{h}^A) \prec \log_2(\mathbf{h}^B)$, or*

$$[\log_2(h_0^A), \dots, \log_2(h_{K-1}^A)]^T \prec [\log_2(h_0^B), \dots, \log_2(h_{K-1}^B)]^T \quad (5.34)$$

which is equivalent to

$$\prod_{i=0}^{N-1} h_{[i]}^A \leq \prod_{i=0}^{N-1} h_{[i]}^B, \quad N = 1, \dots, K-1 \quad (5.35)$$

$$\prod_{i=0}^{K-1} h_{[i]}^A = \prod_{i=0}^{K-1} h_{[i]}^B, \quad (5.36)$$

then the following inequality holds

$$\max_{p_k^A \geq 0} \frac{1}{K} \sum_{k=0}^{K-1} \log_2 \left(1 + p_k^A \frac{h_k^A}{\sigma_n^2 \Gamma} \right) \leq \max_{p_k^B \geq 0} \frac{1}{K} \sum_{k=0}^{K-1} \log_2 \left(1 + p_k^B \frac{h_k^B}{\sigma_n^2 \Gamma} \right) \quad (5.37)$$

where the maximization problems, at the left and right sides of the inequality sign, both have the same power budget: $\sum_{k=0}^{K-1} p_k^A \leq P_T$ and $\sum_{k=0}^{K-1} p_k^B \leq P_T$, respectively. And the proposition holds for any positive value of P_T .

Proof. Assume, without loss of generality, that the components of vectors \mathbf{h}^A and \mathbf{h}^B are with decreasing order, i.e. $\mathbf{h}^A, \mathbf{h}^B \in \mathcal{D}$ (see definition of \mathcal{D} in Proposition 4.5).

From what we have seen earlier in this chapter in Section 5.3, we know that the solutions to the maximization problems in (5.37), are given by the waterfilling policy (5.7)-(5.8). Let us denote these waterfilling solutions (5.7)-(5.8) by $\check{\mathbf{p}}^A = [\check{p}_0^A, \dots, \check{p}_{K-1}^A]^T$ and $\check{\mathbf{p}}^B = [\check{p}_0^B, \dots, \check{p}_{K-1}^B]^T$, respectively. Since $\mathbf{h}^A \in \mathcal{D}$, we deduce from (5.7) that

$$\check{p}_0^A \geq \dots \geq \check{p}_{K-1}^A \geq 0, \quad (5.38)$$

i.e. $\check{\mathbf{p}}^A \in \mathcal{D}_+ = \{\mathbf{x} : x_0 \geq x_1 \geq \dots \geq x_{K-1} \geq 0\}$.

Let us now consider the function $\phi(\mathbf{x}) = \sum_{k=0}^{K-1} g_k(x_k)$, $\mathbf{x} \in \mathcal{D}$, with $g_k(x_k) = \log_2(1 + \check{p}_k^A 2^{x_k})$. Given that

$$\frac{\partial g_k(x_k)}{\partial x_k} = \frac{\check{p}_k^A 2^{x_k}}{1 + \check{p}_k^A 2^{x_k}}, \quad (5.39)$$

it can be easily verified that the inequalities (5.38) ensure that the derivatives (5.39) will satisfy the conditions (4.10). Consequently, by Proposition 4.5, ϕ is a Schur-convex function on \mathcal{D} . Then, noting first that $\log_2(\mathbf{h}^A) \prec \log_2(\mathbf{h}^B)$ implies $\log_2\left(\frac{\mathbf{h}^A}{\sigma_n^2 \Gamma}\right) \prec \log_2\left(\frac{\mathbf{h}^B}{\sigma_n^2 \Gamma}\right)$, we deduce from Proposition 4.3 that

$$\phi\left(\log_2\left(\frac{\mathbf{h}^A}{\sigma_n^2 \Gamma}\right)\right) \leq \phi\left(\log_2\left(\frac{\mathbf{h}^B}{\sigma_n^2 \Gamma}\right)\right) \quad (5.40)$$

i.e.

$$\sum_{k=0}^{K-1} \log_2 \left(1 + \check{p}_k^A 2^{\log_2\left(\frac{h_k^A}{\sigma_n^2 \Gamma}\right)} \right) \leq \sum_{k=0}^{K-1} \log_2 \left(1 + \check{p}_k^A 2^{\log_2\left(\frac{h_k^B}{\sigma_n^2 \Gamma}\right)} \right) \quad (5.41)$$

$$\sum_{k=0}^{K-1} \log_2 \left(1 + \check{p}_k^A \frac{h_k^A}{\sigma_n^2 \Gamma} \right) \leq \sum_{k=0}^{K-1} \log_2 \left(1 + \check{p}_k^A \frac{h_k^B}{\sigma_n^2 \Gamma} \right). \quad (5.42)$$

Finally, by the optimality property of the waterfilling solution $\check{\mathbf{p}}^B$, we have that

$$\sum_{k=0}^{K-1} \log_2 \left(1 + \check{p}_k^A \frac{h_k^B}{\sigma_n^2 \Gamma} \right) \leq \sum_{k=0}^{K-1} \log_2 \left(1 + \check{p}_k^B \frac{h_k^B}{\sigma_n^2 \Gamma} \right). \quad (5.43)$$

Combining (5.42) and (5.43) concludes the proof. \square

Interestingly, putting Propositions 4.9 and 5.4 together, we conclude that the logarithm-majorization $\log_2(\mathbf{h}^A) \prec \log_2(\mathbf{h}^B)$ is a sufficient condition for the bit rate associated with channel realization B to be greater or equal to that of channel realization A , irrespectively of whether the waterfilling power allocation is carried out or not. Let us now illustrate this feature with an example. Two realizations (A and B) of the gains of 8 subcarriers are given in Fig. 5.10. These realizations are such that set B logarithm-majorizes set A , i.e. $\log_2(\mathbf{h}^A) \prec \log_2(\mathbf{h}^B)$. The corresponding achievable bit rate are then given in Fig. 5.11, both without power loading (dashed lines) and with waterfilling power loading (solid lines). First, we can see that realization B outperforms realization A both without and with waterfilling power loading, illustrating Propositions 4.9 and 5.4, respectively. Second, it can be seen that the gain of doing waterfilling is bigger for channel realization B than for A . Finally, as the transmit power P_T increases, this gain decreases less rapidly for realization B .

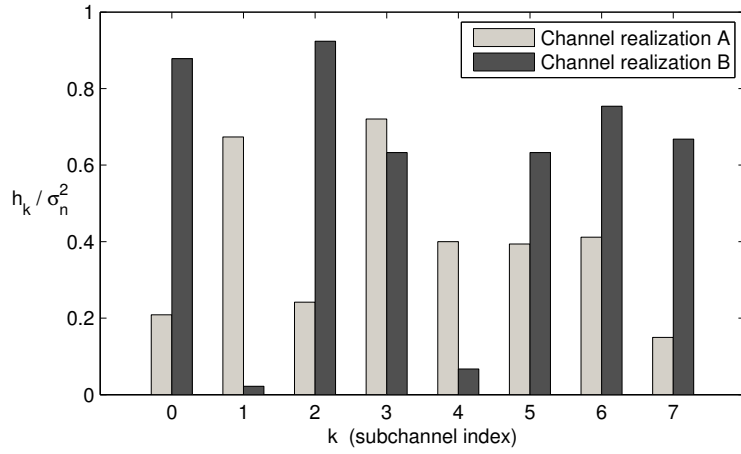


Figure 5.10 Two channel realizations verifying $\log_2(\gamma^A) < \log_2(\gamma^B)$. $K = 8$.

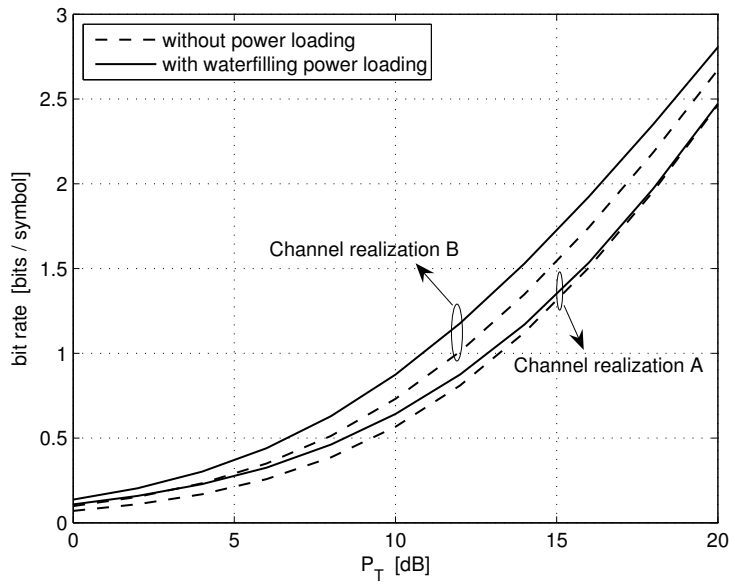


Figure 5.11 Achievable bit rate (with SNR gap $\Gamma = 1$) for channel realizations A and B, without and with waterfilling power allocation.

Exploiting Cyclic Prefix for Performance Improvement in CPSC Systems

6

The content of this chapter has been published in [30].

6.1 Introduction

Remember from Chapter 2 that, in cyclically prefixed block transmission, the role of the cyclic prefix (CP) is twofold. Firstly, it acts as a guard period preventing interference between successive blocks. Secondly, the CP converts the linear convolution with the channel impulse response into a cyclic one and (I)FFT operations then allow the equalization to be held in the frequency domain, with low complexity. To play efficiently these two roles, the CP must be of length greater or equal to the channel impulse response's delay (equal to $L - 1$ symbol periods).

Conventionally, and in all previous chapters of this thesis, the CP is discarded at the receiver side. While it is sometimes used for channel estimation [95,96] or synchronization [97], the part of the received signal corresponding to the CP is conventionally not used for equalization purposes. Recently, an OFDM receiver exploiting the CP for improved data detection was introduced in [98]. However, the proposed receiver only uses the part of the CP that does not suffer from interference from the previous block (in case the

cyclic prefix length is strictly greater than the channel impulse response's delay).

The purpose of this chapter is to propose a new CPSC linear receiver exploiting the whole received signal (including the CP) for data detection. We show that the proposed scheme improves the performance of the communication system, both in terms of BER and goodput. A ZF type of linear equalization is assumed throughout this chapter, without loss of generality.

The chapter is organized as follows. We start in Section 6.2 by first briefly reminding the conventional CPSC scheme and then by presenting the proposed scheme. It is then simulated and compared to the conventional scheme in Section 6.3.

6.2 Proposed CPSC scheme

Let us focus on the transmission of the i th symbol block. The global situation is depicted in Fig. 6.1. The transmitted and received block $i - 1$ and $i + 1$ are also included. We can already mention a difference in Fig. 6.1 with respect to what was presented in Chapter 2: here the CP has length equal to L , instead of $L - 1$ as before. The reason for that will be given later on. The i th block of data symbols is denoted by $\mathbf{d}^i = [d_0^i, \dots, d_{K-1}^i]^T$. After the addition of the CP, we get the following $(K + L) \times 1$ vector

$$\tilde{\mathbf{d}}^i = [d_{K-L}^i, \dots, d_{K-1}^i, d_0^i, \dots, d_{K-1}^i]^T \quad (6.1)$$

$$= [\mathbf{d}_{\text{CP}}^{i,T}, \mathbf{d}_{\text{noCP}}^{i,T}, \mathbf{d}_{\text{CP}}^{i,T}]^T \quad (6.2)$$

where we split the transmitted block \mathbf{d}^i into two components, distinguishing the L symbols belonging to the CP from the others:

$$\mathbf{d}^i = [\mathbf{d}_{\text{noCP}}^{i,T}, \mathbf{d}_{\text{CP}}^{i,T}]^T \quad (6.3)$$

$$\mathbf{d}_{\text{CP}}^i = [d_{K-L}^i, \dots, d_{K-1}^i]^T \quad (6.4)$$

$$\mathbf{d}_{\text{noCP}}^i = [d_0^i, d_1^i, \dots, d_{K-L-1}^i]^T. \quad (6.5)$$

These notations are illustrated in Fig. 6.1.

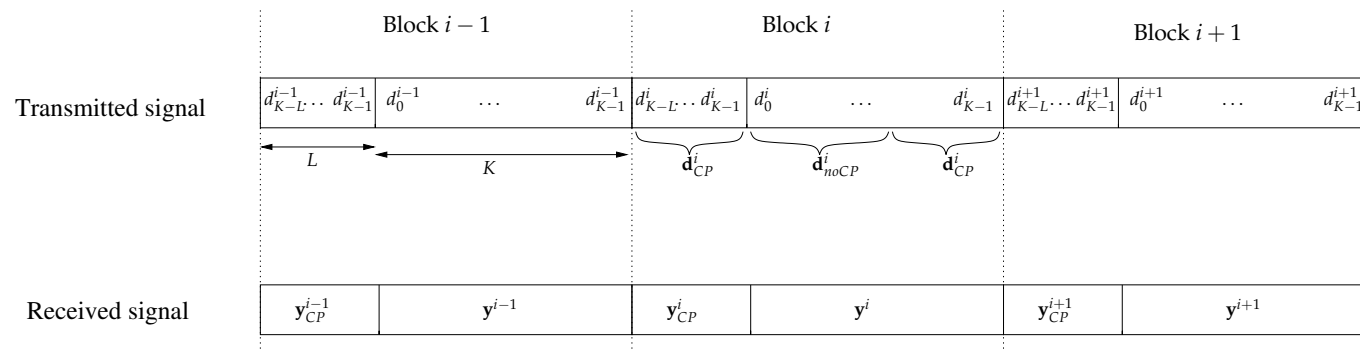


Figure 6.1 The cyclic prefix as guard interval: three consecutive blocks.

6.2.1 Conventional receiver

The conventional ZF linear receiver for CPSC was described in Subsection 2.4.2.2. It does not use the part of the received signal which corresponds to the CP: the $L \times 1$ received block \mathbf{y}_{CP}^i (see definition in Fig. 6.1) is discarded and the following K samples are considered

$$\mathbf{y}^i = \mathbf{G}_{c,K}^i \mathbf{d}^i + \mathbf{n}^i \quad (6.6)$$

$$= \mathbf{W}_K^H \mathbf{\Omega}_K^i \mathbf{W}_K \mathbf{d}^i + \mathbf{n}^i \quad (6.7)$$

which is nothing more than the signal (2.51) with extra sub/superscripts which clearly identify the considered block index (i) and the matrices size (K). The conventional ZF linear receiver was presented in part (a) of Fig. 2.6. The corresponding conventional estimate is given by

$$\hat{\mathbf{d}}_{\text{conv}}^i = \mathbf{W}_K^H \mathbf{\Omega}_K^{i-1} \mathbf{W}_K \mathbf{y}^i \quad (6.8)$$

$$= \mathbf{d}^i + \mathbf{W}_K^H \mathbf{\Omega}_K^{i-1} \mathbf{W}_K \mathbf{n}^i \quad (6.9)$$

$$= \mathbf{d}^i + \mathbf{\ddot{n}}_{\text{conv}}^i \quad (6.10)$$

with $\mathbf{\ddot{n}}_{\text{conv}}^i \triangleq \mathbf{W}_K^H \mathbf{\Omega}_K^{i-1} \mathbf{W}_K \mathbf{n}^i$. As commented in Subsection 3.2.2, the noise effecting this estimate is no longer white, but its covariance matrix is circulant: all symbol estimates in (6.10) are affected by a noise with equal variance, which is given by

$$(\sigma_n^2)_{\text{conv}}^i = \frac{\sigma_n^2}{K} \sum_{k=0}^{K-1} \frac{1}{h_{k,K}^i} \quad (6.11)$$

where, again, sub/superscripts have been added to the definition of the h_k in (3.2).

6.2.2 Proposed receiver

In the last subsection, we reminded that discarding the CP is the first thing a conventional receiver does. In other words, only part of the received signal is used for data estimation. In this subsection, we will present a way to use the entire received signal to generate better estimates.

Let us consider again the situation described in Fig. 6.1, where three consecutive blocks ($i-1$, i and $i+1$) are represented. Having received all blocks

until the $i + 1$ (included), we focus on the detection of the data block i . As a consequence, the reader can already conclude that the proposed scheme increases the detection delay by one block period (i.e. $K + L$ symbol periods). The vector notations are defined in Fig. 6.1. Having received block $i + 1$, we carry out the following steps. The block diagram of the proposed receiver is given in Fig. 6.2, where each individual step can be distinguished (see the legend).

■ **Step 1:**

Using a conventional receiver on received vector \mathbf{y}^{i+1} , we are able to generate the following conventional estimate

$$\hat{\mathbf{d}}_{\text{conv}}^{i+1} = \mathbf{d}^{i+1} + \mathbf{W}_K^H \boldsymbol{\Omega}_K^{(i+1),-1} \mathbf{W}_K \mathbf{n}^{i+1} \quad (6.12)$$

$$= \mathbf{d}^{i+1} + \ddot{\mathbf{n}}_{\text{conv}}^{i+1} \quad (6.13)$$

whose noise samples have variance

$$(\sigma_n^2)_{\text{conv}}^{i+1} = \frac{\sigma_n^2}{K} \sum_{k=0}^{K-1} \frac{1}{h_{k,K}^{i+1}}. \quad (6.14)$$

Note that $\hat{\mathbf{d}}_{\text{conv}}^{i+1}$ can be split into $\hat{\mathbf{d}}_{\text{CP,conv}}^{i+1}$ and $\hat{\mathbf{d}}_{\text{noCP,conv}}^{i+1}$, in a similar fashion as in (6.3). Similarly, from step 1 of previous block period (i.e. block period i), we already have conventional estimates for \mathbf{d}_{CP}^i and $\mathbf{d}_{\text{noCP}}^i$ at our disposal:

$$\hat{\mathbf{d}}_{\text{CP,conv}}^i = \mathbf{d}_{\text{CP}}^i + \ddot{\mathbf{n}}_{\text{CP,conv}}^i \quad (6.15)$$

$$\hat{\mathbf{d}}_{\text{noCP,conv}}^i = \mathbf{d}_{\text{noCP}}^i + \ddot{\mathbf{n}}_{\text{noCP,conv}}^i \quad (6.16)$$

with

$$(\sigma_n^2)_{\text{CP,conv}}^i = (\sigma_n^2)_{\text{noCP,conv}}^i = \frac{\sigma_n^2}{K} \sum_{k=0}^{K-1} \frac{1}{h_{k,K}^i}. \quad (6.17)$$

■ **Step 2:**

On the one hand, from the previous block period, we have decisions on \mathbf{d}^{i-1} at our disposal. Consequently, the contribution of $\mathbf{d}_{\text{CP}}^{i-1}$

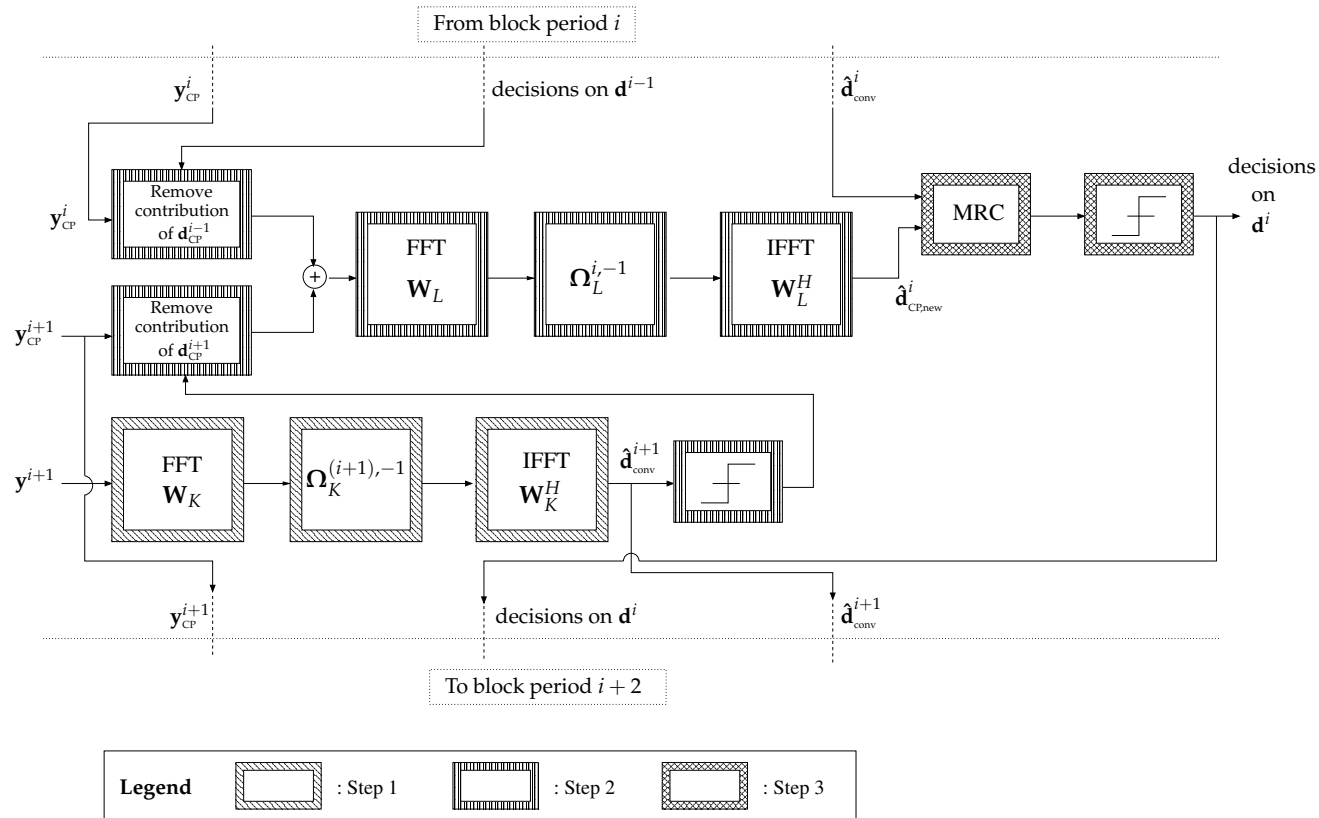


Figure 6.2 Block diagram of the proposed receiver: block period $i + 1$, detection of data block i .

can be subtracted from received vector \mathbf{y}_{CP}^i , leading to $\tilde{\mathbf{y}}_{\text{CP}}^i$:

$$\tilde{\mathbf{y}}_{\text{CP}}^i = \begin{pmatrix} g_0^i & 0 & \cdots & 0 \\ g_1^i & g_0^i & 0 & \cdots & 0 \\ \vdots & & & & \\ & & & \ddots & 0 \\ g_{L-1}^i & \cdots & & g_1^i & g_0^i \end{pmatrix} \mathbf{d}_{\text{CP}}^i + \mathbf{n}_{\text{CP}}^i. \quad (6.18)$$

On the other hand, based on the estimate $\hat{\mathbf{d}}_{\text{CP,conv}}^{i+1}$ from step 1 in (6.13), temporary decisions can be made on the transmitted symbols $\mathbf{d}_{\text{CP}}^{i+1}$. We are thus able to subtract the contribution of $\mathbf{d}_{\text{CP}}^{i+1}$ from $\mathbf{y}_{\text{CP}}^{i+1}$, leading to $\tilde{\mathbf{y}}_{\text{CP}}^{i+1}$:

$$\tilde{\mathbf{y}}_{\text{CP}}^{i+1} = \begin{pmatrix} 0 & g_{L-1}^i & \cdots & g_2^i & g_1^i \\ 0 & 0 & g_{L-1}^i & \cdots & g_2^i \\ \vdots & & & \ddots & \vdots \\ & & & & g_{L-1}^i \\ 0 & \cdots & & 0 & 0 \end{pmatrix} \mathbf{d}_{\text{CP}}^i + \mathbf{n}_{\text{CP}}^{i+1}. \quad (6.19)$$

Note that the errors in all decision makings were neglected. Adding (6.18) and (6.19), we get

$$\tilde{\mathbf{y}}_{\text{CP}} = \tilde{\mathbf{y}}_{\text{CP}}^i + \tilde{\mathbf{y}}_{\text{CP}}^{i+1} \quad (6.20)$$

$$= \mathbf{G}_{c,L}^i \mathbf{d}_{\text{CP}}^i + \mathbf{n}_{\text{CP}}^i + \mathbf{n}_{\text{CP}}^{i+1}. \quad (6.21)$$

We see that we end up with a very simple signal model which involves an $L \times L$ circulant matrix $\mathbf{G}_{c,L}^i$. Note that it is precisely why the proposed scheme requires a CP of length at least equal to L . In fact, a circulant matrix generated from a channel impulse response with L taps is at least of size $L \times L$. Using again the property (2.25) of circulant matrices, we rewrite

$$\tilde{\mathbf{y}}_{\text{CP}} = \mathbf{W}_L^H \boldsymbol{\Omega}_L^i \mathbf{W}_L \mathbf{d}_{\text{CP}}^i + \mathbf{n}_{\text{CP}}^{i+1} + \mathbf{n}_{\text{CP}}^i. \quad (6.22)$$

Finally, (6.22) can easily be ZF equalized using FFT and IFFT operations. However, this time, (I)FFT operations of size L have to be used.

We get the following new estimate

$$\hat{\mathbf{d}}_{\text{CP,new}}^i = \mathbf{d}_{\text{CP}}^i + \mathbf{W}_L^H \boldsymbol{\Omega}_L^{i-1} \mathbf{W}_L (\mathbf{n}_{\text{CP}}^{i+1} + \mathbf{n}_{\text{CP}}^i) \quad (6.23)$$

$$= \mathbf{d}_{\text{CP}}^i + \mathbf{\ddot{n}}_{\text{CP,new}}^i \quad (6.24)$$

and the noise variance is given by

$$(\sigma_n^2)_{\text{CP,new}}^i = \frac{2 \sigma_n^2}{L} \sum_{l=0}^{L-1} \frac{1}{h_{l,L}^i}. \quad (6.25)$$

■ **Step 3:**

At this time, two estimates for \mathbf{d}_{CP}^i , (6.15) and (6.24), have been generated and have to be recombined. These two estimates are affected by noise having different variances, respectively (6.17) and (6.25). We can recombine these two estimates using maximum ratio combining (MRC):

$$\begin{aligned} \hat{\mathbf{d}}_{\text{CP,MRC}}^i &= \frac{(\sigma_n^2)_{\text{CP,conv}}^i \hat{\mathbf{d}}_{\text{CP,new}}^i + (\sigma_n^2)_{\text{CP,new}}^i \hat{\mathbf{d}}_{\text{CP,conv}}^i}{(\sigma_n^2)_{\text{CP,conv}}^i + (\sigma_n^2)_{\text{CP,new}}^i} \\ &= \mathbf{d}_{\text{CP}}^i + \mathbf{\ddot{n}}_{\text{CP,MRC}}^i. \end{aligned} \quad (6.26)$$

The variance associated with this final CP estimate is always smaller than the variance (6.11) associated with the conventional scheme

$$(\sigma_n^2)_{\text{CP,MRC}}^i = \frac{(\sigma_n^2)_{\text{CP,conv}}^i (\sigma_n^2)_{\text{CP,new}}^i}{(\sigma_n^2)_{\text{CP,conv}}^i + (\sigma_n^2)_{\text{CP,new}}^i} \quad (6.27)$$

$$\leq (\sigma_n^2)_{\text{CP,conv}}^i = (\sigma_n^2)_{\text{conv}}^i. \quad (6.28)$$

Using (6.16) and (6.26), the final estimate for \mathbf{d}^i is given by

$$\hat{\mathbf{d}}^i = [\hat{\mathbf{d}}_{\text{noCP,conv}}^{i,T}, \hat{\mathbf{d}}_{\text{CP,MRC}}^{i,T}]^T. \quad (6.29)$$

We see that the proposed scheme generates better estimates with reasonable additional complexity: it increases the complexity of the conventional scheme by one FFT, one IFFT (both of size L) and about L^2 multiplications.

6.2.3 Power loading

As described in last subsection, the proposed scheme is able to generate better estimates (in terms of signal to noise ratio), but only for the symbols belonging to the CP (i.e. the L last symbols of the block \mathbf{d}^i). However, using power loading, this signal to noise ratio gain can easily be distributed among all K symbols of the block. In fact, less transmit power can be allocated to CP symbols and more power to the others: concretely instead of transmitting (6.2), we transmit

$$\tilde{\mathbf{d}}^i = [\sqrt{p_{\text{CP}}} \mathbf{d}_{\text{CP}}^{i,T}, \sqrt{p_{\text{noCP}}} \mathbf{d}_{\text{noCP}}^{i,T}, \sqrt{p_{\text{CP}}} \mathbf{d}_{\text{CP}}^{i,T}]^T \quad (6.30)$$

with $p_{\text{noCP}} \geq p_{\text{CP}}$. Assuming identical constellation size, in order to have equal BER on all K symbols we must impose

$$\frac{p_{\text{noCP}}}{(\sigma_{\tilde{n}}^2)^i_{\text{conv}}} = \frac{p_{\text{CP}}}{(\sigma_{\tilde{n}}^2)^i_{\text{CP,MRC}}} \quad (6.31)$$

under the transmit power constraint

$$2L p_{\text{CP}} + (K - L) p_{\text{noCP}} = K + L. \quad (6.32)$$

Form (6.31) and (6.32), we deduce

$$p_{\text{noCP}} = \frac{K + L}{2L \frac{(\sigma_{\tilde{n}}^2)^i_{\text{CP,MRC}}}{(\sigma_{\tilde{n}}^2)^i_{\text{conv}}} + (K - L)} \quad (6.33)$$

$$p_{\text{CP}} = \frac{K + L}{2L + (K - L) \frac{(\sigma_{\tilde{n}}^2)^i_{\text{conv}}}{(\sigma_{\tilde{n}}^2)^i_{\text{CP,MRC}}}}. \quad (6.34)$$

Note that this solution for the power loading supposes that the quantities (6.11) and (6.27) are known at the transmitter. A limited feedback from the receiver to the transmitter is thus required.

6.3 Performance evaluation

In this section, the performance of the proposed scheme (power loading included) is evaluated and compared to the conventional CPSC scheme. In particular, the BER and goodput will be successively used as comparison criteria. All curves that will be presented result from an average over several

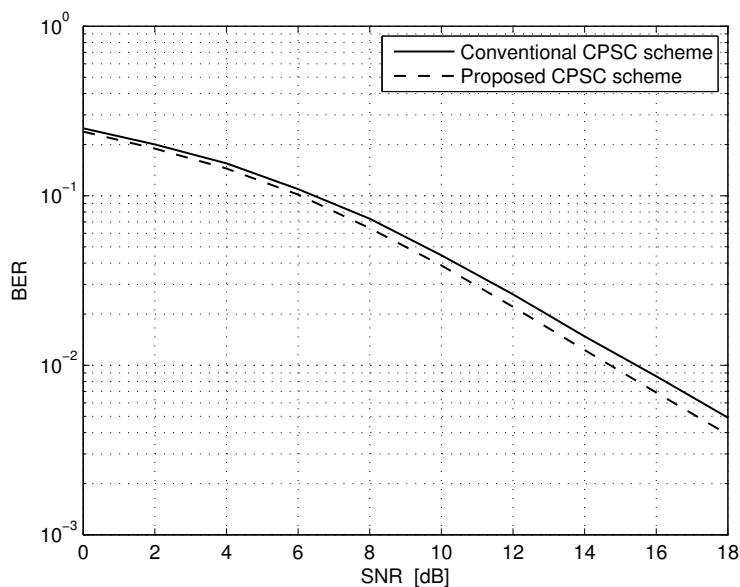


Figure 6.3 BER comparison between the proposed and conventional schemes, for $K = 32$, and $L = 6$.

channel realizations. BPSK modulation is assumed, unless otherwise stated. The transmit power being normalized, the average SNR is defined, as before, as $\gamma = 1/\sigma_n^2$. While the errors in all decisions making were neglected in the derivations of last section, possible error propagations are taken into account in the simulations.

6.3.1 Bit error rate

As described in section 6.2, the proposed scheme generates estimates that are affected by noise with lower variance, in comparison with the conventional scheme. In other words, the proposed scheme always achieves a lower BER than the conventional scheme, theoretically at least (i.e. under the assumption of no error propagation).

Fig. 6.3 shows the BER for the following parameters: $K = 32$, $L = 6$. We see that the proposed scheme outperforms the conventional scheme by almost

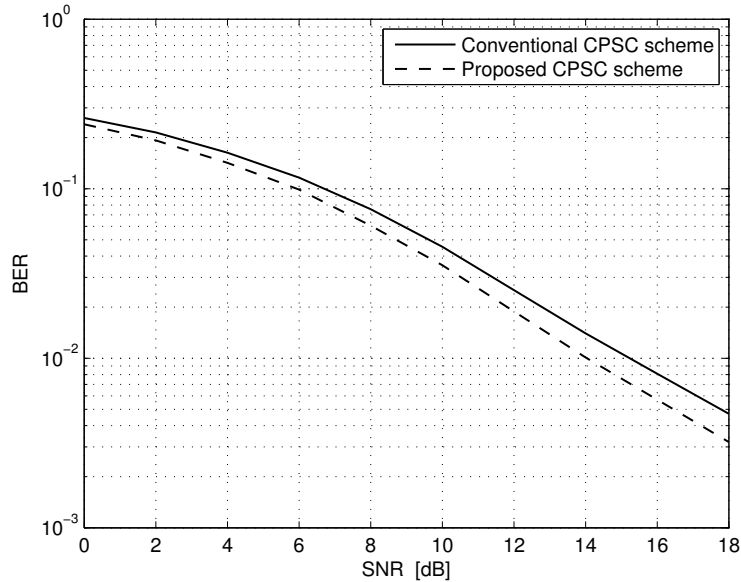


Figure 6.4 BER comparison between the proposed and conventional schemes, for $K = 32$, and $L = 16$.

1 dB at sufficiently high SNR. Note however that the difference between the two schemes is smaller at low SNR. This comes from the fact that, at low SNR, the proposed scheme suffers more from error propagation.

Fig. 6.4 gives the same BER curves but for $L = 16$. Like expected, we see that the BER improvement is greater than for $L = 6$. In fact, the proposed scheme only generates better estimates for the symbols belonging to the CP. As a consequence, the greater the CP length with respect to K , the greater the performance enhancement of the proposed scheme will be (in terms of BER). Not to mislead the reader, let us mention that the situation of Fig. 6.4 is not representative of practical systems: a CP length equal to half of the block size ($L = K/2$) is not acceptable in terms of efficiency and will most probably never be encountered in practice. In other words, Fig. 6.4 should be interpreted as an illustration of the theoretical results from Section 6.2, nothing more.

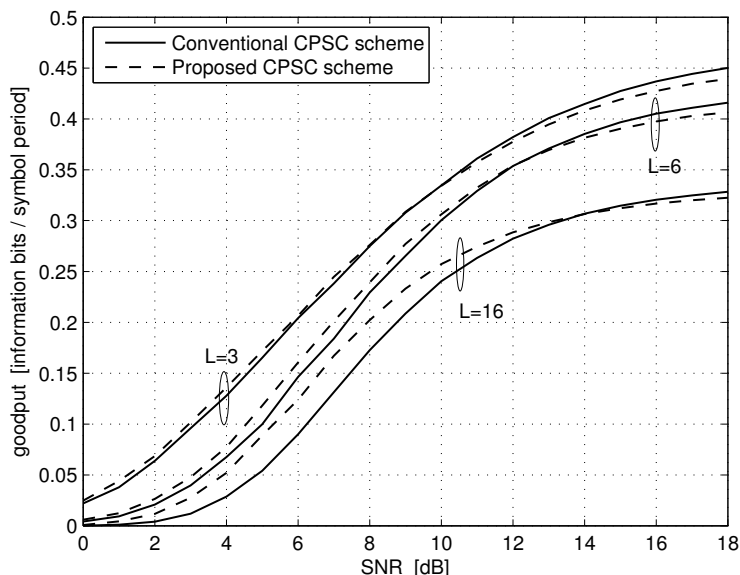


Figure 6.5 Goodput comparison between the proposed and conventional schemes, for $K = 32$ and different values of L .

6.3.2 Goodput

In last subsection, we showed the BER improvement achieved by the proposed scheme. However, the proposed scheme uses a CP length equal to L , instead of $L - 1$ for the conventional scheme. The proposed scheme is thus slightly less efficient than the conventional scheme, in terms of data rate. In this subsection, in order to see if the BER improvement compensates for the loss in data rate efficiency, we compare the two schemes in terms of goodput, i.e. error-free rate as defined in Chapter 5. A frame-oriented transmission with convolutional coding and hard-decision Viterbi decoding is again considered. The convolutional code used in the simulations has rate $1/2$, and generator polynomial $[5,7]$ in octal notation. A frame size of $N_f = 128$ bits is considered. The goodput is again expressed as the average number of bits received correctly (i.e. belonging to an error-free frame) per symbol period.

Fig. 6.5 compares the two schemes for $K = 32$ and different values of L . We see that, even though the proposed scheme uses a longer CP, it always

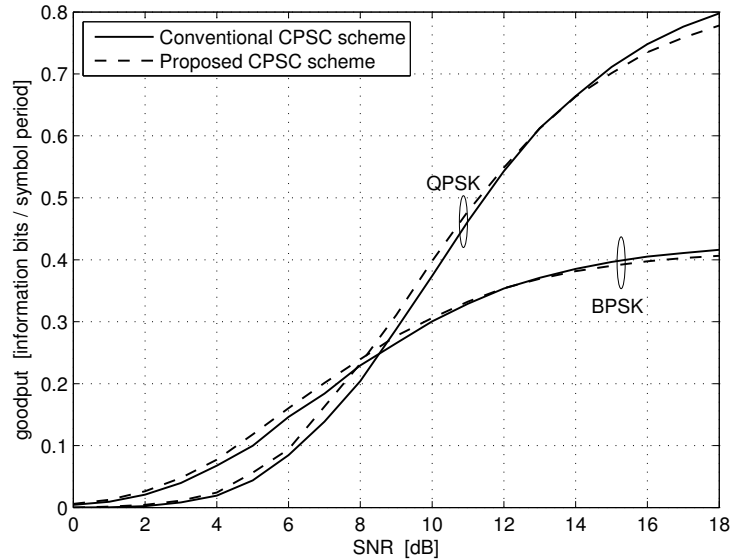


Figure 6.6 Goodput comparison between the proposed and conventional schemes with BPSK and QPSK constellations, for $K = 32$, and $L = 6$.

outperforms the conventional scheme except at high SNR. In fact, at high SNR, the frame success rate is close to one for both schemes, and the loss in data rate efficiency of the proposed scheme (because of the larger CP) directly results in a goodput loss. We also see that the SNR value above which the proposed scheme is outperformed, depends on L : the greater L , the greater this SNR value will be. This is due to the fact that the BER improvement is greater for higher values of L , as shown in the previous subsection.

Having the proposed CPSC scheme outperformed by the conventional one at high SNR in Fig. 6.5 is not a big issue. In fact, as it was shown in Chapter 5, the BPSK constellation would not be used in practice at such high SNR. To illustrate this comment, let us focus on the case $L = 6$, and consider both the BPSK and QPSK constellations. The result is given in Fig. 6.6, and indeed confirms the following: for the range of SNRs where the conventional CPSC outperforms the proposed scheme for BPSK, the QPSK constellation should be employed since it provides a great increase in goodput.

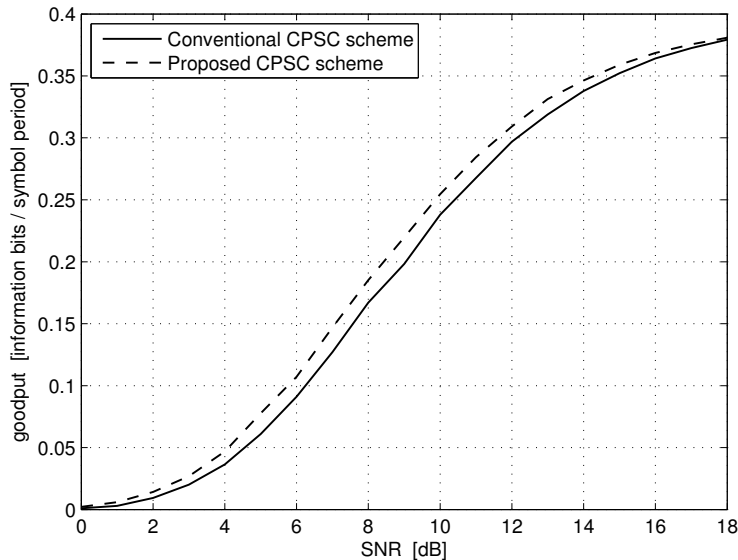


Figure 6.7 Goodput comparison between the proposed and conventional schemes, for $K = 64$, $L = 6$, and CP length = 16.

In practical systems, the CP length is often fixed and chosen to be strictly greater than the channel impulse response's delay. This situation is considered in Fig. 6.7, where the CP length is equal to 16 for both schemes. The parameters are $K = 64$, $L = 6$. As expected, thanks to its BER improvement, the proposed scheme then outperforms the conventional scheme at all SNRs.

6.4 Conclusions

We have presented a new CPSC receiver. The originality lies in the use of the CP for equalization purposes. The proposed scheme requires two FFT sizes and reasonable additional complexity. It always achieves lower BER than the conventional scheme, but requires a slightly longer CP and thus implies an increased loss in data rate efficiency. However, goodput simulations showed that the BER improvement compensates for this loss in efficiency, for the SNRs values consistent with the constellation size considered. Moreover, in practical systems where the CP length is strictly greater than the channel impulse

response's delay, the proposed scheme improves the goodput of the link at all SNRs.

We believe that there is two optimistic (but still honest!) ways of looking at the result presented in this chapter:

- *Mathematical elegance.* Quite surprisingly, the CP can be exploited for equalization in a rather elegant way. In fact, an additional frequency domain equalization can be used, but this time with (I)FFT operations of size equal to the CP length.
- *Practical applicability.* Since the proposed scheme implies extra complexity at the receiver side, it is more suited to the uplink where the base station might be able to afford extra complexity. This is not constraining since CPSC in itself is more adapted to the uplink anyway. Next, the reader might be concerned about the performance enhancement (say in terms of BER) being too small. Then the reader should realize that a performance enhancement of even a fraction of a dB can still be very useful, e.g. in the context of increasing the mobile's battery life.

Conclusions

7

Digital wireless communications have considerably changed not only the way people communicate, but also the way research is conducted in the field of telecommunications. In fact, the nature of the wireless medium has created a number of new challenging and fascinating research topics. In particular, a prerequisite for achieving higher and higher transmission rates in wireless systems is to develop strategies for efficiently dealing with frequency selective channels. A good candidate is the so-called cyclic prefixed block transmission, and in particular its two most popular variants which are the cyclic prefixed single-carrier (CPSC) and orthogonal frequency division multiplexing (OFDM) modulations.

In this context, this thesis aimed at analyzing and optimizing the use of cyclic prefixed block transmission for wireless communications. More specifically, the objective of this thesis was threefold. First, it contributed to the current state-of-the-art on the performance comparison between CPSC and OFDM, focusing on the derivation of analytical results when possible. Second, it aimed at using a system-based or cross-layer criterion for allocating resource, especially in an OFDM system. Third, it discussed the possibility of improving the performance of a CPSC system by exploiting the cyclic prefix (CP) for equalization purposes.

The main contributions of this thesis are summarized hereunder. Each of them actually corresponds to a chapter of this dissertation.

Contributions

A **first contribution** is the analysis of the extraction of the multipath diversity by a CPSC transmission. First, the result in [67] was moderated: if it is true that the asymptotical (i.e. at infinite SNR) diversity order achieved by ML-CPSC is equal to one, we proved that the block size K has an influence on the performance at moderate SNR. In particular, for reasonably large values of K , we saw that the multipath diversity can be extracted by ML-CPSC for the range of BER values typically used in practice. Second, the influence of suboptimal linear receivers on the diversity extraction was investigated. It was proved that the use of a ZF linear receiver in a CPSC system prevents the extraction of any multipath diversity, just as the OFDM modulation. However, the MMSE linear receiver achieves a much better trade-off between performance and complexity: the multipath diversity can also be extracted by MMSE-CPSC for the range of BER values typically used in practice and for sufficiently large values of K .

Publication related to this contribution: [23]

A **second contribution** is the achievable bit rate comparison between OFDM and CPSC, assuming perfect channel state information at the transmitter side (CSIT) and allowing bit loading only. This contribution is the extension of [24], first, to any SNR value and, second, to the MIMO case:

- We analytically proved that, in terms of achievable bit rate and at all SNR, the best performing scheme is OFDM, followed by DFE-CPSC, then MMSE-CPSC, and finally ZF-CPSC. This result was demonstrated thanks to the majorization theory. Note that this specific result was not published yet.
- Focusing on the high SNR region and adding a spatial dimension to the problem, we analytically proved that MIMO DFE-CPSC outperforms MIMO MMSE-OFDM in terms of achievable bit rate. This result is interesting but not surprising: the DFE receiver does a better job than the MMSE receiver at mitigating the spatial interference. However, if spatial precoding is added on a tone basis, leading to a DMMT scheme, both the temporal and spatial interferences are removed. But,

surprisingly again, we have demonstrated that MIMO DFE-CPSC and DMMT perform identically at high SNR.

Publication related to this contribution: [25]

A third contribution is the use of a cross-layer criterion, called goodput, for allocating bits and power in a convolutionally coded adaptive OFDM system with hard Viterbi decoding, and ARQ retransmission protocol. The goodput is defined as the number of information bits delivered without error to the user by unit of time. This criterion has been chosen because it reaches a trade-off between the bit rate and BER criteria, and because it really expresses what a user is specifically looking for in some applications. A mathematical formulation for the goodput was presented, and different strategies were proposed for solving the discrete problem of allocating the bits and power in order to maximize the goodput. The most valuable result is probably the following: rounding the waterfilling solution with adequate SNR gap value (or equivalently target BER) is near-optimal in terms of goodput while having low complexity. Interestingly, we analytically showed how this SNR gap value depends on the convolutional code used, the frame length, the type of ARQ protocol used, the available transmit power, and the harmonic and geometric mean of the subcarrier gains. With this resource allocation strategy, the OFDM modulation was shown to significantly outperforms CPSC in terms of goodput. In fact, since the SNR is equal for all symbols of the block, much less degrees of freedom are available for bit and power loading in a CPSC system, with respect to OFDM.

Publications related to this contribution: [27–29]

A fourth contribution is the exploitation of the CP for equalization purposes in a CPSC system. A new CPSC receiver was proposed, which requires two different FFT sizes and reasonable additional complexity. The proposed receiver was shown to achieve lower BER than the conventional scheme, but to require a slightly longer CP which implies an increased loss in data rate efficiency. However, goodput simulations showed that the BER improvement compensates for this loss in efficiency, for SNRs values consistent with the constellation size considered. Moreover, in practical systems where the CP length is strictly greater than the channel impulse response's delay, the proposed scheme improves the goodput of the link at all SNRs. Finally, since

CPSC in itself is more adapted to the uplink, the extra complexity needed by the proposed scheme might not be such an issue, as the base station might be able to afford it.

Publication related to this contribution: [30]

Discussion and future work

Let us end this dissertation by taking an objective look at the different contributions and discussing them. Additionally, when relevant, potential open issues are identified.

About the performance comparison between CPSC and OFDM, the results derived in this thesis support the following recommendations:

- In the absence of CSIT, one could opt for a CPSC transmission. In fact, as shown in Chapter 3, CPSC is able to outperform OFDM both in terms of instantaneous and average BER. In particular, MMSE-CPSC reaches the best trade-off between performance and complexity: it allows the extraction of the multipath diversity under some realistic hypotheses, and with the same overall complexity as the OFDM modulation.
- With CSIT, however, the OFDM modulation should be preferred, as it offers much more degrees of freedom for adaptive resource allocation. The considerations of Chapter 5 have shown the considerable goodput increase achieved by OFDM, with respect to CPSC.

Interestingly, this performance-based comparison agrees with the system-based comparison. From a system-based point of view, a CPSC transmission suits very well the uplink, thanks to its low PAPR and to having most of its processing complexity at the receiver side. From a performance point of view, CPSC is justified when no CSIT is available, which is also more representative of an uplink scenario. Consequently, as proposed in [11], a hybrid scheme could very well be considered in practice: CPSC in the uplink, and OFDM in the downlink. However, to the best of our knowledge, some open issues remain:

- With perfect CSIT, OFDM is best. Without CSIT, CPSC is best. A more realistic hypothesis would be to consider partial CSIT (imperfect, quantized, or statistical). In such case, it would be useful to derive conditions on how partial the CSIT can get before CPSC outperforms OFDM.
- The same kind of comment holds if realistic non-idealities are included in the comparison. However, as mentioned in the introduction, non-idealities are difficult to analytically include in the performance expressions [14, 15]
- Another feature which is certainly worth taking into account in the comparison, is the scheme's applicability to a multi-user environment. In this context also, the OFDM modulation potentially offers more degrees of freedom for optimization than CPSC [8, 19, 20]. But, again, the level of CSIT will play a role, which would be interesting to investigate.
- Finally, in our opinion, the result in [99] has been under-exploited so far. The authors proposed a "generalized cyclic prefixed" transmission, which allows a parametrized transition between OFDM and CPSC. This elegant framework could allow to choose, depending on the transmit conditions (level of CSIT, non-idealities,...), within a set of hybrid schemes that lies in between OFDM and CPSC (including these).

About the use of the goodput criterion for resource allocation in an OFDM system, the proof of the near-optimality of the waterfilling solution (with adequate SNR gap value, which depends on the transmission parameters) constitutes an interesting results. However, demonstrating that using a well-known technique is more than fine from a goodput point of view, is probably not as promising for future work as we would have hoped. But still:

- This work has considered a system with hard-decision Viterbi decoding, which is known to be suboptimal. An extension of this work to a system with soft Viterbi decoding (i.e. based on Euclidean distances) is under investigation [94].

- This work has assumed perfect CSIT. Unfortunately, its extension to a system with partial CSIT does not seem straightforward.
- Finally, and probably most importantly, the introduction of the coding rate selection into the goodput maximization problem could be considered. The first step towards this goal would be to find an accurate and easy way to express how the frame success rate varies with the coding rate.

Finally, about the use of the CP for equalization purposes in a CPSC system, the proposed scheme trades some additional receive complexity for a performance enhancement of a fraction of a dB, which might be convenient in a practical uplink scenario.

List of Publications

Journal papers

- B. Devillers, J. Louveaux, and L. Vandendorpe, "Bit and power allocation for goodput optimization in coded parallel subchannels with ARQ," *IEEE Trans. on Signal Processing*, vol. 56, no. 8, pp. 3652-3661, Aug. 2008.
- B. Devillers, J. Louveaux, and L. Vandendorpe, "About the diversity in cyclic prefixed single-carrier systems", *Elsevier Physical Communication (PHYCOM) journal*, vol. 1, no. 4, pp. 266-276, Dec. 2008.

Conference papers

- B. Devillers, A. García Armada, J. Louveaux, and L. Vandendorpe, "Resource allocation for goodput optimization in parallel subchannels with error correction and selective repeat ARQ," in *Proc. European Signal Processing Conference, EUSIPCO*, Poznan, Poland, Sept. 2007, pp. 851-855.
- B. Devillers, J. Louveaux, and L. Vandendorpe, "Exploiting cyclic prefix for performance improvement in single carrier systems", in *Proc. IEEE Workshop on Signal Processing Advances in Wireless Communications, SPAWC*, Cannes, France, July 2006, pp. 1-5.
- B. Devillers, and L. Vandendorpe, "Bit and power allocation for goodput optimization in coded OFDM systems", in *Proc. IEEE International*

Conference on Acoustics, Speech and Signal Processing, ICASSP, Toulouse, France, May 2006, pp. 649-652.

- B. Devillers and L. Vandendorpe, "Bit loading for goodput improvement in coded OFDM systems," in *Proc. Joint Conference on Coding and Communications, JCCC, Sölden, Austria, Mar. 2006.*
- B. Devillers, T. Sartenaer, and Luc Vandendorpe, "Bit rate comparison between MIMO cyclically prefixed single carrier and multicarrier transmissions", in *Proc. European Signal Processing Conference, EU-SIPCO, Antalya, Turkey, Sept. 2005.*

Bibliography

- [1] R.W. Chang, "Synthesis of band-limited orthogonal signals for multi-channel data transmission," *Bell Sys Tech. J.*, vol. 45, pp. 1775–1796, Dec. 1966.
- [2] B.R. Saltzberg, "Performance of an efficient parallel data transmission system," *IEEE Trans. Commun.*, vol. 15, no. 6, pp. 805–811, Dec. 1967.
- [3] S.B. Weinstein and P.M. Ebert, "Data transmission by frequency division multiplexing using the discrete Fourier transform," *IEEE Trans. Commun.*, vol. 19, no. 5, pp. 628–634, Oct. 1971.
- [4] A. Peled and A. Ruiz, "Frequency domain data transmission using reduced computational complexity algorithms," in *Proc. IEEE International Conference on Acoustics, Speech and Signal Processing, ICASSP*, vol. 5, May 1980, pp. 964–967.
- [5] B. Hirosaki, "An orthogonally multiplexed QAM system using the discrete Fourier transform," *IEEE Trans. Commun.*, vol. 29, no. 7, pp. 982–989, July 1981.
- [6] J.A.C. Bingham, "Multicarrier modulation for data transmission: An idea whose time has come," *IEEE Commun. Mag.*, vol. 28, pp. 5–14, May 1990.
- [7] Z. Wang and G.B. Giannakis, "Wireless multicarrier communications: where Fourier meets Shannon," *Signal Processing Magazine, IEEE*, vol. 17, no. 3, pp. 29–48, May 2000.
- [8] C. Wong, R. Cheng, K. Letaief, and R. Murch, "Multiuser OFDM with adaptive subcarrier, bit, and power allocation," *IEEE J. Selected Areas Comm.*, vol. 17, no. 10, pp. 1747–1758, Oct. 1999.

- [9] H. Sari, G. Karam, and I. Jeanclaude, "Transmission techniques for digital terrestrial TV broadcasting," *IEEE Commun. Mag.*, vol. 33, no. 2, pp. 100–109, Feb. 1995.
- [10] A. Czylik, "Comparison between adaptive OFDM and single carrier modulation with frequency domain equalization," in *Proc. IEEE 47th Vehicular Technology Conf.*, vol. 2, 1997, pp. 865–869.
- [11] D. Falconer, S. L. Ariyavisitakul and A. Benyamin-Seeyar, and B. Eidson, "Frequency domain equalization for single-carrier broadband wireless systems," *IEEE Commun. Mag.*, vol. 40, no. 4, pp. 58–66, Apr. 2002.
- [12] J. Tubbax, B. Come, L. V. der Perre, L. Deneire, and M. Engels, "OFDM versus single carrier with cyclic prefix: a system-based comparison for binary modulation," in *Proc. of IEEE Vehicular Technology Conference Fall*, vol. 2, Oct. 2001, pp. 1115–1119.
- [13] T. Pollet, M. V. Bladel, and M. Moeneclaey, "BER sensitivity of OFDM systems to carrier frequency offset and wiener phase noise," *IEEE Trans. Commun.*, vol. 43, no. 2-4, pp. 191–193, Feb-Apr. 1995.
- [14] F. Horlin and A. Bourdoux, "Comparison of the sensitivity of OFDM and SC-FDE to CFO, SCO, and IQ imbalance," in *Proc. 3rd International Symposium on Communications, Control and Signal Processing, ISCCSP, Malta*, Mar. 2008, pp. 111–116.
- [15] L. Rugini and P. Banelli, "BER of OFDM systems impaired by carrier frequency offset in multipath fading channels," *IEEE Trans. Wireless Commun.*, vol. 4, no. 5, pp. 2279–2288, Sept. 2005.
- [16] N. Al-Dhahir, "Single-carrier frequency domain equalization for space-time block-coded transmissions over frequency-selective fading channels," *IEEE Commun. Lett.*, vol. 5, no. 7, pp. 304–306, July 2001.
- [17] J. Coon, J. Siew, M. Beach, A. Nix, S. Armour, and J. McGeehan, "A comparison of MIMO-OFDM and MIMO-SCFDE in WLAN environments," in *Proc. IEEE Global Communications Conference, GLOBECOM*, vol. 22, San Francisco, Dec. 2003, pp. 3296–3301.

- [18] F. Horlin, J. Tubbax, L. V. der Perre, and H. D. man, "OFDM vs. single-carrier: a multi-antenna comparison," in *Proc. IEEE International Conference on Acoustics, Speech and Signal Processing, ICASSP*, vol. 4, Montreal, Canada, May 2004, pp. 753–756.
- [19] R. Dinis, D. Falconer, C. T. Lam, and M. Sabbaghian, "A multiple access scheme for the uplink of broadband wireless systems," in *Proc. IEEE Global Communications Conference, GLOBECOM*, vol. 6, Dallas, Texas, Dec. 2004, pp. 3808–3812.
- [20] H.G. Myung, "Introduction to single carrier FDMA," in *Proc. IEEE European Signal Processing Conference, EUSIPCO*, Poznan, Poland, Sept. 2007.
- [21] Y.P. Lin and S.M. Phoong, "BER optimized channel independent precoder for OFDM system," in *Proc. IEEE Global Communications Conference, GLOBECOM*, vol. 1, Taipei, Nov. 2002, pp. 350–354.
- [22] ———, "MMSE OFDM and prefixed single carrier systems: BER analysis," in *Proc. IEEE International Conference on Acoustics, Speech and Signal Processing, ICASSP*, vol. 4, Hong-Kong, Apr. 2003, pp. 229–232.
- [23] B. Devillers, J. Louveaux, and L. Vandendorpe, "About the diversity in cyclic prefixed single-carrier systems," *Elsevier Physical Communication (PHYCOM) journal*, vol. 1, no. 4, pp. 266–276, dec 2008.
- [24] J. Louveaux, L. Vandendorpe, and T. Sartenar, "Cyclic prefixed single carrier and multicarrier transmission: bit rate comparison," *IEEE Commun. Lett.*, vol. 7, no. 4, pp. 180–182, Apr. 2003.
- [25] B. Devillers, T. Sartenar, and L. Vandendorpe, "Bit rate comparison between MIMO cyclically prefixed single carrier and multicarrier transmissions," in *Proc. European Signal Processing Conference, EUSIPCO*, Antalya, Turkey, Sept. 2005.
- [26] T.M. Cover and J.A. Thomas, *Elements of information theory*. New York: Wiley, 1991.
- [27] B. Devillers, J. Louveaux, and L. Vandendorpe, "Bit and power allocation for goodput optimization in coded parallel subchannels with ARQ," *IEEE Trans. Signal Processing*, vol. 56, no. 8, pp. 3652–3661, Aug. 2008.

- [28] B. Devillers and L. Vandendorpe, "Bit and power allocation for goodput optimization in coded OFDM systems," in *Proc. IEEE International Conference on Acoustics, Speech and Signal Processing, ICASSP*, vol. 4, Toulouse, France, May 2006, pp. 649–652.
- [29] B. Devillers, A. García Armada, J. Louveaux, and L. Vandendorpe, "Resource allocation for goodput optimization in parallel subchannels with error correction and selective repeat ARQ," in *Proc. IEEE European Signal Processing Conference, EUSIPCO*, Poznan, Poland, Sept. 2007, pp. 851–855.
- [30] B. Devillers, J. Louveaux, and L. Vandendorpe, "Exploiting cyclic prefix for performance improvement in single carrier systems," in *Proc. IEEE Workshop on Signal Processing Advances in Wireless Communications, SPAWC*, Cannes, France, July 2006, pp. 1–5.
- [31] D. Tse and P. Viswanath, *Fundamentals of wireless communication*. Cambridge University Press, 2005.
- [32] A. Paulraj, R. Nabar, and D. Gore, *Introduction to space-time wireless communications*. Cambridge University Press, 2003.
- [33] B. Muquet, Z. Wang, G. Giannakis, M. de Courville, and P. Duhamel, "Cyclic prefixing or zero padding for wireless multicarrier transmissions?" *IEEE Trans. Commun.*, vol. 50, no. 12, pp. 2136–2148, Dec. 2002.
- [34] Z. Wang, X. Ma, and G.B. Giannakis, "Optimality of single-carrier zero-padded block transmissions," in *proc. IEEE Wireless Communications and Networking Conference*, vol. 2, Orlando, FL, Mar. 2002, pp. 660–664.
- [35] —, "OFDM or single-carrier block transmissions?" *IEEE Trans. Commun.*, vol. 52, no. 3, pp. 380–394, Mar. 2004.
- [36] L. Deneire, B. Gyselinckx, and M. Engels, "Training sequence versus cyclic prefix - a new look on single carrier communication," *IEEE Commun. Lett.*, vol. 5, no. 7, pp. 292–294, July 2001.
- [37] H. Witshnig, T. Mayer, A. Springer, A. Koppler, L. Maurer, M. Huemer, and R. Weigel, "A different look on cyclic prefix for SC/FDE," in *Proc. IEEE International Symposium on Personal, Indoor and Mobile Radio Communications, PIMRC*, Lisbon, Portugal, Sept. 2002.

- [38] H. Witshnig, T. Mayer, A. Springer, L. Maurer, M. Huemer, and R. Weigel, "The advantages of a known sequence versus cyclic prefix in a SC/FDE system," in *Proc. of the 5th international symposium on wireless personal multimedia communications*, vol. 3, Honolulu, Hawaii, USA, Oct. 2002, pp. 1328–1332.
- [39] R. M. Gray, "Toeplitz and circulant matrices: A review," *Foundations and Trends in Communications and Information Theory*, vol. 2, no. 3, pp. 155–239, 2006.
- [40] "Further higher-speed physical layer extension in the 2.4 GHz band," IEEE Std. 802.11g, 2003.
- [41] "IEEE standard for local and metropolitan area networks part 16: Air interface for fixed broadband wireless access systems," IEEE Std 802.16-2004 (Revision of IEEE Std 802.16-2001), 2004.
- [42] S. Muller and J. Huber, "A comparison of peak power reduction schemes for OFDM," in *Proc. IEEE Global Communications Conference, GLOBECOM*, vol. 1, Phoenix, AZ, Nov. 1997, pp. 1–5.
- [43] T. May and H. Rohling, "Reducing the peak-to-average power ratio in OFDM radio transmission systems," in *Proc. IEEE 48th Vehicular Technology Conf.*, vol. 3, May 1998, pp. 2474–2478.
- [44] R. Van Nee and A. de Wild, "Reducing the peak-to-average power ratio of OFDM," in *Proc. IEEE 48th Vehicular Technology Conf.*, vol. 3, May 1998, pp. 2072–2076.
- [45] L. Cimini and N. Sollenberger, "Peak-to-average power ratio reduction of an OFDM signal using partial transmit sequences," in *Proc. International Conference on Communications, ICC*, vol. 1, Vancouver, June 1999, pp. 511–515.
- [46] J. Tellado-Mourelo, "Peak to average power reduction for multicarrier modulation," Ph.D. dissertation, Stanford University, Stanford, CA, Sept. 1999.
- [47] V. Tarokh and H. Jafarkhani, "On the computation and reduction of the peak-to-average power ratio in multicarrier communications," *IEEE Trans. Commun.*, vol. 48, no. 1, pp. 37–44, Jan. 2000.

- [48] A. Salvekar, J. Tellado, and J. Cioffi, "Peak-to-average power ratio reduction for block transmission systems in the presence of transmit filtering," in *Proc. International Conference on Communications, ICC*, vol. 1, Helsinki, Finland, June 2001, pp. 175–178.
- [49] "Air interface for fixed broadband wireless access systems part A: systems between 2 and 11 GHz," *IEEE Std. 802.16ab-01/01*, 2001.
- [50] N. Benvenuto and S. Tomasin, "On the comparison between OFDM and single carrier modulation with DFE using a frequency-domain feedforward filter," *IEEE Trans. Commun.*, vol. 50, no. 6, pp. 947–955, June 2002.
- [51] G.H. Golub and C.F. Van Loan, *Matrix Computations*. Baltimore, MD: Johns Hopkins University Press, 1983.
- [52] I.E. Telatar, "Capacity of multi-antenna Gaussian channels," *Europ. Trans. Telecommun.*, vol. 10, pp. 585–595, Nov. 1999.
- [53] D. Palomar, "A unified framework for communications through MIMO channels," Ph.D. dissertation, Universitat politècnica de Catalunya, Barcelona, Spain, May 2003.
- [54] L. Zheng and D. Tse, "Diversity and multiplexing: a fundamental trade-off in multiple-antenna channels," *IEEE Trans. Inform. Theory*, vol. 49, no. 5, pp. 1073–1096, May 2003.
- [55] G.G. Raleigh and J.M. Cioffi, "Spatio-temporal coding for wireless communication," *IEEE Trans. Commun.*, vol. 3, no. 46, pp. 357–366, Mar. 1998.
- [56] R.A. Horn and C.R. Johnson, *Matrix analysis*. New York: Cambridge University Press, 1985.
- [57] D. Divsalar and M. K. Simon, "The design of trellis coded MPSK for fading channels: Performance criteria," *IEEE Transactions on Communications*, vol. 36, no. 9, pp. 1004–1012, Sept. 1988.
- [58] J. Boutros and E. Viterbo, "Signal space diversity: a power- and bandwidth-efficient diversity technique for the rayleigh fading channel," *IEEE Trans. Inform. Theory*, vol. 44, no. 4, pp. 1453–1467, July 1998.

- [59] V. Tarokh, N. Seshadri, and A. R. Calderbank, "Space-time codes for high data rate wireless communication: performance criterion and code construction," *IEEE Trans. Inform. Theory*, vol. 44, no. 2, pp. 744–765, Mar. 1998.
- [60] S. Alamouti, "A simple transmitter diversity scheme for wireless communications," *IEEE Journal on Selected Areas in Communication*, vol. 16, no. 8, pp. 1451–1458, Oct. 1998.
- [61] V. Tarokh, H. Jafarkhani, and A. R. Calderbank, "Space-time block codes from orthogonal designs," *IEEE Trans. Inform. Theory*, vol. 48, no. 5, pp. 1456–1467, July 1999.
- [62] B. Hassibi and B. Hochwald, "High-rate codes that are linear in space and time," *IEEE Trans. Inform. Theory*, vol. 48, no. 7, pp. 1804–1824, July 2002.
- [63] R. Knopp and P. Humblet, "Information capacity and power control in single cell multiuser communications," in *Proc. International Conference on Communications, ICC*, Seattle, June 1995.
- [64] D. Tse, "Optimal power allocation over parallel gaussian channels," in *Proc. of International Symposium on Information*, Ulm, Germany, June 1997.
- [65] —, "Multiuser diversity in wireless networks," Wireless communications seminar, Stanford University, 2001.
- [66] Z. Liu, "Maximum diversity in single-carrier frequency-domain equalization," *IEEE Trans. Inform. Theory*, vol. 51, no. 8, pp. 2937–2940, Aug. 2005.
- [67] W. Zhang, "comments on 'maximum diversity in single-carrier frequency-domain equalization'," *IEEE Trans. Inform. Theory*, vol. 52, no. 3, pp. 1275–1277, Mar. 2006.
- [68] J. Proakis, *Digital communications*. New-York: McGraw-Hill, 2000.
- [69] J. Sándor, "Generalizations of Lehman's inequality," *Soochow Journal of Mathematics*, vol. 32, no. 2, pp. 301–309, Apr. 2006.

- [70] N. Wang and S.D. Blostein, "Comparison of CP-based single carrier and OFDM with power allocation," *IEEE Trans. Commun.*, vol. 53, no. 3, pp. 391–394, Mar. 2005.
- [71] E. Viterbo and J. Boutros, "A universal lattice code decoder for fading channels," *IEEE Trans. Inform. Theory*, vol. 45, no. 5, pp. 1639–1642, July 1999.
- [72] W. Zhao and G. Giannakis, "Sphere decoding algorithms with improved radius search," *IEEE Trans. Commun.*, vol. 53, no. 7, pp. 1104–1109, July 2005.
- [73] B. Hassibi and H. Vikalo, "On the sphere-decoding algorithm I. expected complexity," *IEEE Trans. Signal Processing*, vol. 53, no. 8, pp. 2806–2818, Aug. 2005.
- [74] H. Vikalo and B. Hassibi, "On the sphere-decoding algorithm II. generalizations, second-order statistics, and applications to communications," *IEEE Trans. Signal Processing*, vol. 53, no. 8, pp. 2819–2834, Aug. 2005.
- [75] A.W. Marshall and I. Olkin, *Inequalities: theory of majorization and its applications*. New York, NY: Academic Press, 1979.
- [76] T. Guess, "Optimal sequences for CDMA with decision-feedback receivers," *IEEE Trans. Inform. Theory*, vol. 49, no. 4, pp. 886–900, Apr. 2003.
- [77] J. Starr, J.M. Cioffi, and P.J. Silverman, *understanding digital subscriber line technology*. Prentice Hall, 1999.
- [78] J.M. Cioffi, "A multicarrier primer," Tutorial, Amati Communications Corporation and Stanford University, 1991.
- [79] A. García Armada, "SNR gap approximation for M-PSK-based bit loading," *IEEE Trans. Wireless Commun.*, vol. 5, no. 1, pp. 57–60, Jan. 2006.
- [80] J.E. Gentle, *Matrix Algebra: Theory, Computations and Applications in Statistics*. Springer, 2007.
- [81] A.J. Goldsmith and P. Varaiya, "Capacity of fading channels with channel side information," *IEEE Trans. Inform. Theory*, vol. 43, no. 6, pp. 1986–1992, Nov. 1997.

- [82] P.S. Chow, J.M. Cioffi, and J.A.C. Bingham, "A practical discrete multi-tone transceiver loading algorithm for data transmission over spectrally shaped channels," *IEEE Trans. Commun.*, vol. 43, no. 2-4, pp. 773–775, Feb-Apr 1995.
- [83] J. Campello, "Practical bit loading for DMT," in *Proc. International Conference on Communications, ICC*, vol. 2, Vancouver, June 1999, pp. 801–805.
- [84] D. Qiao, S. Choi, and K.G. Shin, "Goodput analysis and link adaptation for IEEE 802.11a wireless LANs," *IEEE Trans. Mobile Comput.*, vol. 1, no. 4, pp. 278–292, Dec. 2002.
- [85] M. Realp, A.I. Perez-Neira, and C. Mecklenbrauker, "A cross-layer approach to multi-user diversity in heterogeneous wireless systems," in *Proc. International Conference on Communications, ICC*, vol. 4, Seoul, Korea, May 2005, pp. 2791–2796.
- [86] Q. Liu, S. Zhou, and G.B. Giannakis, "Cross-layer combining of adaptive modulation and coding with truncated ARQ over wireless links," *IEEE Trans. Wireless Commun.*, vol. 3, no. 5, pp. 1746–1755, Sept. 2004.
- [87] S. Lin, D. Costello, and M.J. Miller, "Automatic-repeat-request error-control schemes," *IEEE Commun. Mag.*, vol. 22, no. 12, pp. 5–17, Dec. 1984.
- [88] M.B. Pursley and D.J. Taipale, "Error probabilities for spread-spectrum packet radio with convolutional codes and viterbi decoding," *IEEE Trans. Commun.*, vol. 35, no. 1, pp. 1–12, Jan. 1987.
- [89] S.T. Chung and A.J. Goldsmith, "Degrees of freedom in adaptive modulation: a unified view," *IEEE Trans. Commun.*, vol. 49, no. 9, pp. 1561–1571, Sept. 2001.
- [90] A. Lozano, A. Tulino, and S. Verdú, "Optimum power allocation for parallel gaussian channels with arbitrary inputs distributions," *IEEE Trans. Inform. Theory*, vol. 52, no. 7, pp. 3033–3051, July 2006.
- [91] A.P. Iserte, A.I. Perez-Neira, and M.A. Lagunas Hernandez, "On power allocation strategies for maximum signal to noise and interference ratio in an OFDM-MIMO system," *IEEE Trans. Wireless Commun.*, vol. 3, no. 3, pp. 808–820, May 2004.

- [92] D. Hughes-Hartogs, "Ensemble modem structure for imperfect transmission media," U.S. Patents Nos 4,679,227 (July 1987), 4,731,816 (March 1988), and 4,883,706 (May 1989).
- [93] H. Taha, *Integer programming, theory, applications, and computations*. New York, NY: Academic press, 1975.
- [94] I. Stupia, F. Giannetti, V. Lottici, L. Vandendorpe, and J. Louveaux, "Power and bit allocation for goodput optimization in BIC-OFDM systems," in *Proc. IEEE International Symposium on Personal, Indoor and Mobile Radio Communications, PIMRC*, Cannes, France, Sept. 2008.
- [95] X. Wang and K.J Ray Liu, "Adaptive channel estimation using cyclic prefix in multicarrier modulation system," *IEEE Commun. Lett.*, vol. 3, no. 10, pp. 291–293, Oct. 1999.
- [96] W.A. Syafe, K. Nishijo, Y. Nagao, M. Kurosaki, and H. Ochi, "Adaptive channel estimation using cyclic prefix for single carrier wireless system with FDE," in *Proc. 10th International Conference on Advanced Communication Technology, ICACT*, vol. 2, Feb. 2008, pp. 1032–1035.
- [97] M. Sandell, J-J. Beek, and P.O. Brjesson, "Timing and frequency synchronization in OFDM systems using the cyclic prefix," in *in Proc. Int. Symp. Synchronization*, 1995, pp. 16–19.
- [98] A. Tarighat and A.H. Sayed, "An optimum OFDM receiver exploiting cyclic prefix for improved data estimation," in *Proc. IEEE International Conference on Acoustics, Speech and Signal Processing, ICASSP*, vol. 4, Hong Kong, China, Apr. 2003, pp. 217–220.
- [99] L. Feng and W. Namgoong, "Generalization of single-carrier and multi-carrier cyclic prefixed communication," in *Proc. IEEE Global Communications Conference, GLOBECOM*, vol. 4, St. Louis, Dec. 2005, pp. 2174–2178.